STRUCTURAL SYSTEMS
RESEARCH PROJECT

Report No.
SSRP–05/01
Final

SEISMIC TESTING OF PRECAST SEGMENTAL BRIDGES PHASE III: BRIDGE SYSTEM TEST

by

KELLY P. BURNELL
SAMI H. MEGALLY
JOSÉ I. RESTREPO
FRIEDER SEIBLE

Final Report Submitted to the California Department of Transportation (Caltrans) Under Contract No. 59A0337

June 2005

Department of Structural Engineering
University of California, San Diego
La Jolla, California 92093-0085

University of California, San Diego
Department of Structural Engineering
Structural Systems Research Project

Report No. SSRP–05/01

SEISMIC TESTING OF PRECAST SEGMENTAL BRIDGES PHASE III: BRIDGE SYSTEM TEST

By

Kelly P. Burnell
Graduate Student Researcher

Sami H. Megally
Graduate Student Researcher

José I. Restrepo
Professor of Structural Engineering

Frieder Seible
Dean of the Jacobs School of Engineering
Professor of Structural Engineering

Final Report Submitted to the California Department of Transportation (Caltrans) Under Contract No. 59A0337

Department of Structural Engineering
University of California, San Diego
La Jolla, California 92093-0085

June 2005

Technical Report Documentation Page

1. Report No.	2. Government Accession No.	3. Recipient's Catalog No.

4. Title and Subtitle	5. Report Date
Seismic Testing of Precast Segmental Bridges Phase III: Bridge System Test	June, 2005
	6. Performing Organization Code UCSD/ SSRP-2005/01
7. Author(s) Kelly P. Burnell, Sami H. Megally, Jose I. Restrepo, Frieder Seible	8. Performing Organization Report No. UCSD / SSRP-2005/01
9. Performing Organization Name and Address Department of Structural Engineering School of Engineering University of California, San Diego La Jolla, California 92093-0085	10. Work Unit No. (TRAIS) 11. Contracts or Grant No. 59A0337
12. Sponsoring Agency Name and Address California Department of Transportation Division of Engineering Services 1801 30th St., West Building MS #9/5I Sacramento, California 95807	13. Type of Report and Period Covered Final Report - June 2003 to June 2004 14. Sponsoring Agency Code

15. Supplementary Notes
Prepared in cooperation with the State of California Department of Transportation.

16. Abstract

This report discusses the main findings of a test examining the seismic behavior of a precast, post-tensioned, segmental bridge superstructure with a cast-in-place, hollow, rectangular column. The half-scale specimen modeled a prototype bridge from midspan to midspan and down to midheight of the column. The bridge was built using the balanced cantilever method and the tendon layout of the specimen was designed to most closely match that of the prototype segment joints nearest to the column.

The test was completed in two stages; the first stage prestressing level was designed to avoid any joint openings. This was a validation of existing bridge design procedures in which damage is limited to the column, and the superstructure remains elastic. The second stage involved removing some of the tendons to enable inelastic deformations of the joints in the superstructure and to impose on the joints nearest the column a more severe loading condition. The second stage of the test was done as an introductory examination of the performance of a bridge when damage is not limited to the column and inelastic motion is allowed in the superstructure.

The primary objectives of the test were to investigate the response of the opening of the superstructure joints, column-superstructure interaction, plastic hinge formation in the column, and the anticipated system failure mechanism. Extensive instrumentation was used in the column as well as the joints of the superstructure to record the damage and performance of those bridge components.

17. Key Words	18. Distribution Statement
post-tensioning, precast, segmental construction, balanced cantilever, seismic, superstructures, segment joints	Unlimited

19. Security Classification (of this report)	20. Security Classification (of this page)	21. No. of Pages	22. Price
No restrictions	Unclassified	~125	

Form DOT F 1700.7 (8-72) Reproduction of completed page authorized

Disclaimer

The accuracy of the information presented in this report is the sole responsibility of the authors. All recommendations, opinions, and conclusions presented in the report are those of the authors, and do not necessarily express the beliefs of the California Department of Transportation or the State of California.

Acknowledgments

This research project was made possible by funding from the California Department of Transportation under contract No. 59A0337. The input of Charly Sikorsky and others at Caltrans was greatly appreciated.

The test was performed at the Charles Lee Powell Structural Systems Laboratory at the University of California, San Diego. As always, the capable assistance of the lab staff was essential to the completion of the test. In particular we acknowledge L. Berman and C. Latham, as well as B. Parks, J. Ward, M. Dyson, A. Sherman, C. Stearns, F. Ho, and the truly incomparable undergraduate staff.

The assistance of the following groups was greatly appreciated in the material's procurement and manufacture of the bridge system. F. Mazloom and Keicon Precasters for the construction of the superstructure segments. Dywidag-Systems International, Headed Reinforcement Corporation of California, and Sika Corporation were all generous in their assistance and with special materials needed for the project.

Abstract

This report discusses the main findings of a test examining the seismic behavior of a precast, post-tensioned, segmental bridge superstructure with a cast-in-place, hollow, rectangular column. The half-scale specimen modeled a prototype bridge from midspan to midspan and down to midheight of the column. The bridge was built using the balanced cantilever method and the tendon layout of the specimen was designed to most closely match that of the prototype segment joints nearest to the column.

The test was completed in two stages; the first stage prestressing level was designed to avoid any joint openings. This was a validation of existing bridge design procedures in which damage is limited to the column, and the superstructure remains elastic. The second stage involved removing some of the tendons to enable inelastic deformations of the joints in the superstructure and to impose on the joints nearest the column a more severe loading condition. The second stage of the test was done as an introductory examination of the performance of a bridge when damage is not limited to the column and inelastic motion is allowed in the superstructure.

The primary objectives of the test were to investigate the response of the column-superstructure interaction, opening of the superstructure joints, plastic hinge formation in the column, and the anticipated system failure mechanism. Extensive instrumentation was used in the column as well as the joints of the superstructure to record the damage and performance of those bridge components.

Table of Contents

List of Figures

List of Tables

1 Introduction

1.1 Precast Segmental Bridges

Since beginning in Western Europe over fifty years ago precast segmental construction has spread throughout the world, and in the 1970s the United States. The benefits of segmental construction are most apparent in areas where conventional falsework is prohibitive, shorter construction times are needed, or higher quality construction is desired. One area in which segmental construction is still used sparingly is areas prone to seismic activity.

The process of building precast segmental bridges begins with the production of components, or segments, of the bridge in a precasting plant or factory. The superstructure segments are then shipped to the site of the bridge and lifted into place. Using high strength steel tendons, the segments are post-tensioned together. Two methods of assembling the superstucture segments dominate segmental construction. For shorter span lengths (75'-200' (23-70m)) span-by-span construction is used, and in longer spans (150'-500' (46-152m)) the balanced cantilever method. The span-by-span method entails connecting an entire span of the bridge and then lifting the span into place or assembling it in place atop a temporary steel support. A bridge constructed by the balanced cantilever method will be erecting by placing one segment at a time on either side of the bridge column, thus gradually reaching out across the span distance from the column.

Several advantages are inherent to both building methods. Because of the modular nature of these bridges there is no need for the extensive formwork used in conventional cast-in-place (CIP) concrete. This is an enormous advantage in areas such as high valleys and rivers where formwork is difficult and expensive. Also a minimal footprint is left on the environment below the bridge whether it is an environmentally sensitive habitat or a busy surface street. The savings accumulated by not shutting down streets located below the bridge can be significant, especially in urban areas with high traffic flow.

Other advantages to segmental construction can be achieved as a result of precasting the segments. Because the pieces are cast at a central fabrication facility where mix designs and curing conditions are more easily controlled, higher quality control of segments is achieved. Several construction tasks can also be achieved simultaneously allowing for a reduction in the bridge's construction schedule. For example superstructure segments can be cast at the precast plant while preparation for and construction of piers and abutments occurs at the construction site.

Despite the many advantages to precast segmental construction its use in earthquake-prone areas of the United States has been hampered due to a lack of research on segmental bridges' performance under seismic loads. One concern is for the joints where the segments connect. Because of a lack of experimental research in this area, very conservative design guidelines not based on actual research currently govern the joint region. Some previous work at the University of Texas at Austin dealt with segmental bridges but did not address seismic issues [1,2] The current American Associtation of State Highway and Transportation Officials (AASHTO) guidelines [3,4] require segmental

bridge adhesive (high-strength epoxy) be used on the joints as well as limiting the number of external or unbonded tendons to 50 percent of the total prestressing in the superstructure. The California Department of Transportation (Caltrans) requires that mild steel cross the joint requiring a CIP closure joint and negating many of the benefits of the segmental construction process [5].

1.2 Test Program

A test program examining issues involving the use of precast segmental bridge structures in seismic areas began in 2000 at the University of California, San Diego (UCSD). This program was a cooperative effort involving Caltrans, the American Segmental Bridge Institute (ASBI), and UCSD. The first two phases of the program looked at specific segment to segment connections [6]. The first phase examined joints where high moments and low shears are present such as the midspan of a bridge. Joints with high moments as well as high shears like those nearest to a column were examined in phase two. The early phases tested a series of joints with bonded tendons, unbonded tendons, and a mix of bonded and unbonded. One notable finding was the ability of the joints to open significantly and close with very little residual displacement or damage to the structure when undergoing single direction loading. Further testing involving bi-directional loading is also needed.

The third and final large-scale testing phase, and the subject of this report, was a segmental bridge system test modeling a complete superstructure with pier segment and column. This was done to examine issues relating to the interaction of the column and superstructure as well as corroborating the findings of the earlier phases of the test

program. The prototype bridge modeled had span lengths of 100’ (30.5m) and was assumed to be constructed using the balanced cantilever method. The model bridge was built at half scale of this prototype and erected according to the balanced cantilever method to approximately match the time-dependant stresses across the joints. A series of hydraulic actuators and hollow-core jacks provided boundary conditions matching those on an interior span of the prototype structure. The column used for the test was a hollow CIP column with highly confined boundary elements. A similar column was also used in a previous test and subjected an aggressive bi-directional seismic loading pattern [7].

The test was split into two stages. The first stage was designed to validate the existing design philosophy of maintaining the superstructure of the bridge undamaged. To achieve this the level of post-tensioning in the superstructure was selected to not allow any opening of the segment-to-segment joints under plastic hinging of the column. The second stage sought to allow some opening of the joints. For this purpose a portion of the superstructure tendons were left unbonded in the initial stage and later removed. Additional vertical loads simulating a vertical acceleration, were added to the structure resulting in a more severe loading demand as well as a reduced capacity of the superstructure joints.

1.3 Issues To Be Addressed in Testing

The principle issues addressed by the segmental bridge test are listed below. A brief explanation of the instrumentation and test setup designed to address each issue is also listed.

- The potential for superstructure joints opening under seismic loading
    - At least one linear potentiometer was placed across each of the joints and several across the more critical joints to measure any opening across the joints. Surface strain gauges were also placed near the joints to measure the concrete strains.

- Different design objectives in the superstructure behavior under seismic loading
    - In order to change the amount of prestressing present in the superstructure a portion of the tendons were left unbonded to facilitate their removal during the second stage of testing, and allow for different internal stress conditions.

- Any issues arising between the interaction of the column and superstructure
    - A number of strain gauges were placed on the pier segment rebars that could possibly undergo significant strains during testing. These gauges as well as the gauges in the column were used to gather strain data in the pier segment region of the specimen.

- The formation and performance of the plastic hinge in a hollow rectangular column
    - An extensive array of strain gauges was placed throughout the plastic hinge region at the top of the column. Linear potentiometers were also used to gather curvature information from the column. Three separate shear panels were placed on the west side of the column to measure any shear deformations of the column.

- Failure of the bridge system
    - As well as the instrumentation on the test specimen clustered on the northern and western faces of the unit, these sides were also used to mark the formation and progression of cracks in the column and pier segment. This allowed the other sides of the bridge to be clear for observation of cracks and photographs with minimal obstructions. The strength and stiffness of the system was measured to capture any deterioration during testing.

1.4 Report Outline

The pages that follow discuss in detail the design, construction, analysis, and testing results of the precast segmental bridge system test. A summary of each chapter follows.

Section 2: Test Unit Design and Details

In this chapter the selection and design of the prototype bridge is discussed and the tendon layout considerations are presented. An overview of the design philosophy and detailing of the half-scale test specimen constructed in the lab is also given.

Section 3: Construction and Material Properties

Chapter 3 presents the processes and challenges faced in construction of the test specimen. An explanation of the precast segment construction process as well as the erection of the column and placement of the segments in the lab is given. Material properties for all concrete and steel reinforcing are tabulated.

Section 4: Test Setup, Instrumentation, and Loading Protocol

In this chapter the test setup, instrumentation, and loading procedures for both phases of the segmental bridge test are explained. The test specimen was designed to be loaded in the longitudinal direction under reversed-cyclic loading. The west and north faces of the column were heavily instrumented, leaving the south and east faces for crack observation and photographs.

Section 5: Analytical Considerations and Test Predictions

The analytical considerations of the testing program are presented in chapter 5. The moment-curvature analysis performed and used to predict column deflection is outlined. The post-tensioning loss estimates are presented. The predictions regarding the moments and forces required to open the joints during both stages of the test are also given.

Section 6: Test Observations

Test observations are presented for each stage of the test. The formation and size of cracks as witnessed during the test are explained. Additional photographs of the marked and unmarked crack patterns are found in the photo appendix section. Cracks were marked at the peaks of the first cycle at each ductility level. The cracks were marked with a blue pen in the positive (northward) push, and a red pen in the negative (southward) direction. Photographs and discussions of the joint opening and closing are also explained.

Section 7: Discussion of Test Results

Chapter 7 examines the measured results of each stage of the test. The hysteretic behavior of the bridge system is presented and compared between the two stages of the test. System displacements are examined and relevant strain gauge data is presented. Also the measured joint behavior is presented in detail.

Section 8: Conclusions

This report discussed the design and testing of a half-scale bridge system built using the balanced cantilever method of precast segmental construction. Issues regarding design and analysis of precast segmental bridges are discussed based on the results from the segmental bridge system test as well previous phases of the testing program [6]. Issues for future research are highlighted where applicable.

2 Test Unit Design and Details

2.1 Overview

In this chapter the selection and design of the prototype bridge is discussed and the tendon layout considerations are presented. An overview of the design philosophy and detailing of the half-scale test specimen constructed in the lab is also given.

2.2 Prototype Bridge Structure

The prototype used throughout all phases of the segmental bridge test program was meant to be a general bridge reflecting the types of situations in which a segmental bridge construction scheme would be advantageous while still resulting in a test specimen that the lab could accommodate. The prototype does not seek to model a specific existing bridge; rather it was designed using characteristics generally associated with this type of bridge.

The prototype structure modeled in the bridge system test is a five-span segmental bridge designed according to Caltrans seismic design criteria [3] with three interior 100’ (30.5m) spans and exterior spans of 75’ (22.9m). The column height is 50’ (15.2m). The test specimen models from mid-height of the column and to the midspan on each side of the column (Figure 2.1).

The bridge was designed with a segmental superstructure constructed using the balanced cantilever method. This is different from the previous phases of the research project in which a span-by-span construction scheme was used. However, for the systems test it was decided that a balanced cantilever system would provide data more relevant to current

research needs. Although a 100’ span would be considered a very short span length for a balanced cantilever bridge, lab space limitations and consistency with previous test phases led to a decision not to lengthen the prototype bridge’s span length.

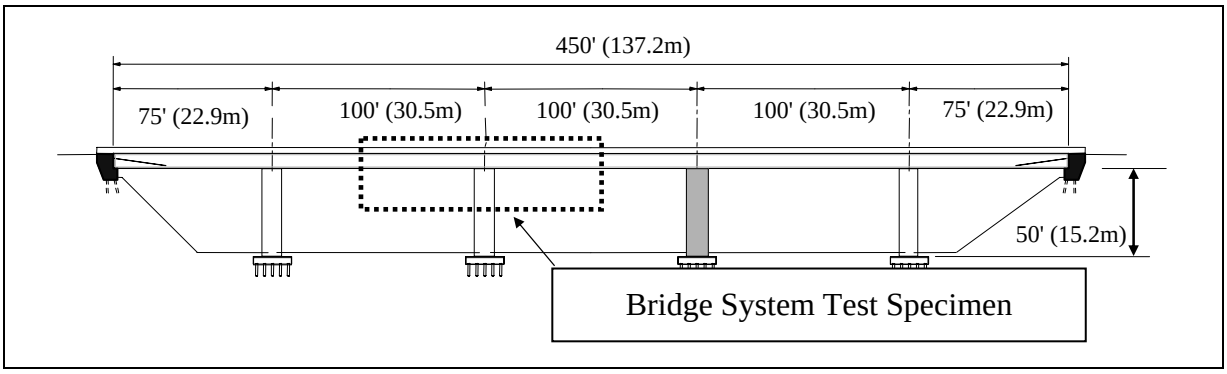

Figure 2.1 Prototype bridge structure

The superstructure box girder shape was based on the ASBI standard section for short balanced cantilever span lengths [8]. The superstructure cross-section had a depth of 71 in. (1800 mm) and a total width of 331 in. (8400 mm). For the segments nearest to the column a thicker bottom flange was needed due to the high negative moments during construction and under seismic loading. Figure 2.2 shows the cross section of the main prototype bridge box girder segment.

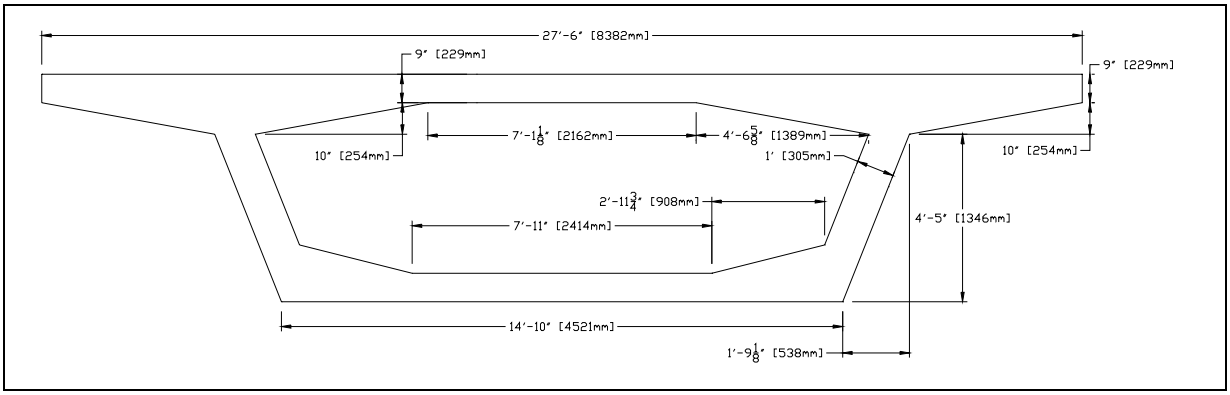

Figure 2.2 Prototype box girder cross section

2.3 Prototype Column

The prototype substructure was hollow rectangular column with octagonal boundary elements on each of the corners. These types of columns have been used recently in several bridges in the San Francisco Bay Area [9,10]. High strength concrete (8000 psi) was assumed in the prototype column.

The corner elements were sized to ensure that under a bi-directional seismic load (V_s) and plastic hinging of the column (M_p) the confined portion of the corner would not crush (see Figure 2.3). The confined corner area's compressive capacity (C_{cap}) must be greater than the axial load (P) of the column plus resisting the compression force of all other corner longitudinal bars yielding without crushing shown in equation 2.1.

$$C_{cap} \geq A_{sl} * N_o * f_u + P \tag{2.1}$$

where A_{sl} is the area of the longitudinal steel and N_o is the number of longitudinal steel bars excluding the bars in compression. The corner capacity is given by

$$C_{cap} = A_{cc} * f'_{cc} \tag{2.2}$$

Where A_{cc} is the confined corner area. Combining equations 2.1 and 2.2 gives the required area of each confined corner:

$$A_{cc} \geq \frac{A_{sl} * N_o * f_u + P}{f'_{cc}} \tag{2.3}$$

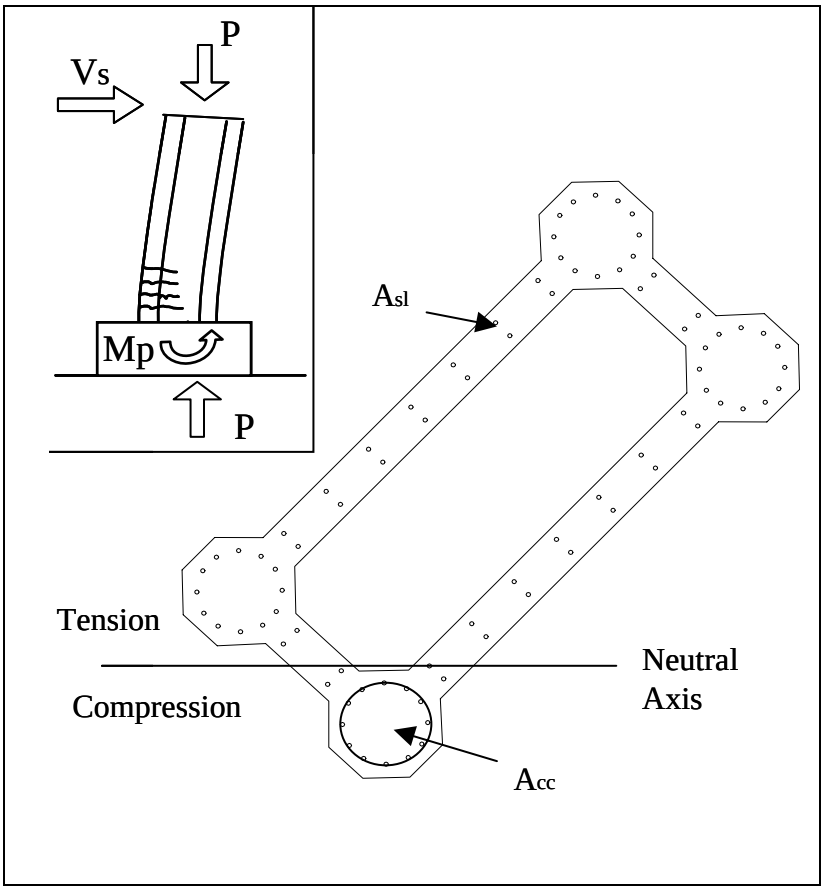

Figure 2.3 Location of neutral axis in column under diagonal seismic loading

2.4 Prototype Tendon Layout

The layout of post-tensioning tendons in balanced cantilever construction involves two steps. First the tendons are placed in the top flange of the superstructure to hold up the segments during construction and resist the negative moment (tension on top) of the cantilevered arms. Then, once all the segments are in place the tendons are placed in the bottom flange of the superstructure to resist positive moments.

Two separate design criteria were used to arrive at the desired tendon layouts for stages 1 and 2 of the test. For stage 1 the governing tendon condition was to limit all damage to the column, thus a capacity design approach was used based on the ultimate moment (M_u) of the column. The seismic moment (M_s) transferred to the superstructure was calculated as follows.

$$M_s = \frac{(M_u + V_s * \frac{h_s}{2})}{2} \qquad (2.1)$$

Where V_s is the seismic shear in the column and h_s is the height of the superstructure (see Figure 2.4).

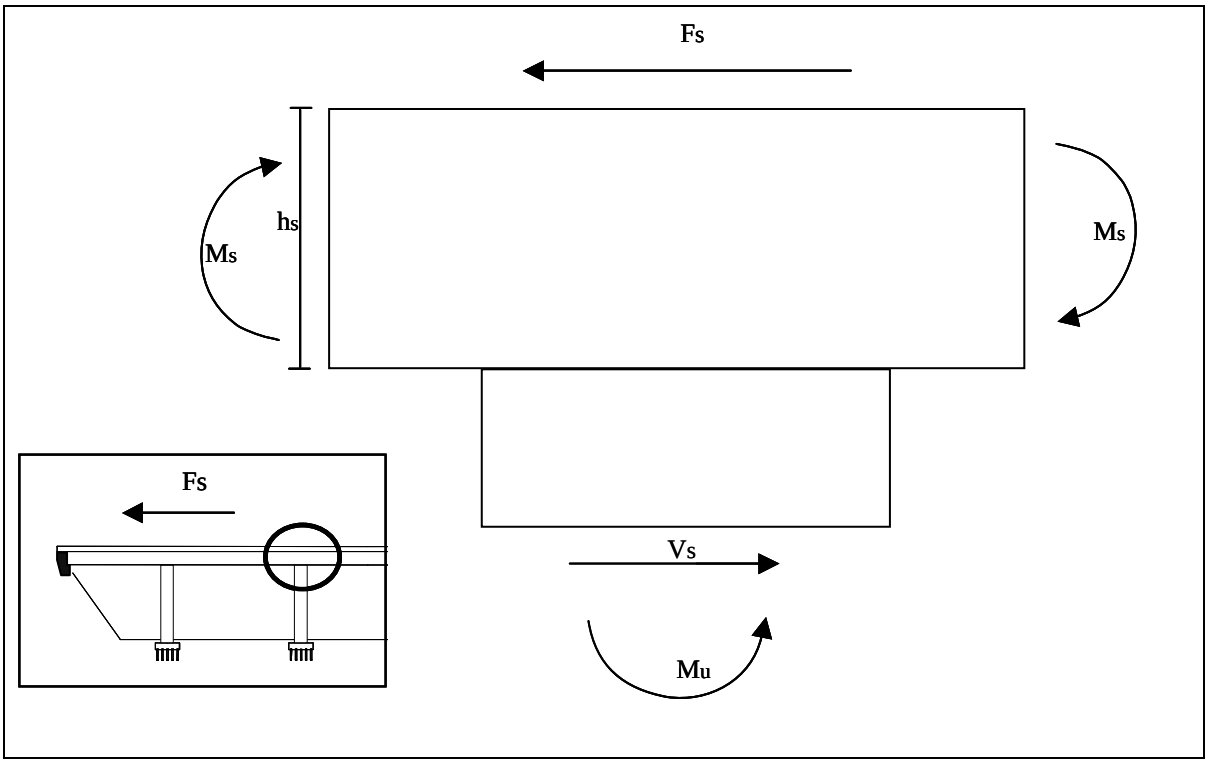

Figure 2.4 Transfer of forces to superstructure during plastic hinging of column

The tendon design for stage 2 sought to place the minimum number of strands in the superstructure to achieve an inelastic response in the superstructure joints under severe seismic loading. This design level was based on AASHTO strength design [1] and allowing $3\sqrt{f'_c}$ tension under service loads.

Table 2-1 summarizes the minimum number of 0.6" (15 mm) strands required across each joint of the prototype for both design scenarios. Overall the reduction was approximately 25-30% in the top joints and up to 70% in the bottom joints.

Table 2-1 Minimum number of tendons required at each joint

		Joint					
		Near Pier	2nd	3rd	4th	5th	Midspan
Stage 1	Top	110	86	62	40	20	16
	Bottom	46	58	66	68	70	72
Stage 2	Top	76	50	32	24	12	12
	Bottom	12	18	24	36	44	46

2.5 Prototype Pier Segment

The pier segment of the prototype structure was initially designed according to standard design principles [1,3,11]. One consideration was whether or not an access opening would be needed through the pier segment. Due to the congestion of mild reinforcement and tendon ducts in the limited area, the access opening was omitted under the assumption that

access to the interior of the box girder sections would be via an opening on the underside of the bridge in each span.

Special attention was paid to the transfer of forces from the superstructure to the column under opening of the first joint nearest the pier segment. Because the pier segment extended past the face of the column additional reinforcement was needed to transfer shear from the superstructure to the column. Once the joints open all the shear force would be transferred through the compression region at the edge of the pier segment. This high shear force was transferred via vertical headed bars to the column. Figure 2.5 shows the transfer of the shear force V_b into the column using a strut-and-tie model in which the compression struts are dashed lines and the tension ties solid lines. The tension of the headed reinforcement is labeled T_h.

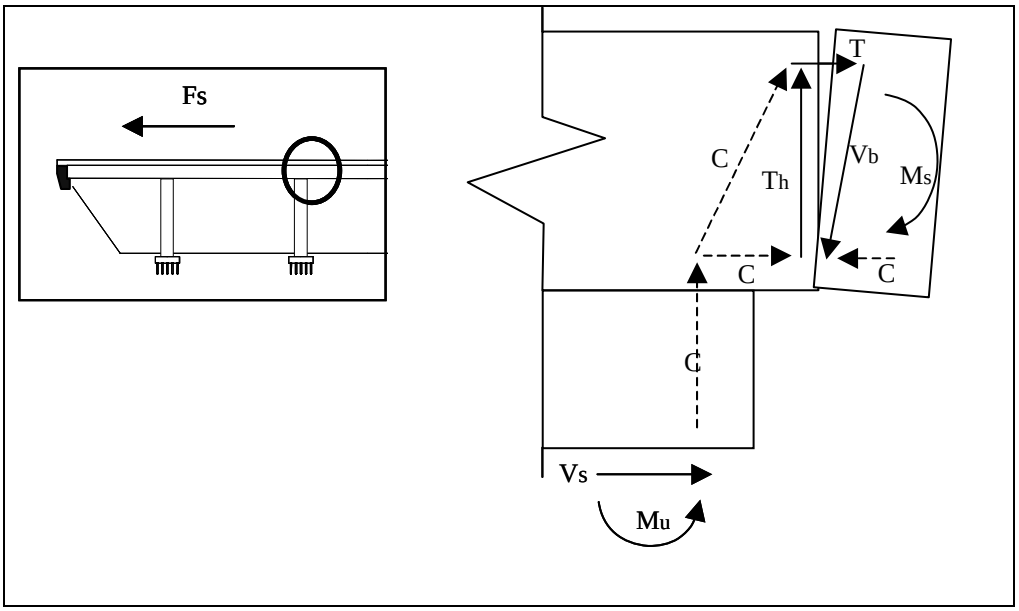

Figure 2.5 Shear transfer through pier segment with opened joint

2.6 Test Unit Design and Details

The test specimen was built at half-scale of the prototype. Figure 2.6 shows the overall layout of the test specimen. The superstructure segments are labeled 1 to 10 starting at the south end of the bridge. The basic geometry and reinforcement configurations of the test specimen are given in Figure 2.7 to Figure 2.14. The tendon layout geometry is shown in Figure 2.15.

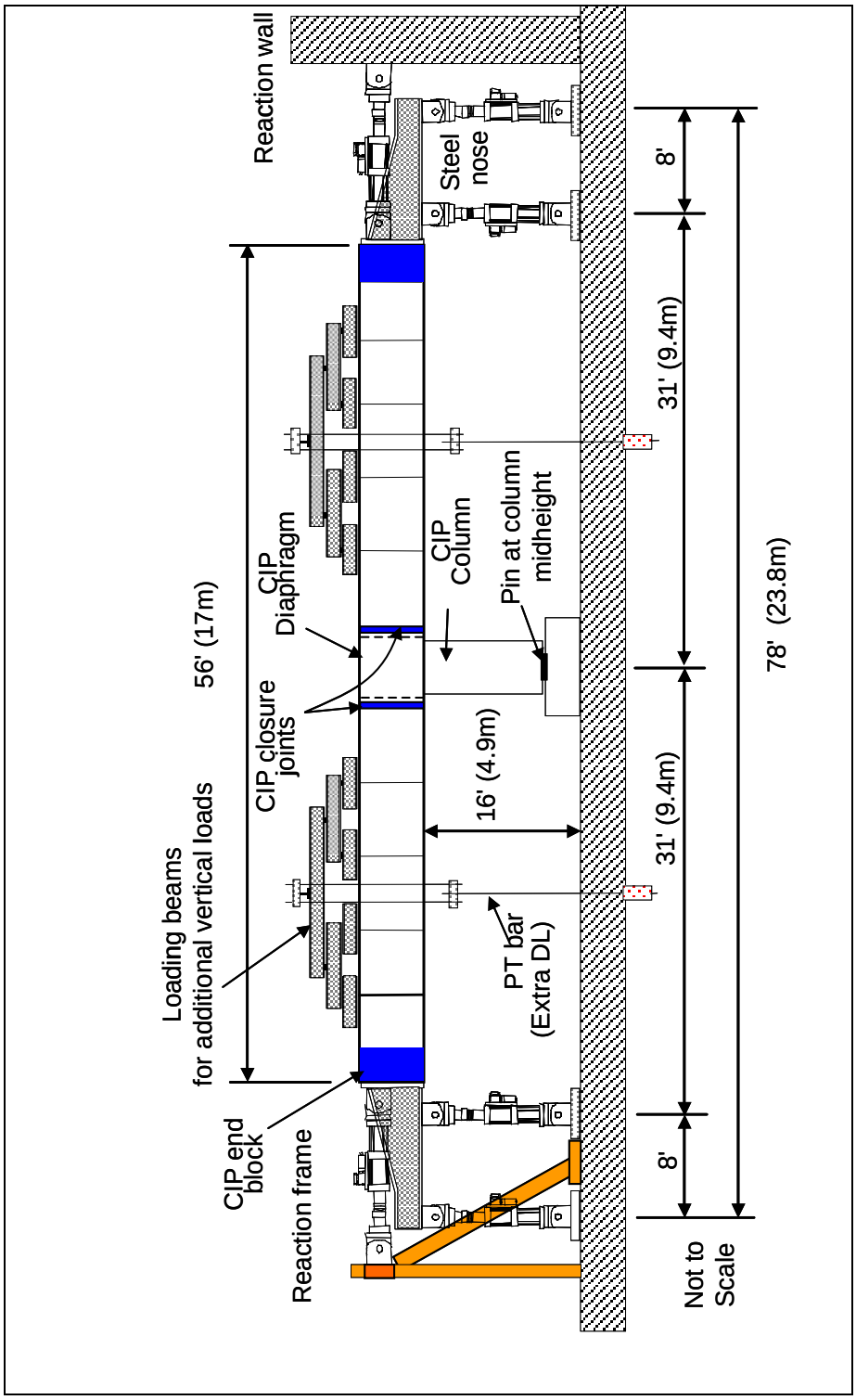

Figure 2.6 Test unit setup elevation view (not to scale)

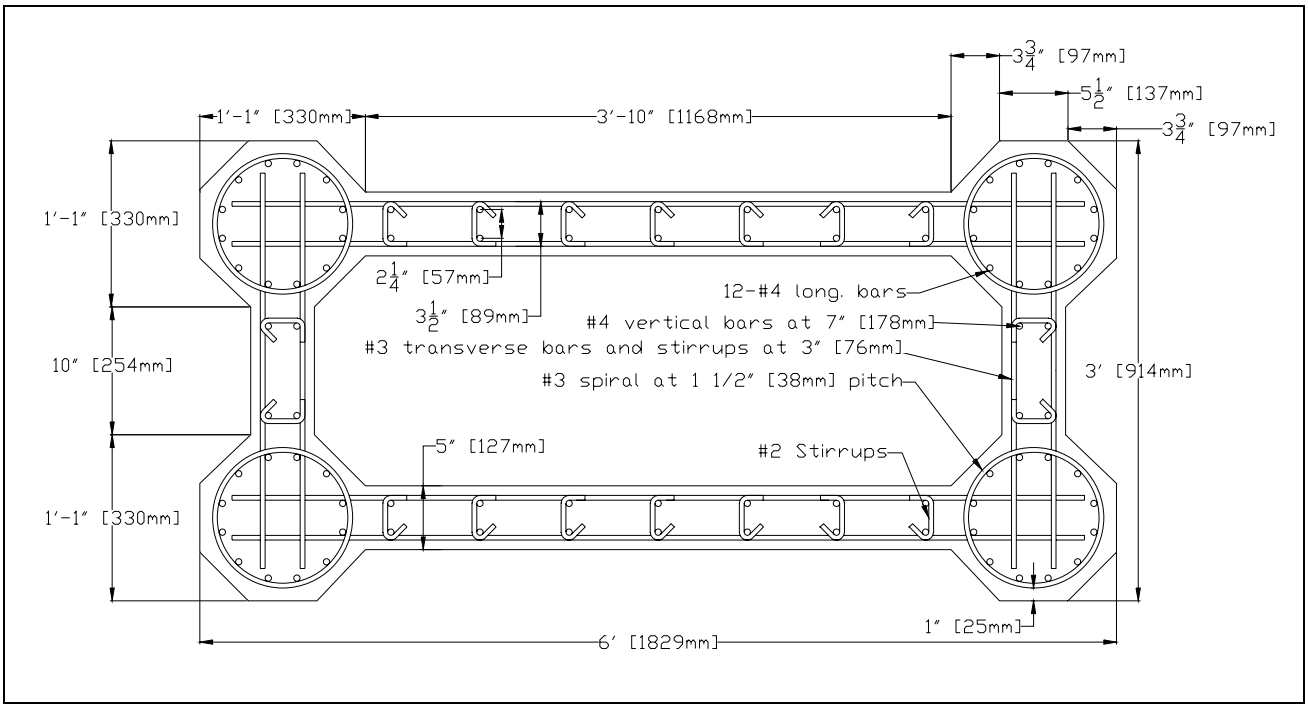

Figure 2.7 Cross section of test unit column plastic hinge region

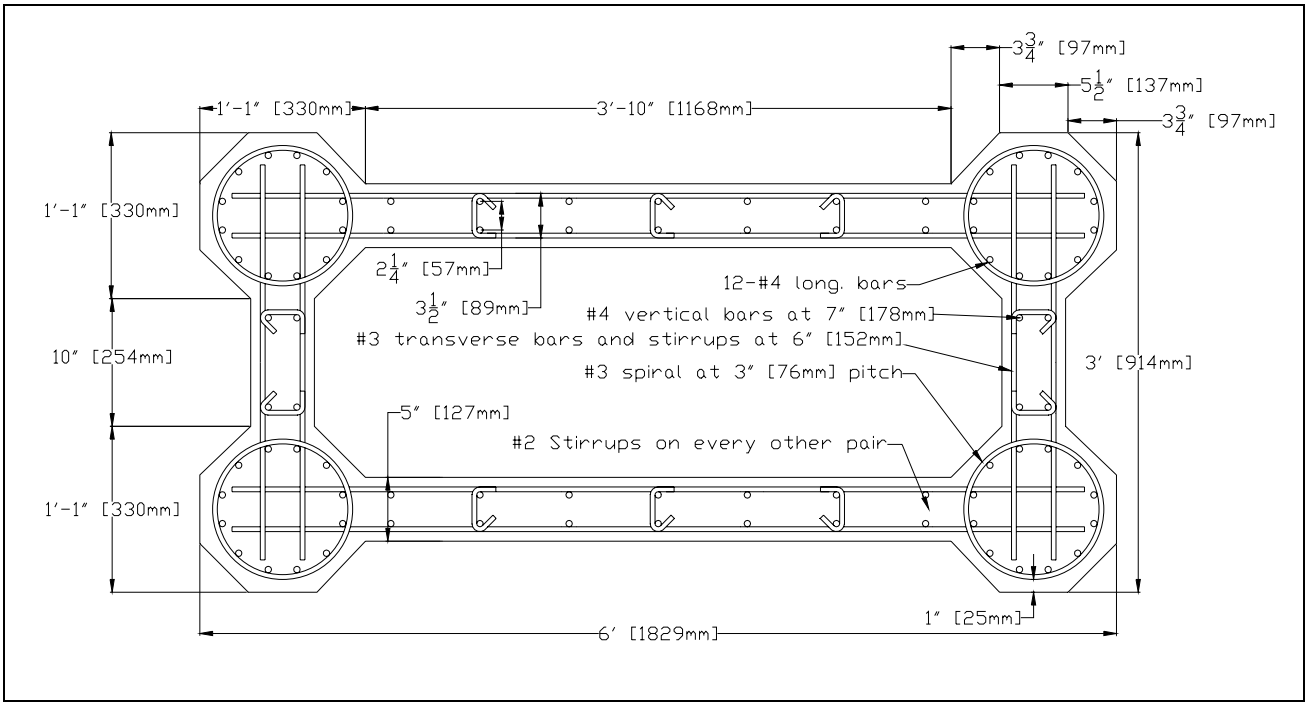

Figure 2.8 Cross section of test unit column non-plastic hinge region

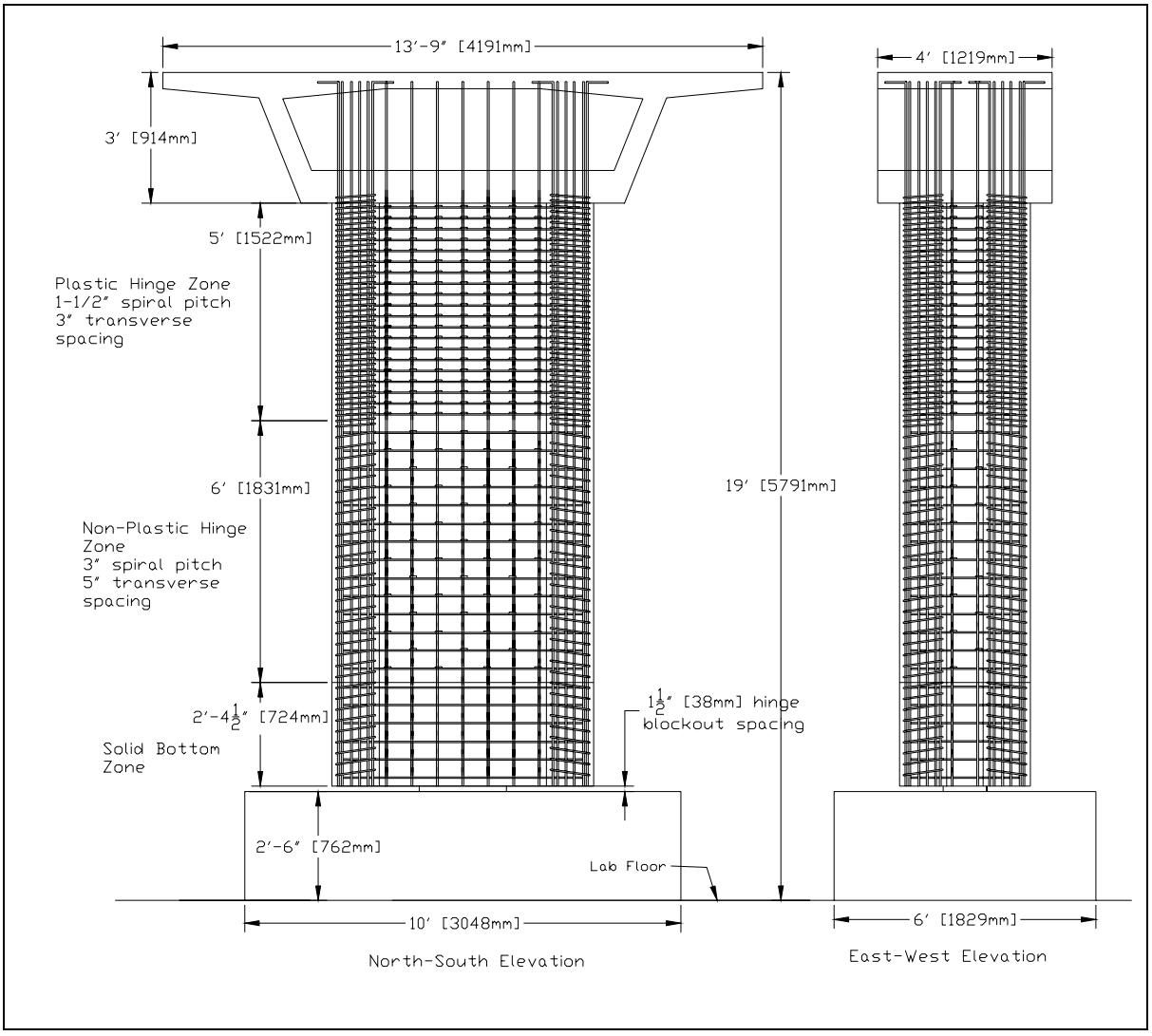

Figure 2.9 Elevation of test unit column and footing

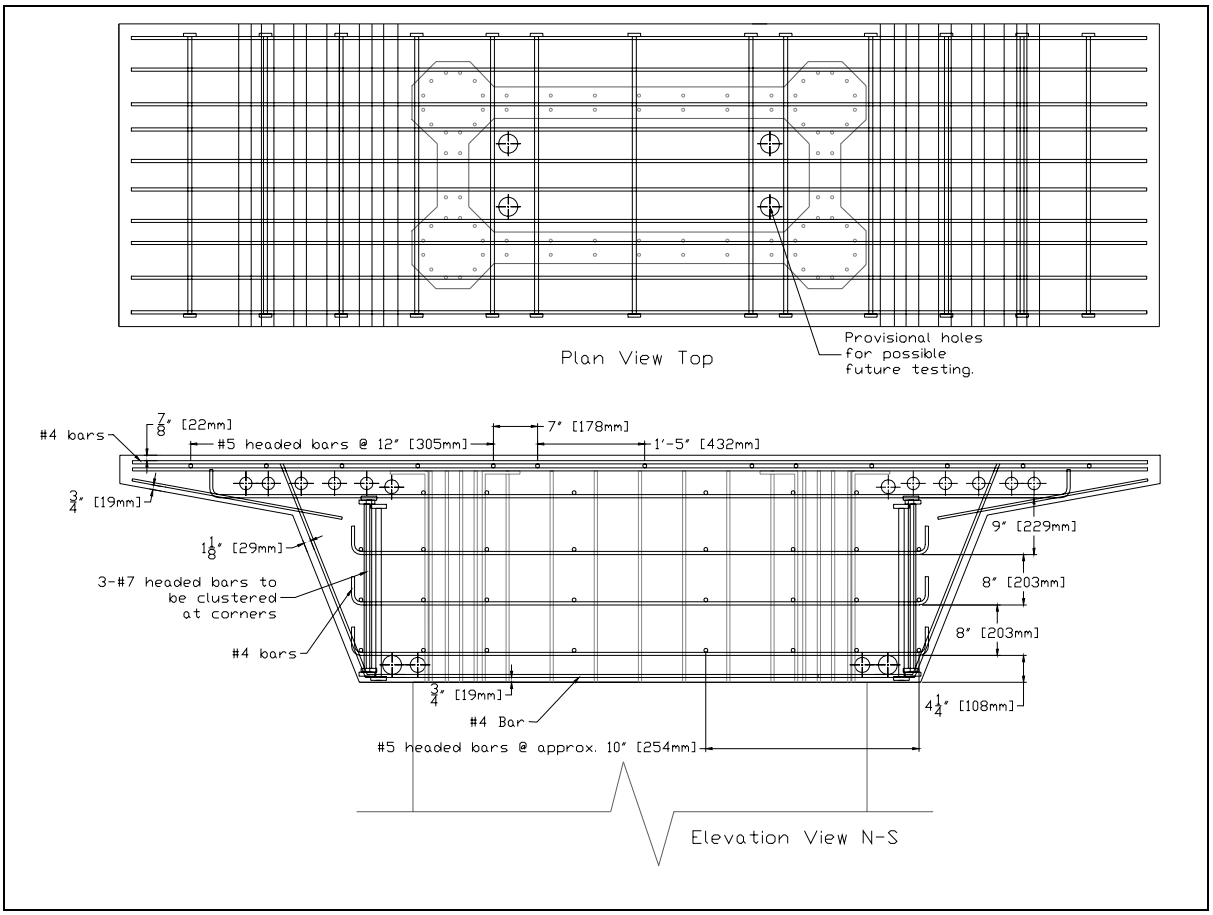

Figure 2.10 Test unit pier segment reinforcement detail

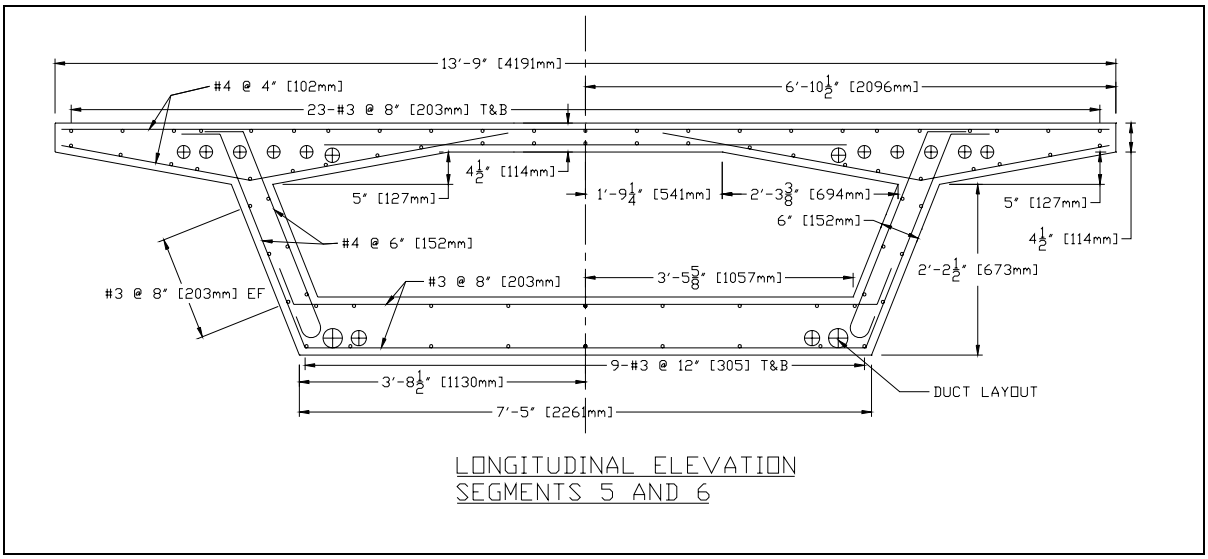

Figure 2.11 Cross section of test unit segments 5 and 6

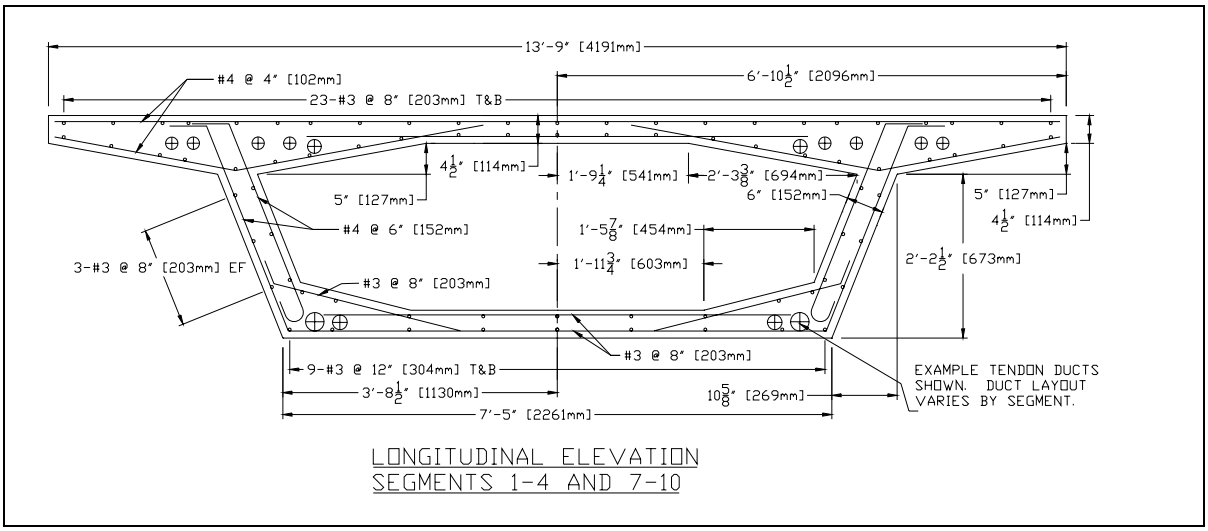

Figure 2.12 Cross section of test unit segments 1-4 and 7-10

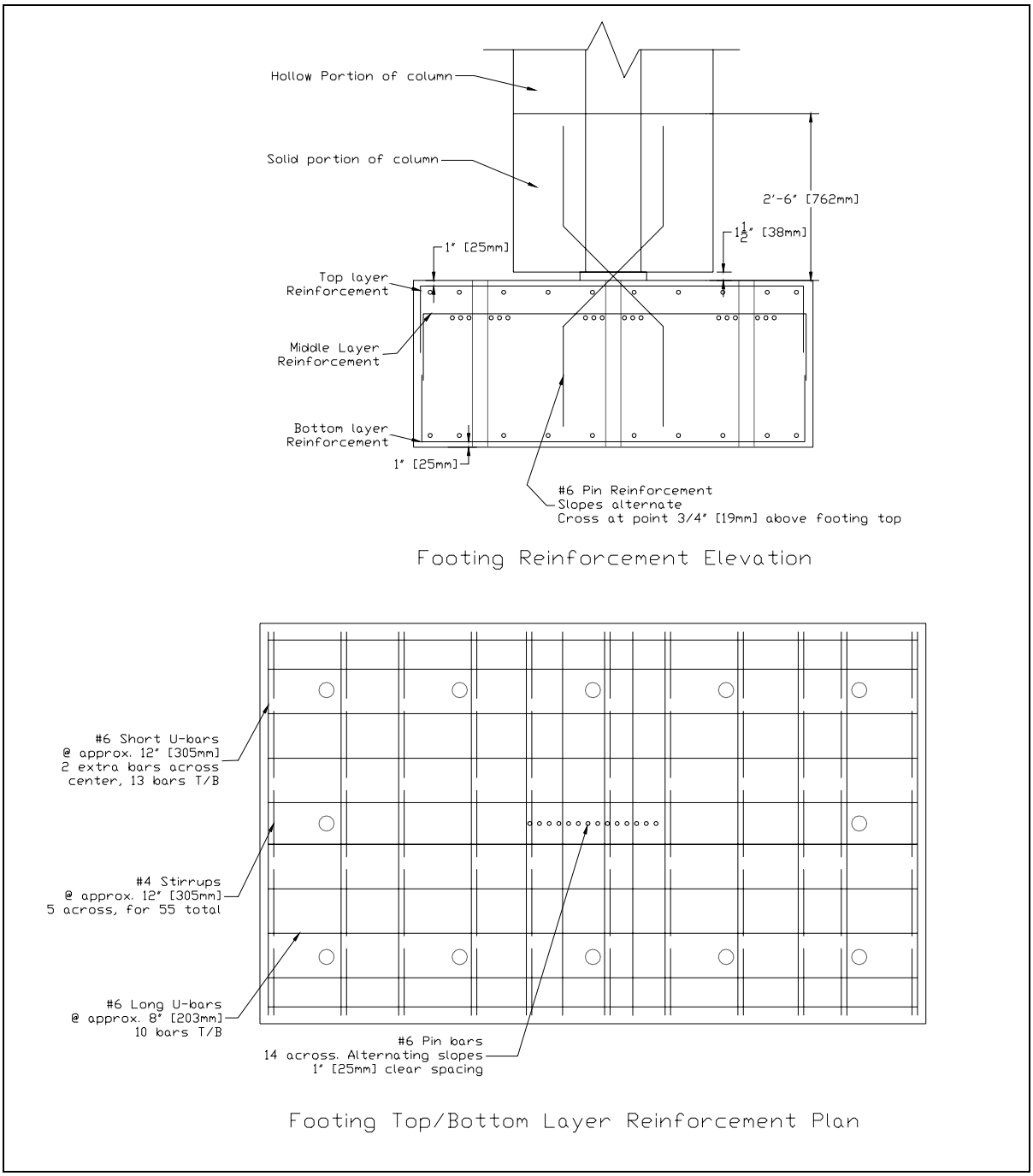

Figure 2.13 Test unit footing reinforcement detail

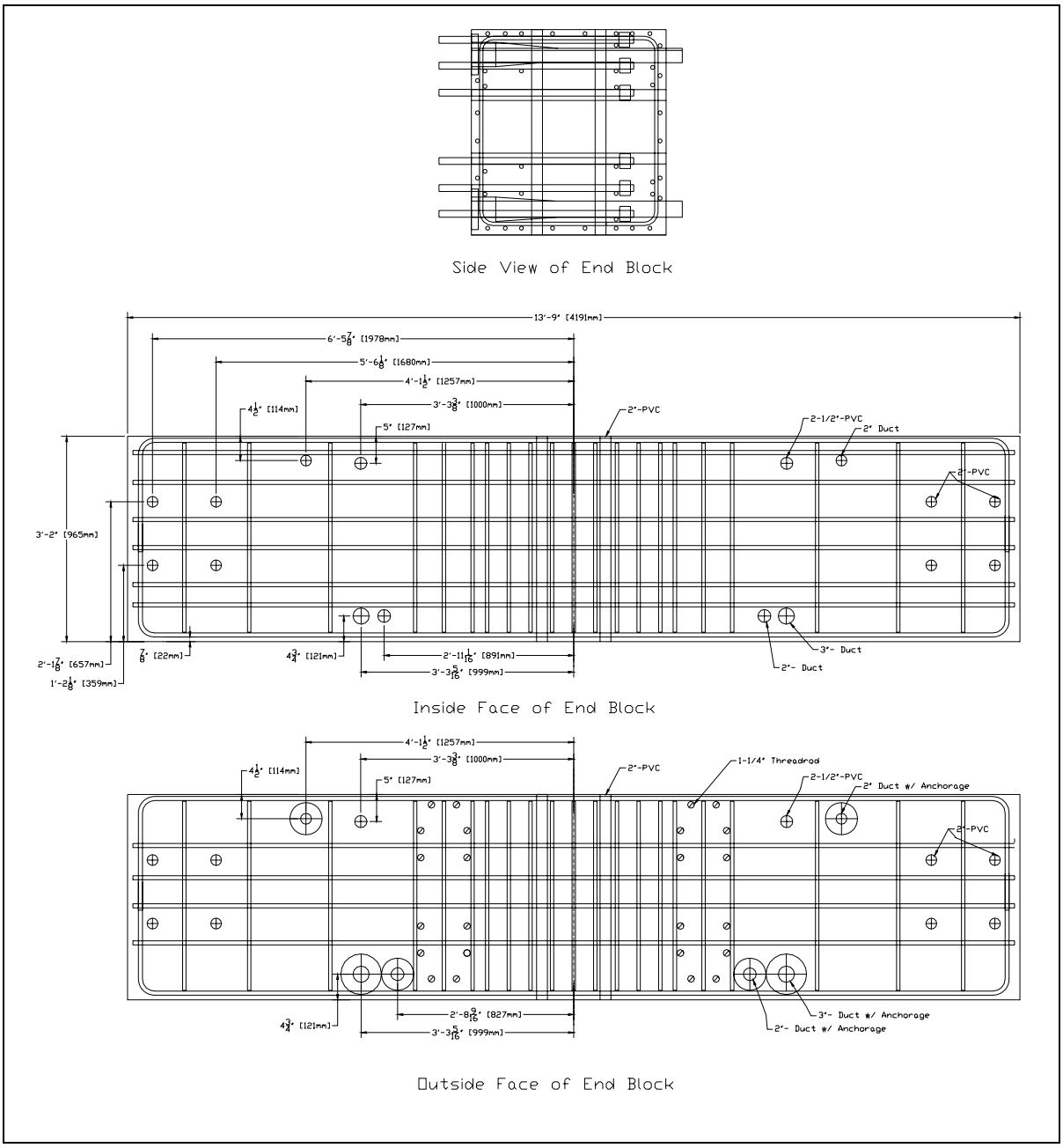

Figure 2.14 Test unit end block reinforcement detail

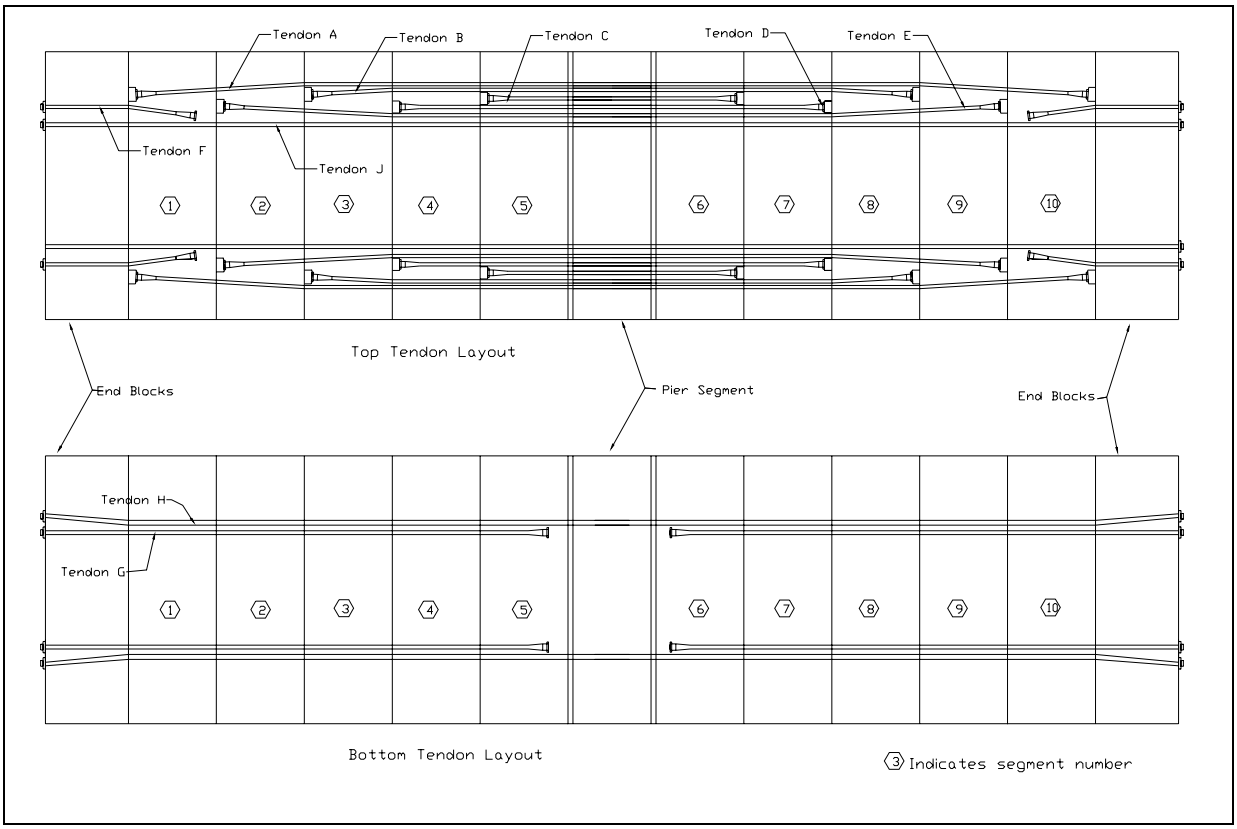

Figure 2.15 Test unit tendon layout

2.7 Strand Bond Area Scaling

Matching the bond area as closely as possible in the scaled down model was important to accurately portray the debonded length of the grouted segments. It was found that by using 0.5" strands in the test unit compared to the 0.6" strands in the prototype resulted in very close bond area matches of the bonding area necessary in the key tendons nearest the column [12].

The bond area per unit length (U) was calculated according to Eqn 2.4 (8).

$$U = \pi * d_s * n_s * r_s * N * a_{ave} \quad (2.4)$$

Where d_s is the diameter a strand, n_s is the number of exterior wires on each strand, r_s is the ratio of the exterior portion of each wire to the interior portion (assumed to be 220/360), N is the number of exterior strands, and a_{ave} is the average number of exposed sides of the exterior strands.

3 Construction and Material Properties

3.1 Overview

Chapter 3 presents the processes and challenges faced in construction of the test specimen. An explanation of the precast segment construction process as well as the erection of the column and placement of the segments in the lab is given. Material properties for all concrete and steel reinforcing are tabulated.

3.2 Construction of the Bridge System Test Unit

A series of additional illustrative photographs of the construction are found in the appendix of this report. The scale and precarious nature of the test unit made its construction an interesting and challenge task. To begin with the footing was cast and moved into position on the lab floor. After this each spiral corner of the column was tied separately and lifted into position on the footing. A foam blockout was used to maintain the gap between the footing and the column base. All the longitudinal steel of the column was placed and the bottom 30 in., the solid section, was poured. Following this the remainder of the column transverse steel and stirrups were placed and the middle and top sections of the column were cast in two separate pours. The same set of forms was used for all three pours, moved up and fastened higher on the column each time. A platform was then constructed around the column top upon which the forms and steel for the pier segment were erected. Careful consideration was given to the location of all post-tensioning ducts to insure that the tendons would be able to pass through the section once all the segments were in place.

While the construction of the column and pier segment was going on at the Powell Labs in San Diego, California; the individual segments were cast by Keicon Precasters located in Stockton, California. The ten precast segments were cast using a single steel form with interchangeable interior pieces to accommodate the different interior dimensions and blister details. The pieces were match-cast starting one of the segments closest to the column and then proceeding along one side. After the five on one side of the column were finished those on the opposite column side would be cast in a similar manner. Once begun, the casting of all ten precast segments was completed in ten working days.

Once the segments were delivered to the lab, platforms were raised on either side of the column and the first pair of segments positioned atop them leaving space for the three inch closure gap. The closure gap was poured and allowed to set for two weeks before the permanent cantilever tendons for the first pair of segments were post-tensioned. The process of post-tensioning the sequential pairs of segments was then repeated as shown in Figure 3.1. First the platforms moved out from the previous pair, and the new segments were lifted into place and segmental bridge adhesive epoxy was applied to each face to be joined (Step A). Next, four temporary post-tensioning bars were placed through the bridge structure to provide an even pressure across the faces during curing of the epoxy, and to hold the segments in place before the permanent tendons were installed (Step B). After the permanent tendons were installed (Step C) the temporary bars were removed and the process repeated until all ten segments (five pairs) were erected.

The end blocks used to apply the boundary conditions were then placed and a closure joint was poured between the blocks and the outermost pair of segments of the test specimen.

With the blocks in place it was then possible to install the tendons along the bottom of the superstructure as well as the continuity tendons and unbonded tendons along the top.

After all tendons were installed in the bridge, the fixtures were attached to the bridge. The wiffle tree and steel nose systems were installed and all eight actuators hooked up to allow the application of loads and boundary conditions.

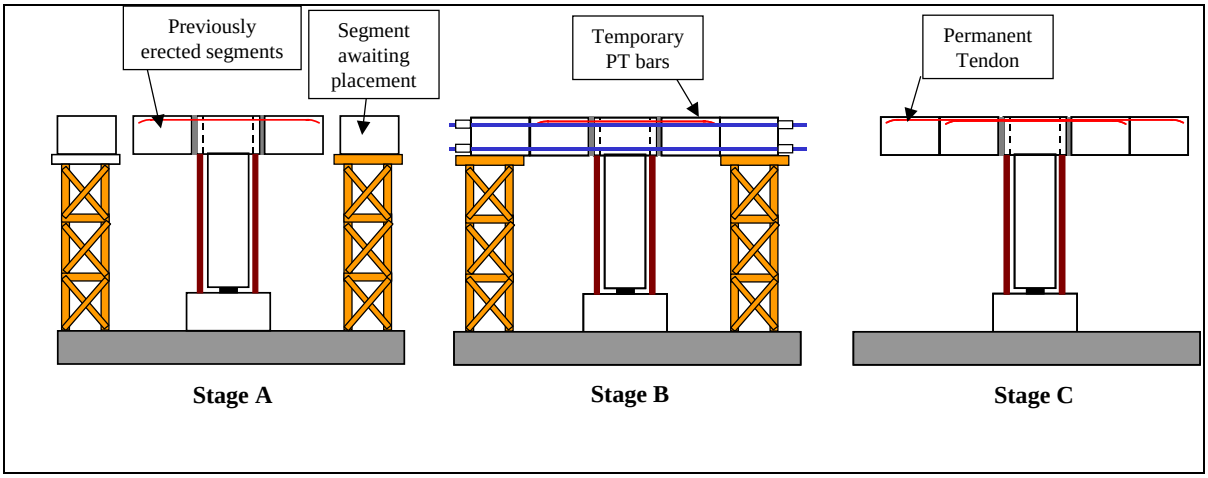

Figure 3.1 Erection sequence of precast segments

3.3 Material Properties

The following section outlines the material properties for concrete and steel used in the test. Design concrete strength was f'_c = 8 ksi (55 MPa) for the column and pier segment and 5 ksi (35MPa) for the segments.

3.3.1 Concrete Properties

The column was poured in five stages. The footing block first, followed by the solid pin section which made up the bottom 30 inches (762mm) of the column. The hollow portion of the column was poured in two separate lifts called column middle and column top. Lastly the pier segment was poured on top of the column. The 3" closure gaps on either side of the pier segment and those connecting the end blocks to the precast segments used the same concrete mix design as the column and pier segment.

In order to insure the concrete was properly distributed throughout the closely spaced reinforcement of the corner elements and walls a self-consolidating concrete was used. This required practically no vibration of the concrete resulting in limited aggregate separation, and ease of placing the concrete. A minimal spread of 25 inches was specified for the self-consolidating concrete.

The compressive strengths were determined according to the average of three 12 in. tall by 6 in. diameter cylinder tests according to standard practice. The day-of-test (DOT) strengths were taken during the first two days of testing. Because the critical concrete pour sections of the column top, pier segment, and pier segment closure gap were old at the beginning of testing (at least 91 days), no significant differences in strength were anticipated over the weeks of testing. A few smaller cylinders of the grout mix were also tested. The DOT strength of the segments was taken as the average of two cylinders shipped with each segment. All post-test analysis were done using the average DOT strength for each component. Table 3-1 and Table 3-2 give the results of the compressive

strength tests for all sections. Split cylinder tests were performed on the column top to gauge the DOT tensile strength. The result was a splitting stress of 0.64 ksi (4.4 MPa).

Table 3-1 Test unit concrete compressive cylinder strengths (ksi)

	Date Cast	**7-day**	**14-day**	**28 day**	**DOT**	**Age on DOT (days)**
Column Bottom	11-13-03				12.1	201
Column Middle	12-5-03				11.5	179
Column Top	1-13-04				11.6	140
Pier Segment	2-24-04	7.7	9.0	10.0	11.6	98
Pier Gap	3-2-04	7.8		10.3	12.5	91
End Gap	4-27-04	8.1			10.2	35
Grout	5-10-04				4.3	31

Table 3-2 Test unit segment compressive day of test strengths (ksi)

Segment	**1**	**2**	**3**	**4**	**5**	**6**	**7**	**8**	**9**	**10**
DOT Strength	8.8	9.3	9.7	9.1	9.2	9.0	7.8	8.9	8.2	5.9

Table 3-3 Test unit concrete compressive cylinder strengths (MPa)

	Date Cast	**7-day**	**14-day**	**28 day**	**Day of Test**	**Age on DOT (days)**
Column Bottom	11-13-03				83	201
Column Middle	12-5-03				79	179
Column Top	1-13-04				80	140
Pier Segment	2-24-04	53	62	69	80	98
Pier Gap	3-2-04	54		71	86	91
End Gap	4-27-04	56			70	35
Grout	5-10-04				30	31

Table 3-4 Test unit segment compressive day of test strengths (MPa)

Segment	1	2	3	4	5	6	7	8	9	10
DOT Strength	61	64	67	63	63	62	54	61	57	41

3.3.2 Steel Properties

Table 3-5 and Table 3-6 give the properties for the mild reinforcement used in the test specimen. The reinforcement used in the footing, the segments, and the end blocks is not included. The numbers given are the averages of three separate bars of each size taken from each batch of steel used. The high-strength strands used were 0.5” (13 mm) diameter, low relaxation strands. Since no yielding of the strands was anticipated and due to the difficulty in producing reliable material test results from the 7-wire strands, no material tests were performed. In case of unexpected yielding, strand sections from the main spool were retained for possible future testing.

Table 3-5 Test unit mild steel reinforcement properties (ksi)

	F_y	F_u
#3 bar – Column. Long wall transverse bar	65.9	103.8
#3 bar – Column. Short wall transverse bar	65.6	99.2
#4 bar – Column, Longitudinal group A	64.8	105.7
#4 bar – Column. Longitudinal group B	65.1	105.0
#4 bar – Pier Segment	66.5	87.8

Table 3-6 Test unit mild steel reinforcement properties (MPa)

	F_y	F_u
#3 bar – Column. Long wall transverse bar	455	716
#3 bar – Column. Short wall transverse bar	453	684
#4 bar – Column, Longitudinal group A	447	729
#4 bar – Column. Longitudinal group B	449	725
#4 bar – Pier Segment	459	606

4 Test Setup and Instrumentation

4.1 Overview

In this chapter the test setup, instrumentation, and loading procedures for both phases of the segmental bridge test are explained. The test specimen was designed to be loaded in the longitudinal direction under reversed-cyclic loading. The west and north faces of the column were heavily instrumented, leaving the south and east faces for crack observation and photographs.

4.2 Test Setup

The test unit was loading in the longitudinal direction according to a displacement-based, incrementally-increased, fully-reversed cyclic loading pattern. The lateral load was applied via four +/- 225 kip, 48 in. (1000kN, 1.2m) stroke MTS actuators. The two northern horizontal load actuators were anchored to the lab strong wall and the southern horizontal actuators were held in place by steel a-frames atop concrete blocks. Two 300 kip (1320kN) hollow core jacks provided the gravity load. Each jack was attached to a high strength steel bar and applied the force to a series of steel beams called a wiffle tree. These wiffle trees spreads the single point load on either side of the span to 64 points across the deck of the bridge structure better simulating a distributed load. The axial load ratio of the column during stage 1 was 0.027 and 0.047 during stage 2. Because the bridge system represents a single span of a continuous span bridge the moments at the ends of the spans are not zero. A pair of vertical actuators on each end applied a constant moment at the bridge ends. These actuators were +/- 225 kip, 18 in. (1000kN, 0.46m) stroke MTS actuators. One applied a force directly under the end block and the other and equal and

opposite force with a moment arm of 8ft via the steel nose pieces attached to the bridge ends. Figure 4.1 and Figure 4.2 show the scale schematics of the test set-up and a photo is shown in Figure 4.3.

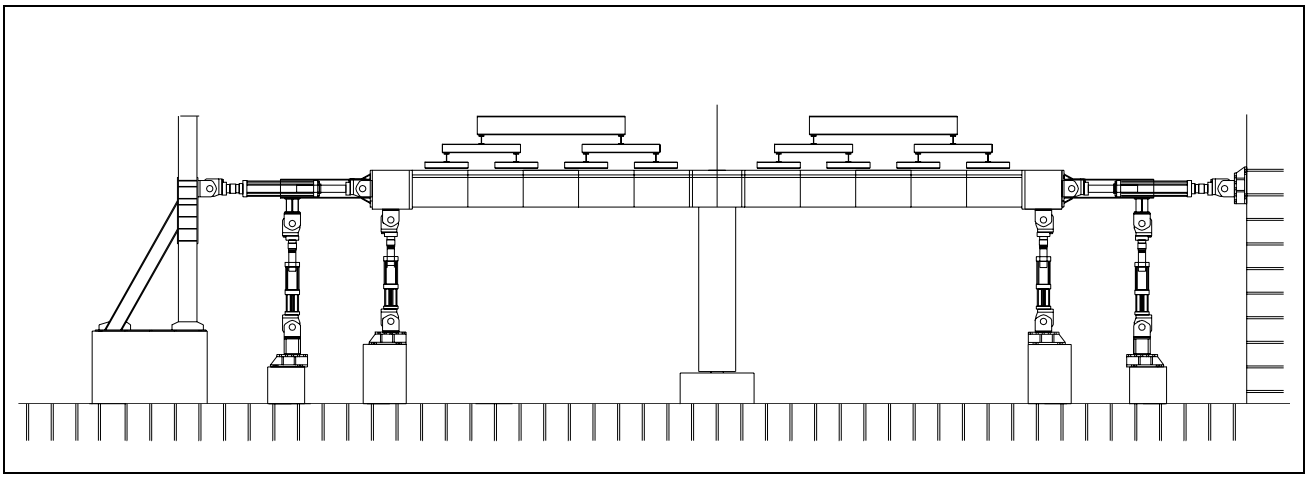

Figure 4.1 Test unit east-west elevation view

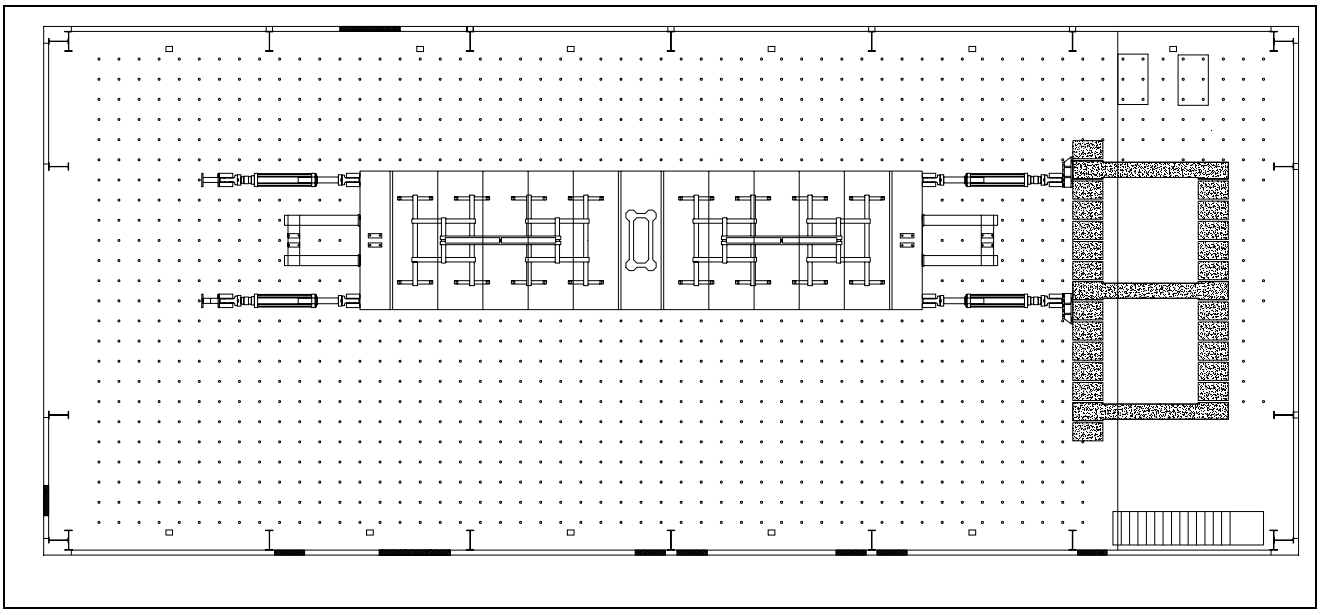

Figure 4.2 Test unit plan view

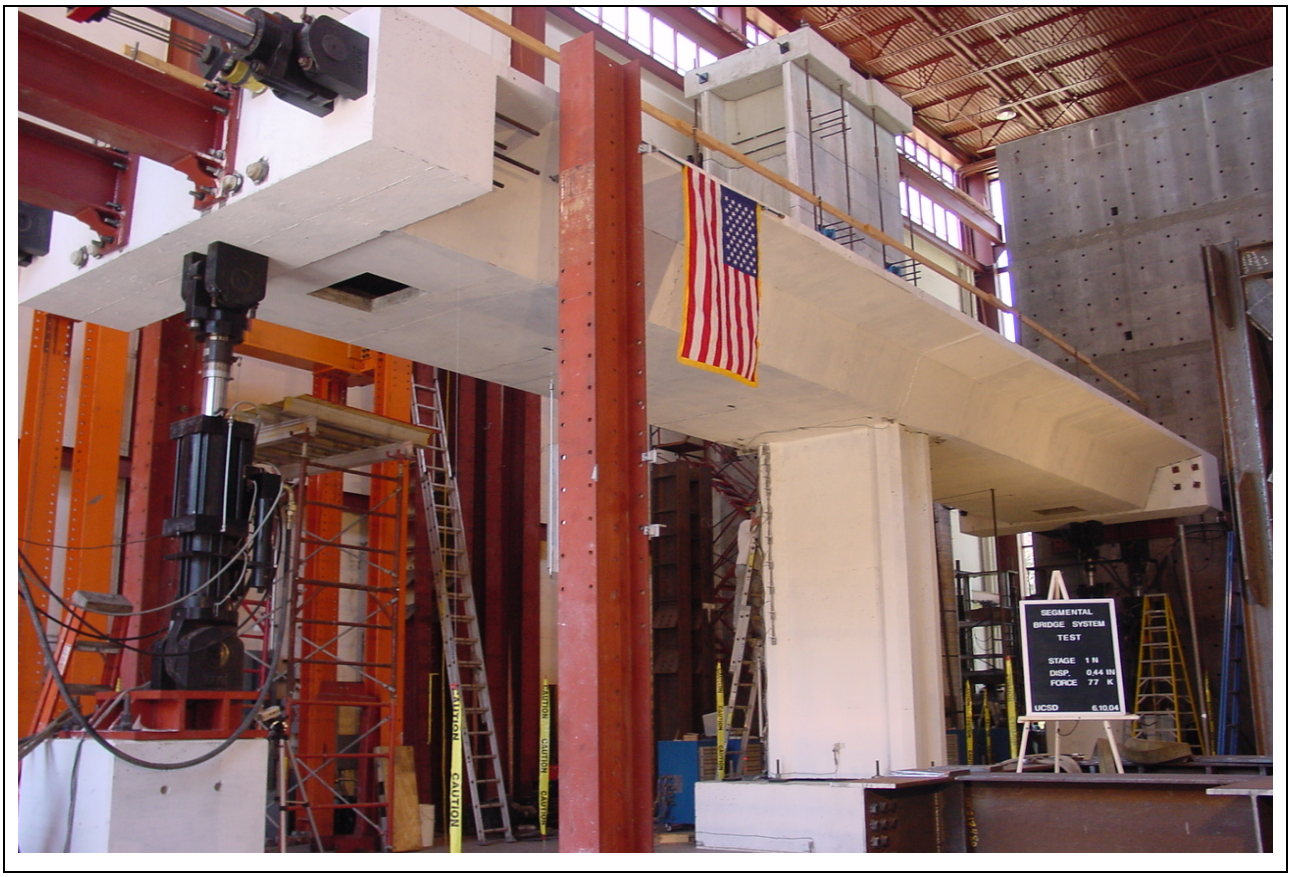

Figure 4.3 Test unit photo

4.3 Loading History

The test unit was subjected to a reversed cyclic loading pattern in the longitudinal direction. The loading history is shown in Figure 4.4. Two cycles at increasing ductility levels were used in order to allow for further testing of the system without considerable strength deterioration in the column. Testing stage 1 consisted of the cycles up to and including a system displacement ductility of 4 (μ=4) which is a minimum requirement for seismically designed bridges. During stage 1 the vertical load and end moments applied to the superstructure were equivalent to those caused only by gravity loads.

At the commencement of stage 2 a cycle was repeated at μ=4 to easily compare any differences in behavior between the two stages. During stage 2 the vertical load and end moments applied to the superstructure were equivalent to a vertical acceleration of 0.75g plus the gravity load.

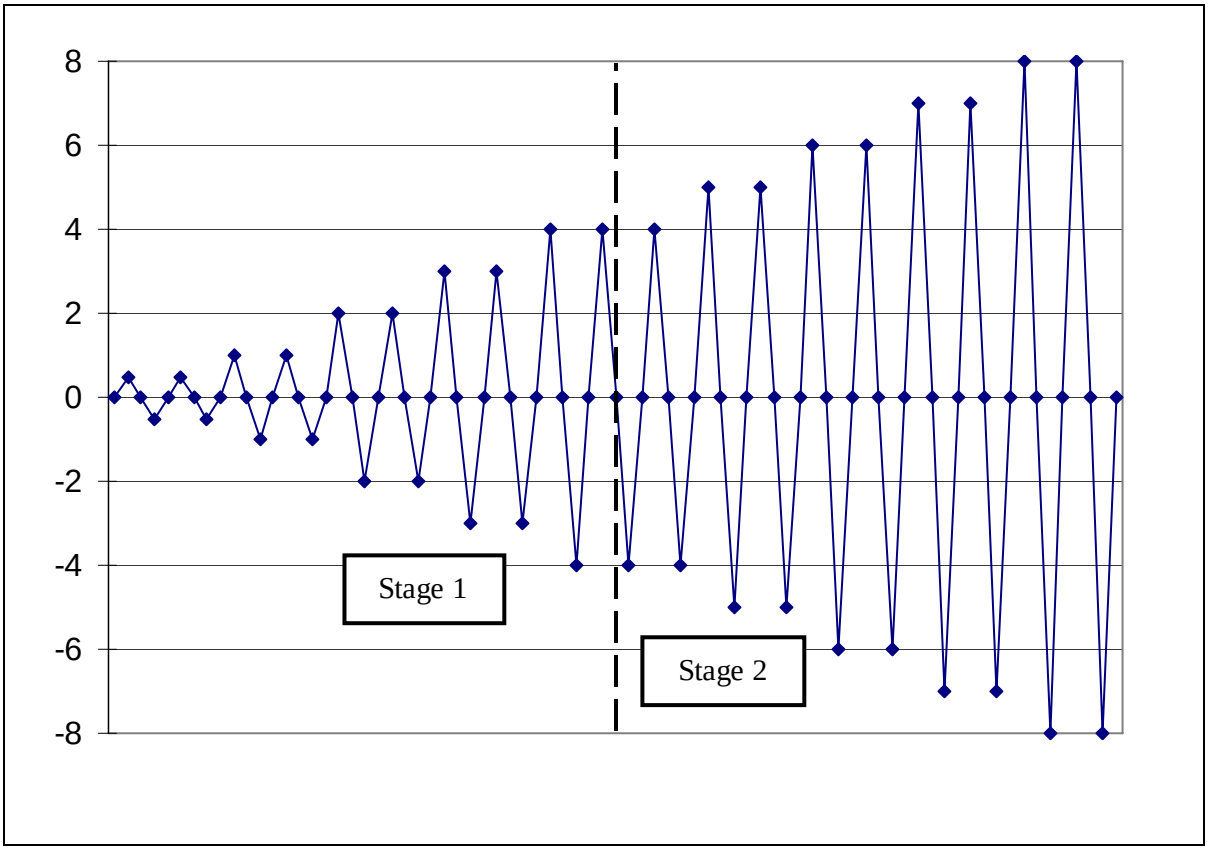

Figure 4.4 Loading history

4.4 Instrumentation

4.4.1 Mild Reinforcement Strain Gages

The strain of reinforcing bars in the column and pier segment were monitored using strain gauges. Most gauges were 12Ω resistance gages with a 5mm (0.2 in.) gauge length. In a

few locations near the column-pier segment interface, post-yield gauges were used to capture post-yield strains in the bars. The reinforcing bars were prepared by grinding smooth a section of bar, roughening the surface, and cleaning it with methyl ethyl-keytone. The gauges were then applied to the prepared surface with an adhesive (alpha cyanoacrylate monomer). To protect them from water and mechanical abrasions an acrylic based water-proofing agent and a vinyl mastic membrane were applied over the gauges.

Figure 4.5 and Figure 4.6 show the strain gauge details of the bridge column. The longitudinal bar gauge locations were selected to give a strain profile of the column. On the transverse bars gauges were added to measure overall strain in the bar as well as gain information on development of the straight bars (13). The strain gauge layout of the pier segment is shown in Figure 4.7. These gauges were intended to monitor the transition of forces through the pier segment.

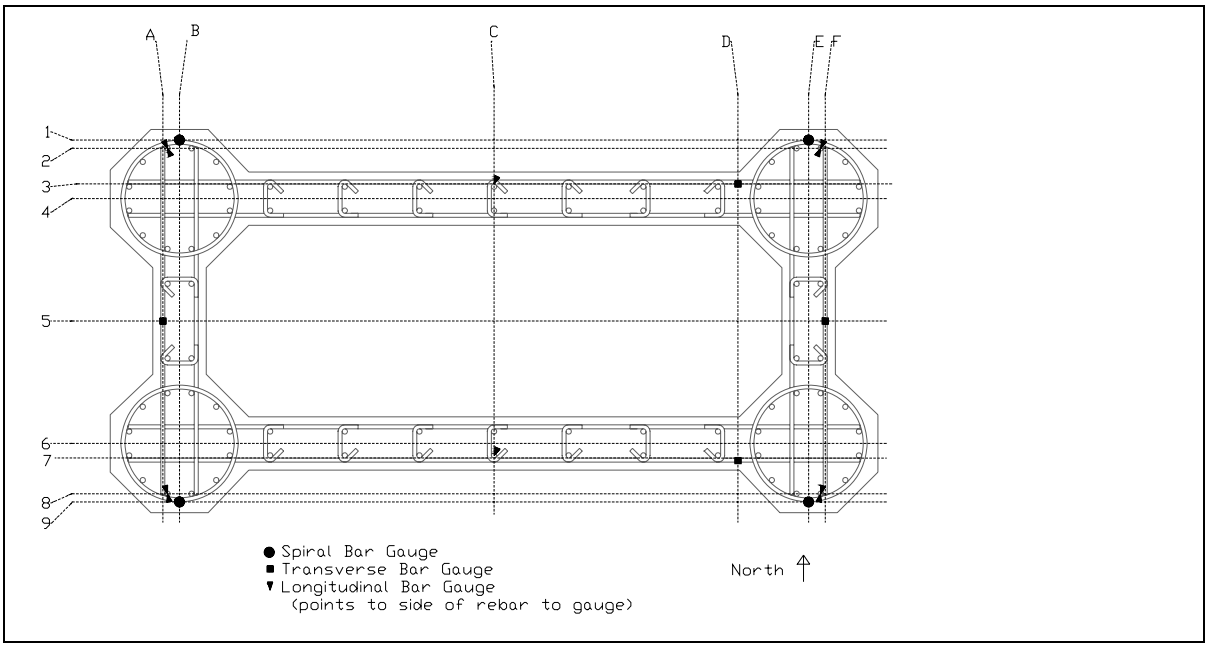

Figure 4.5 Column reinforcement strain gauge layout

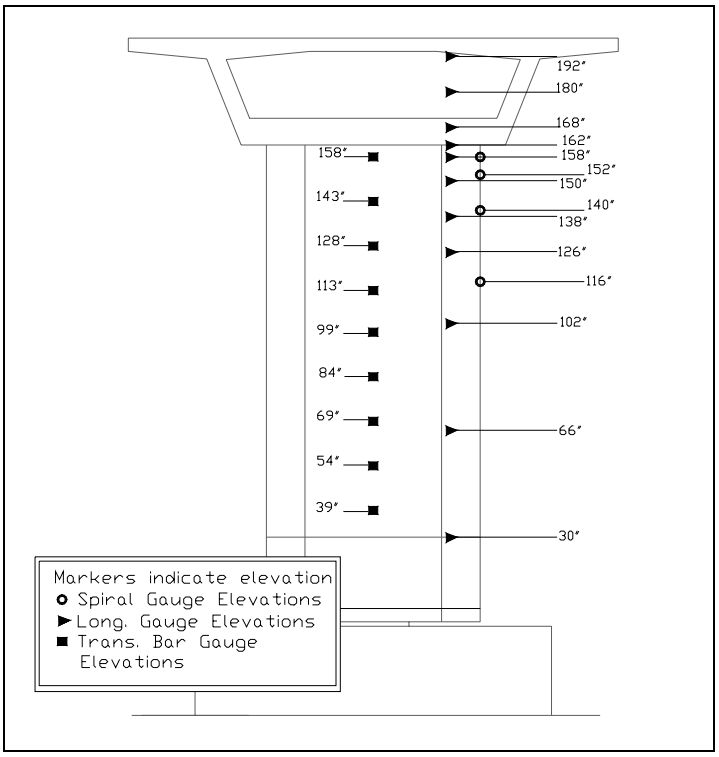

Figure 4.6 Column reinforcement strain gauge elevation view

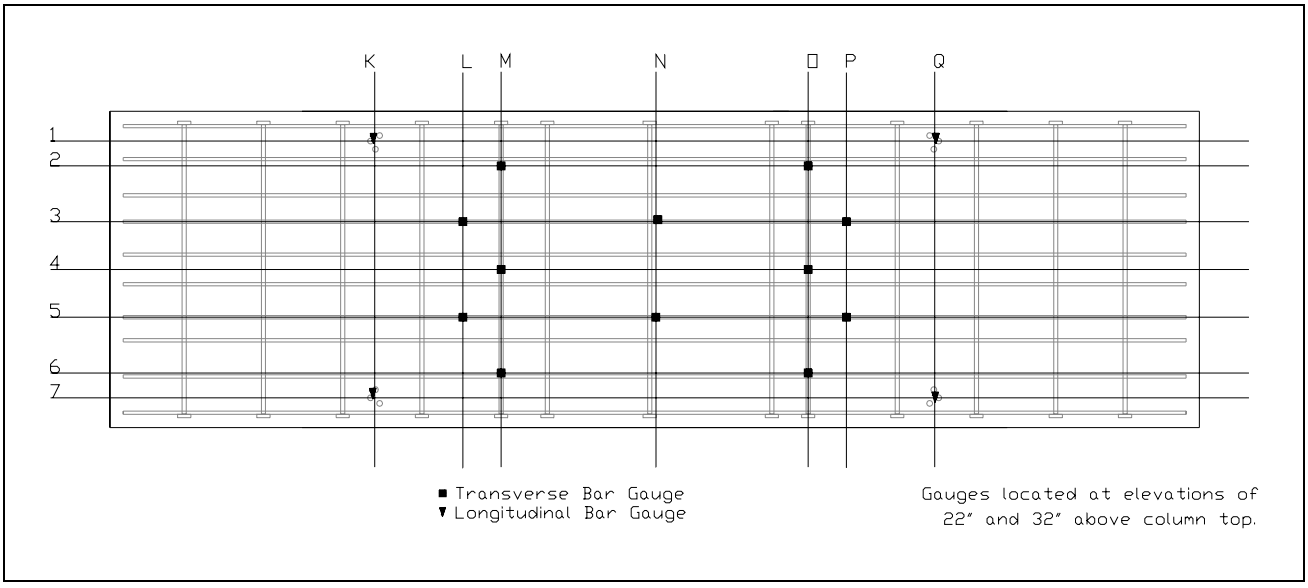

Figure 4.7 Pier segment reinforcement strain gauge layout

4.4.2 Tendon Strain Gauges

Numerous strain gauges were attached to the high strength steel strands in a similar manner to the mild reinforcement gauges. There was a very high failure rate of these gauges during insertion of the strands, stressing, and grouting of the tendons. After stressing and grouting of the tendons only a third of the gauges on the tendons survived. Due to these difficulties, which increased with the lengths of the tendons gauged, limited reliable test data was gleaned from these gauges. All the gauges that survived the rigors of stressing and grouting are shown in Figure 4.8.

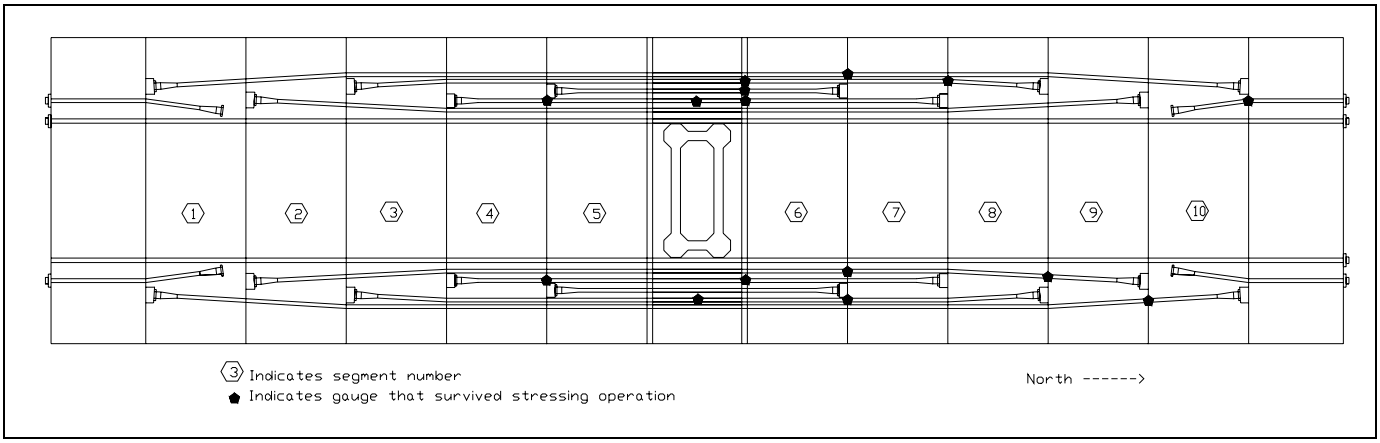

Figure 4.8 Tendon strain gauge layout

4.4.3 Concrete Strain Gauges

Surface gauges were used to monitor the strain along the top and bottom of the superstructure. Figure 4.9 shows the layout of these gauges on either face of the bridge deck. The gauges were placed close to the superstructure joint so that upon opening an easily detectable difference between the strain gauges and the linear potentiometers crossing the joints would exist.

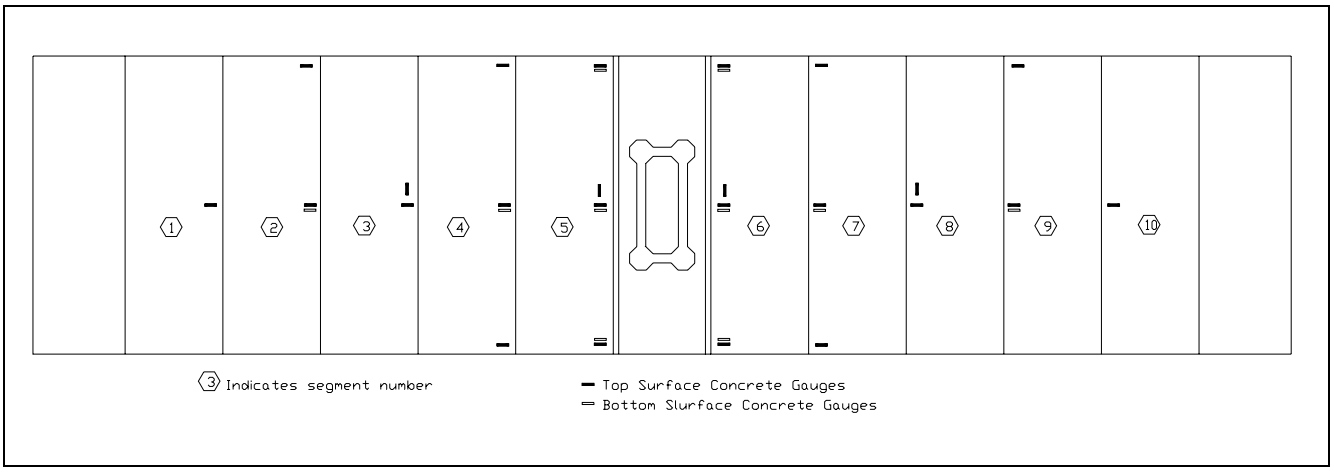

Figure 4.9 Concrete gauge layout

4.4.4 Curvature Instrumentation

Along the length of the column's west side displacement potentiometers were placed to calculate curvature of the column. This was done according to Eqn. 4.1

$$\phi = \frac{\Delta_n - \Delta_s}{D_\phi * L_g} \tag{4.1}$$

Where Φ is the average curvature at the elevation of the devices along the gauge length, Δ_n and Δ_s are the potentiometer readings on the north and south sides, D_Φ is the distance between the potentiometers, and L_g is the gauge length. Curvatures were calculated as positive in the push (north) direction and negative in the pull (south) direction. Figure 4.10 shows the layout of curvature instrumentation. To avoid disturbances from crushing and spalling of cover concrete the gauges were anchored inside the corner spiral element reinforcing.

At the boundary of the column and pier segment a single crack was expected, therefore the topmost instrument measure the rotation of the column relative to the pier segment. This rotation (θ) was calculated as

$$\theta = \frac{\Delta_n - \Delta_s}{D_\phi} \tag{4.2}$$

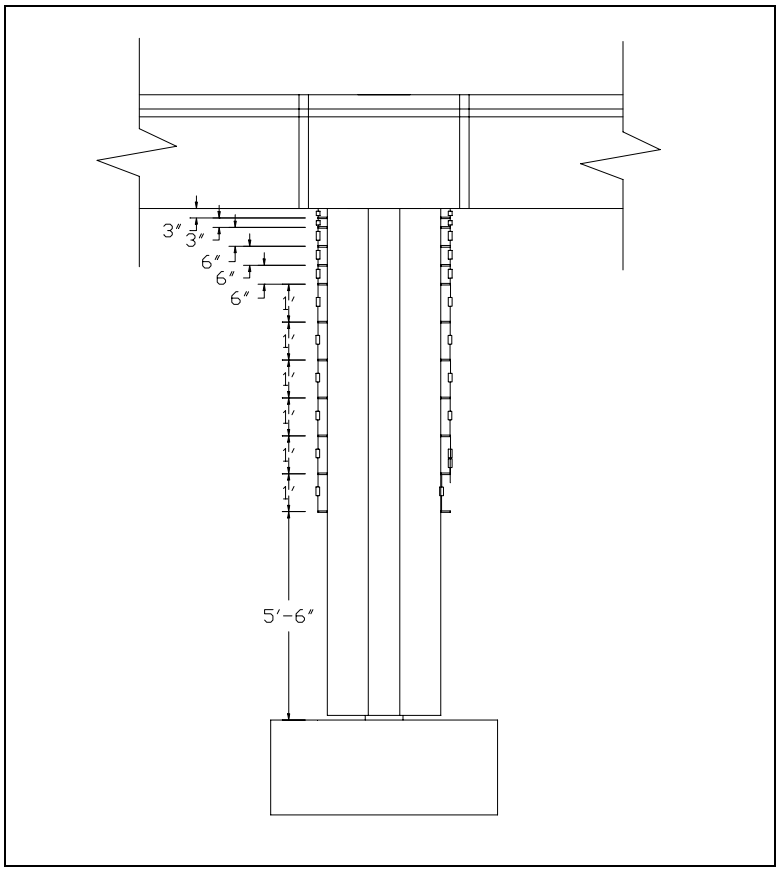

Figure 4.10 Column curvature instrumentation layout

4.4.5 Shear Instrumentation

The measurement of shear deformation in the column was achieved by two independent linear potentiometers arranged diagonally on the west face forming a shear panel.

Under flexure and expansion of the panel region the diagonal deformations remain equal as shown in Figure 4.11 and Figure 4.12. The following figure (Figure 4.13) shows that only in shear do the diagonal deformations differ.

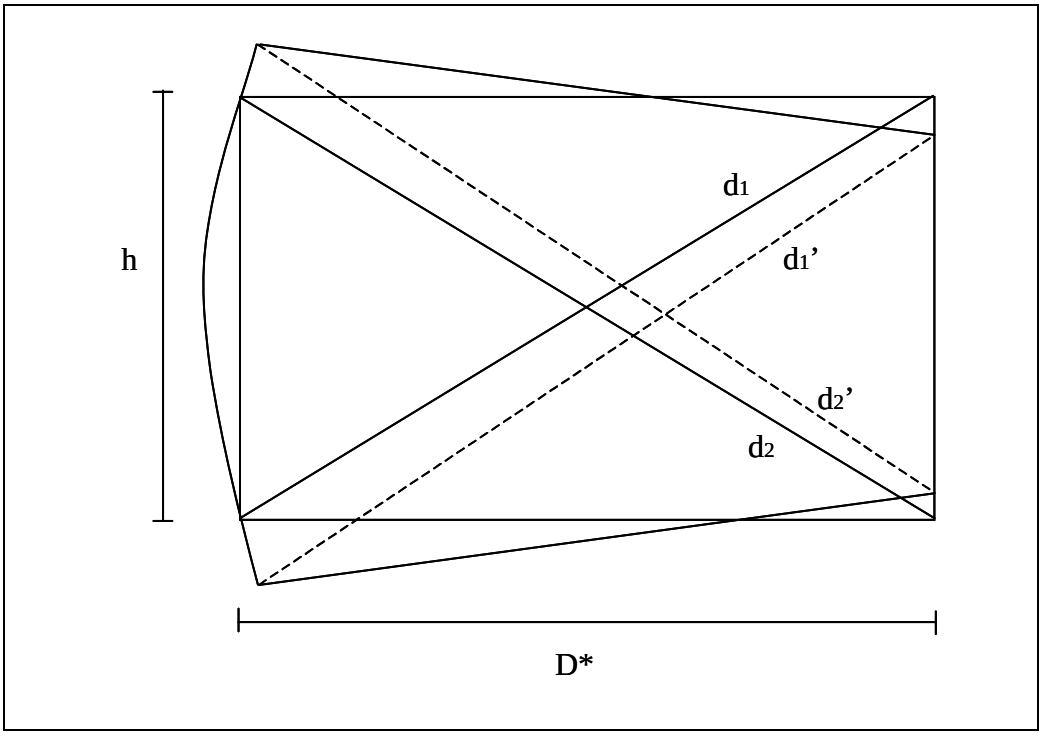

Figure 4.11 Equivalent diagonal deformations under flexure

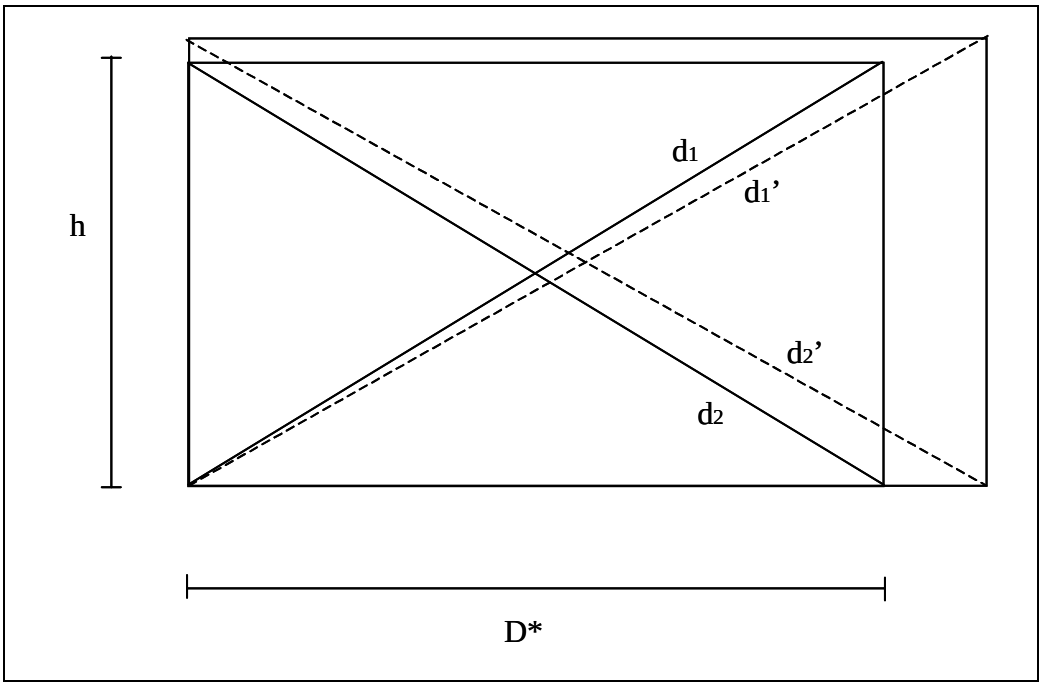

Figure 4.12 Equivalent diagonal deformations under horizontal and vertical expansion

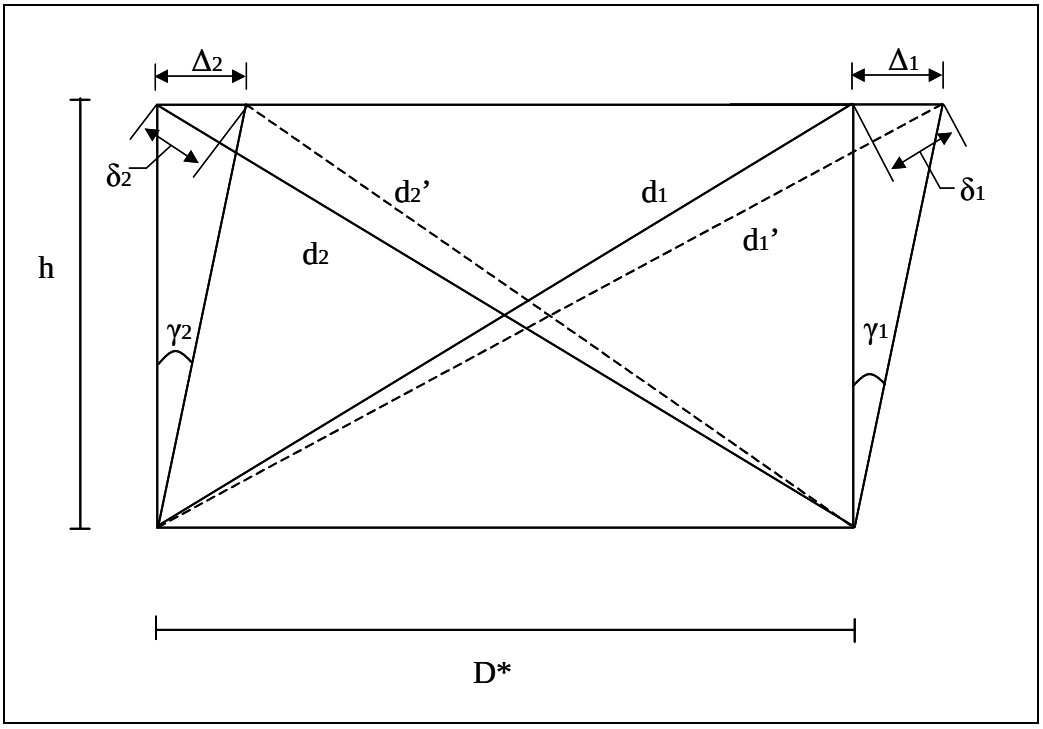

Figure 4.13 Diagonal deformations used to calculate shear deformation

Using these diagonal displacement measurements and assuming small angles, the average shear deformation was calculated according to equation 4.3.

$$\gamma = \frac{\gamma_1 + \gamma_2}{h} = \frac{\Delta_1 + \Delta_2}{2h} \tag{4.3}$$

The lateral deformations Δ_1 and Δ_2 due to shear deformation are calculated from the diagonal deformations using the ratio

$$\frac{\Delta}{\delta} = \frac{d}{D^*} \tag{4.4}$$

where

$$\delta = d' - d \tag{4.5}$$

Combining equations 4.3 and 4.4 yields the equation

$$\gamma = \frac{\delta_1 d_1 - \delta_2 d_2}{2hD^*} \tag{4.6}$$

This equation gives the average shear deformation over a given region with height h, and depth D*. Figure 4.14 shows the shear panel instrumentation on the west face of the column. The panels where attached to the column corners by imbedded 3/8 in. (9.5mm) anchors.

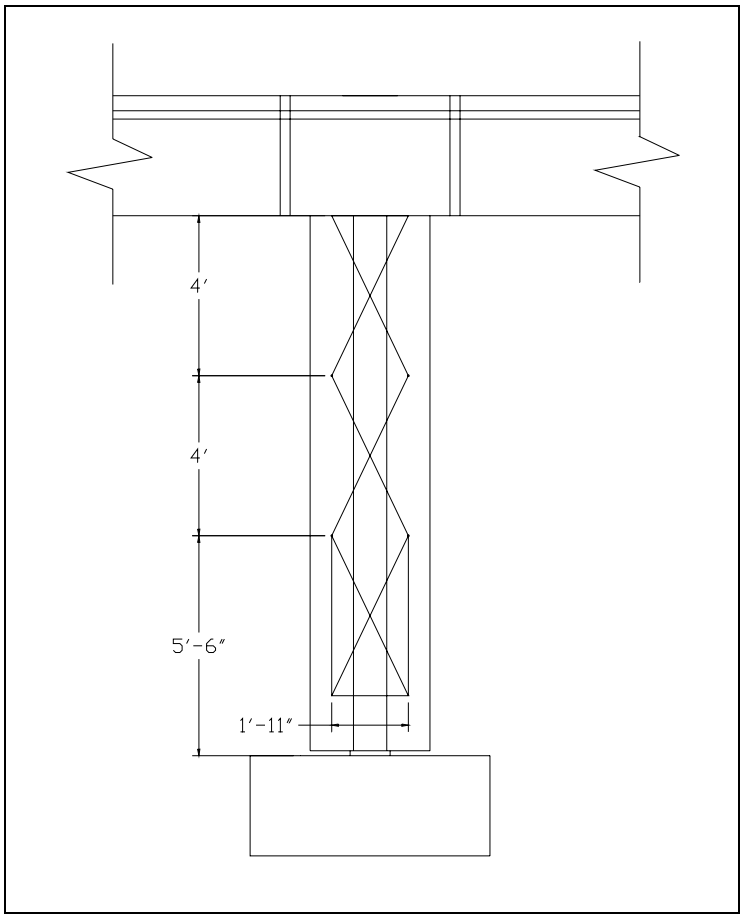

Figure 4.14 Shear instrumentation layout

4.4.6 Linear Potentiometers

Linear displacement devices were used in a variety of locations on the test specimen to monitor its performance. In order to have a record of the deformations along the length of the superstructure vertical displacements of the superstructure were monitored by string potentiometers at each end, the midspans, and center of the bridge. Across most of the superstructure joints displacements were measured on the top and some along the bottom as well. The locations of these potentiometers are shown in Figure 4.15. Linear devices were also used to monitor rotation at the column pin as well as any uplift in the footing.

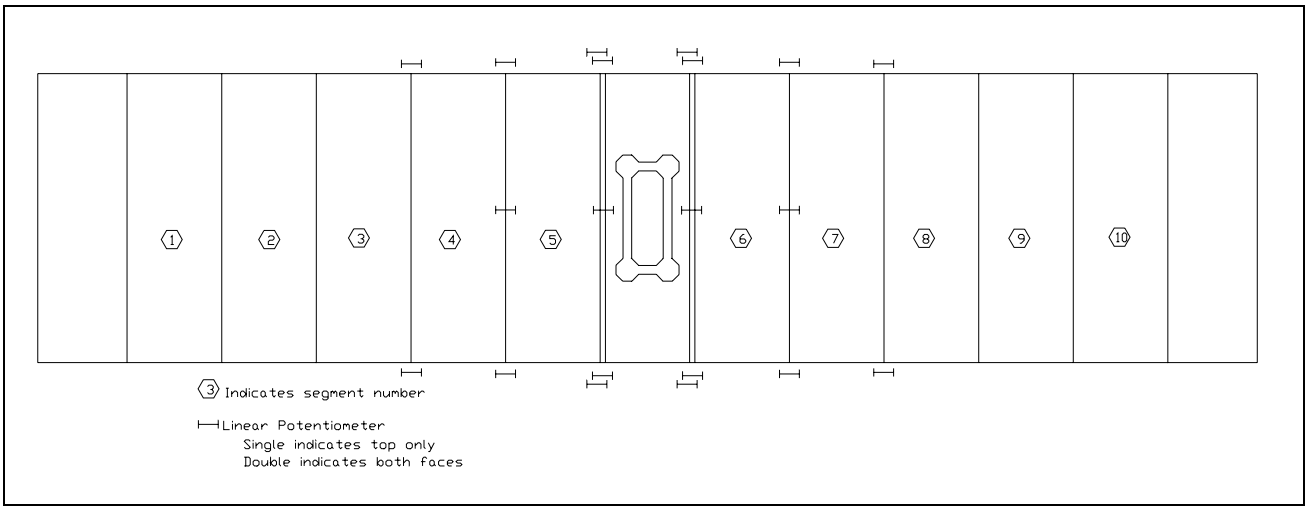

Figure 4.15 Joint displacement potentiometer layout

4.4.7 Inclinometers

Inclinometers were placed on the bridge specimen to measure rotations and corroborate information gained from linear displacement devices. The inclinometers were placed at each end block, at the base of the column, and on the pier segment as shown in Figure 4.16.

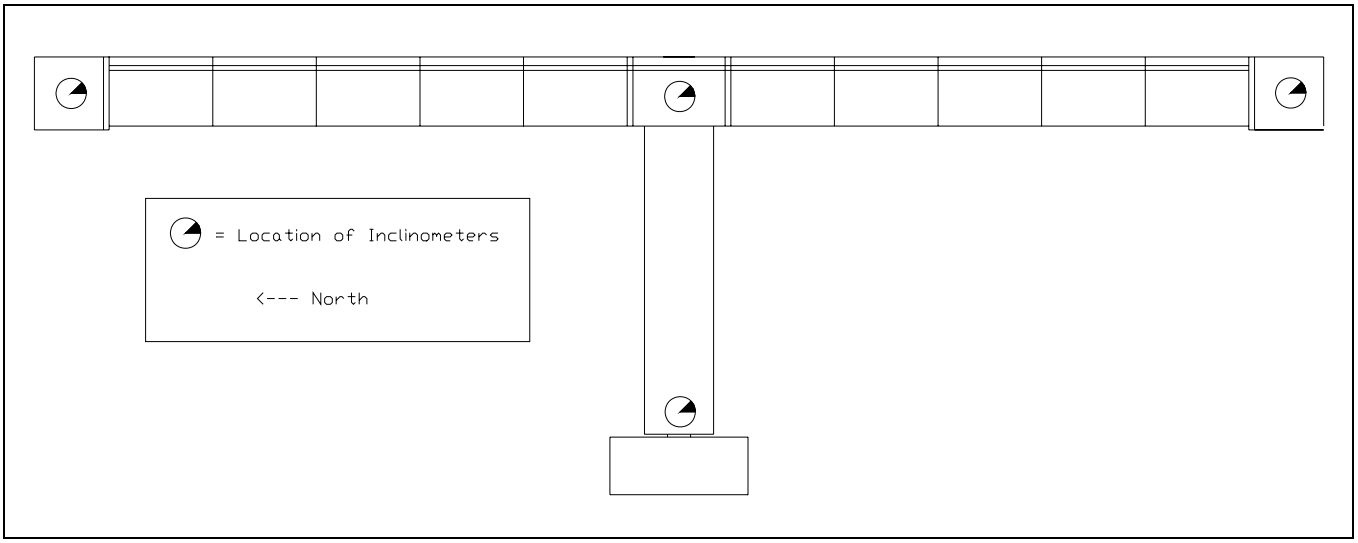

Figure 4.16 Inclinometer device layout

5 Analysis and Predictions

5.1 Overview

The analytical considerations of the testing program are presented in chapter 5. The moment-curvature analysis performed and used to predict column deflection is outlined. The post-tensioning loss estimates are presented. The predictions regarding the moments and forces required to open the joints during both stages of the test are also given.

5.2 Moment-Curvature Analysis

Using the program ANDRIANNA, moment curvature analysis were performed for the column and superstructure using non-linear material models for the concrete (both confined and unconfined), the mild reinforcement, and the prestressing steel in the superstructure.

As outlined in the program manual [14] the concrete material model used in the program for both confined and unconfined concrete uses a stress-strain curve based on Mander's Model [15]. The program allows for tensile cracking as well as compressive strain hardening and softening. The mild steel reinforcement is linear elastic up until reaching the yield stress, at which point a perfectly plastic yield plateau occurs in the stress-strain diagram. Strain hardening occurs after the yield plateau, curving parabolically until the ultimate stress is reached. The prestressing steel uses the model by Collins and Mitchell [16], based on the Minegotto-Pinto function [17]. Figure 5.1 to Figure 5.3 show the material models used. Figure 5.4 and Figure 5.5 show the results of the moment curvature

analysis for the column under dead load and the analysis for the superstructure segments nearest the column.

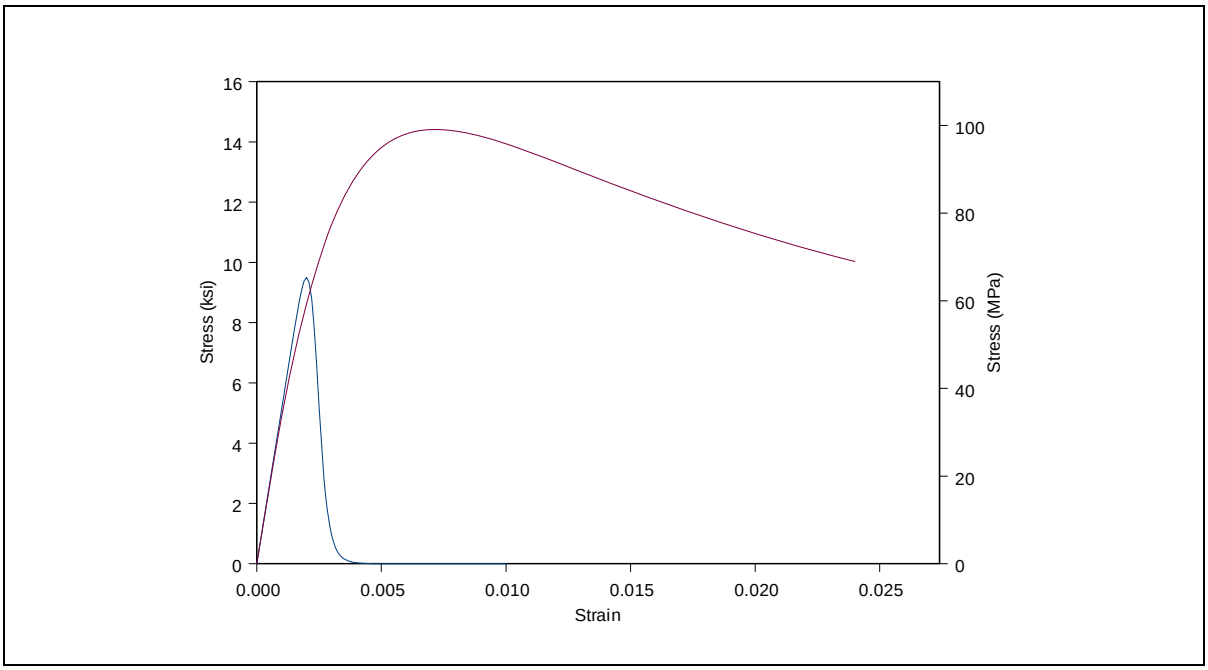

Figure 5.1 Concrete material model

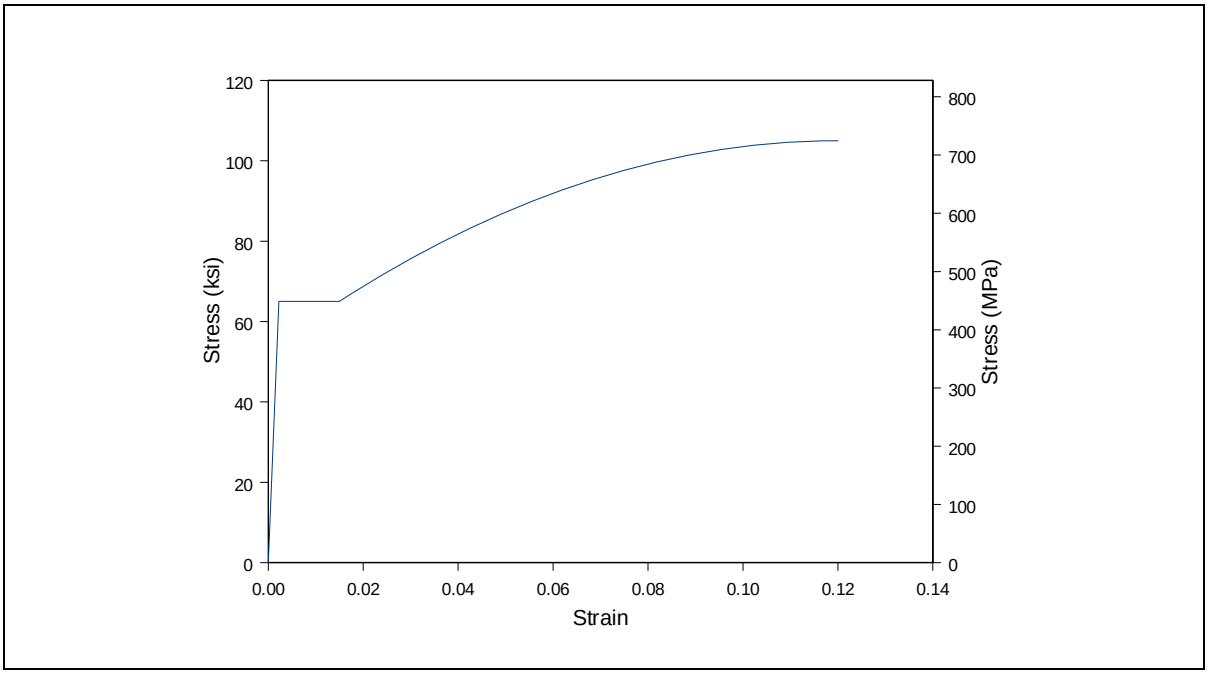

Figure 5.2 Mild steel material model

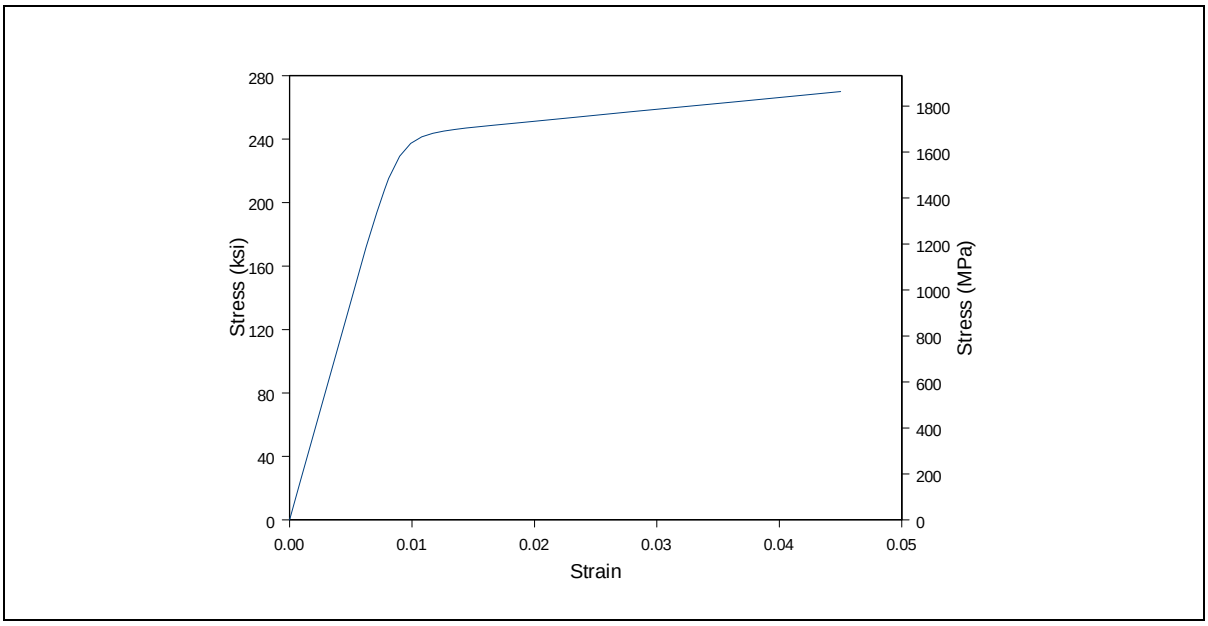

Figure 5.3 Prestressing steel material model

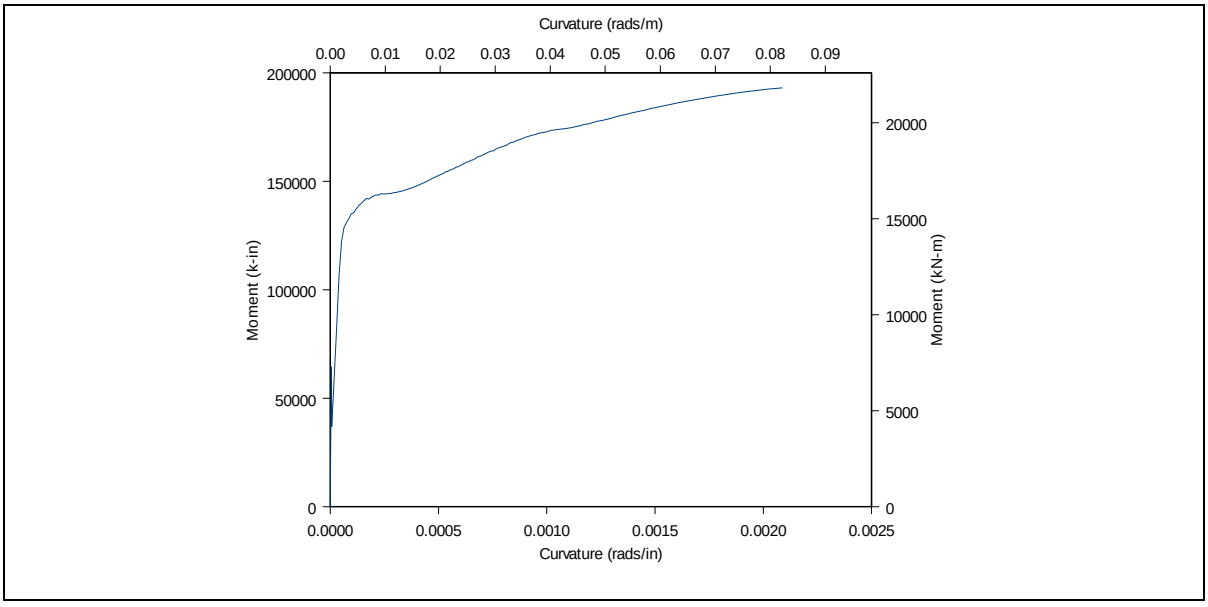

Figure 5.4 Column moment-curvature results

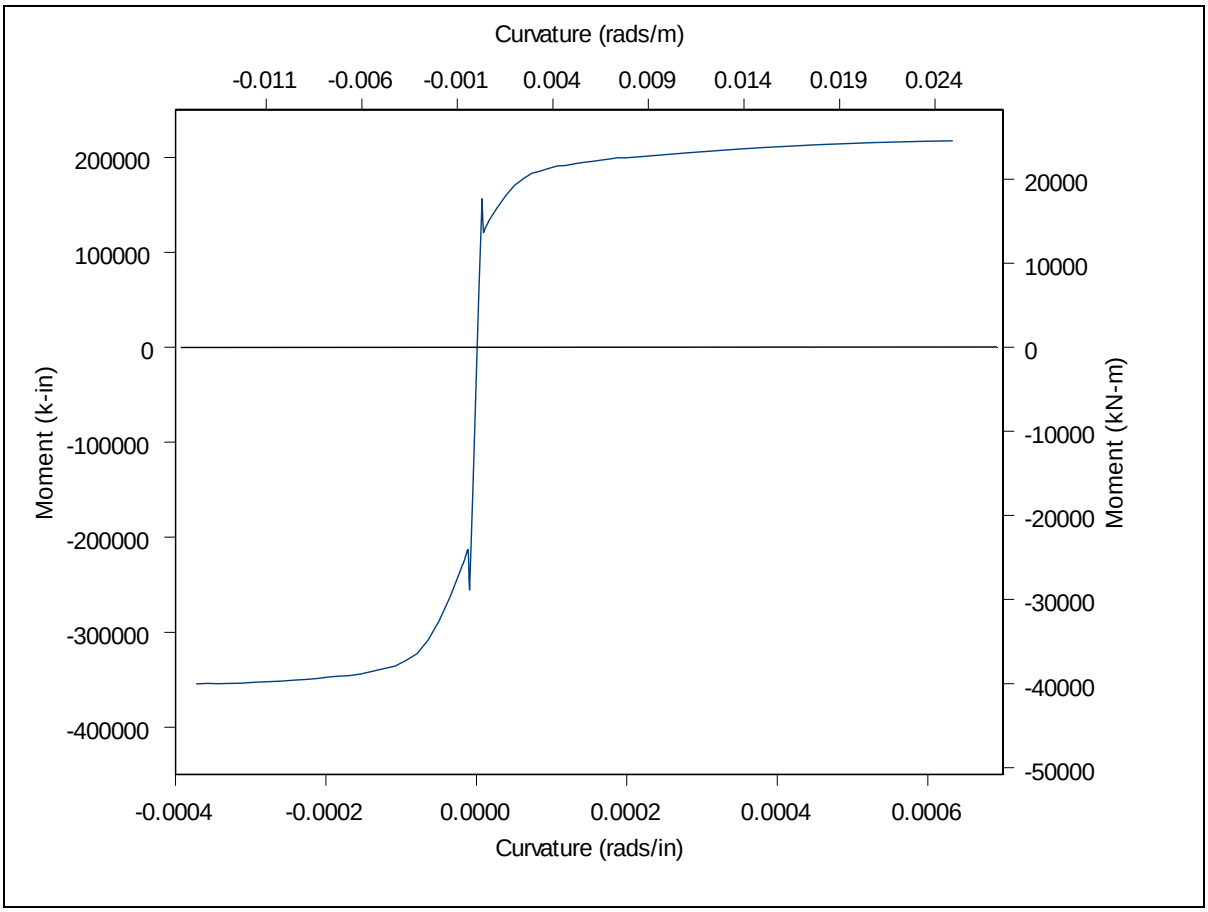

Figure 5.5 Superstructure moment-curvature results

5.3 Column Deflection

The total deflection of the column (Δ_t) was predicted as the sum of the elastic (Δ_e) and plastic (Δ_p) displacement components.

$$\Delta_t = \Delta_e + \Delta_p \tag{5.1}$$

With

$$\Delta_e = \frac{\Phi_y' L^2 * M}{3M_y'} \tag{5.2}$$

$$\Delta_p = (\Phi - \Phi_y' \frac{M}{M_y'}) L_p * L \qquad (5.3)$$

Where M is the moment at a given displacement, Φ is the curvature at that displacement, Φ_y' is the theoretical yield curvature, M_y' is the theoretical yield moment, L is the column shear span, and L_p is the column plastic hinge length.

The plastic hinge length (L_p) is calculated according to Eqn. 5.4 [10].

$$L_p = 0.08L + \alpha D^* + 9d_b \qquad (5.4)$$

Where D* is the confined concrete section depth, d_b is the diameter of reinforcing bar, and the constant α is assumed to be 0.30. The force-displacement predictions for the test unit are shown in Figure 5.6.

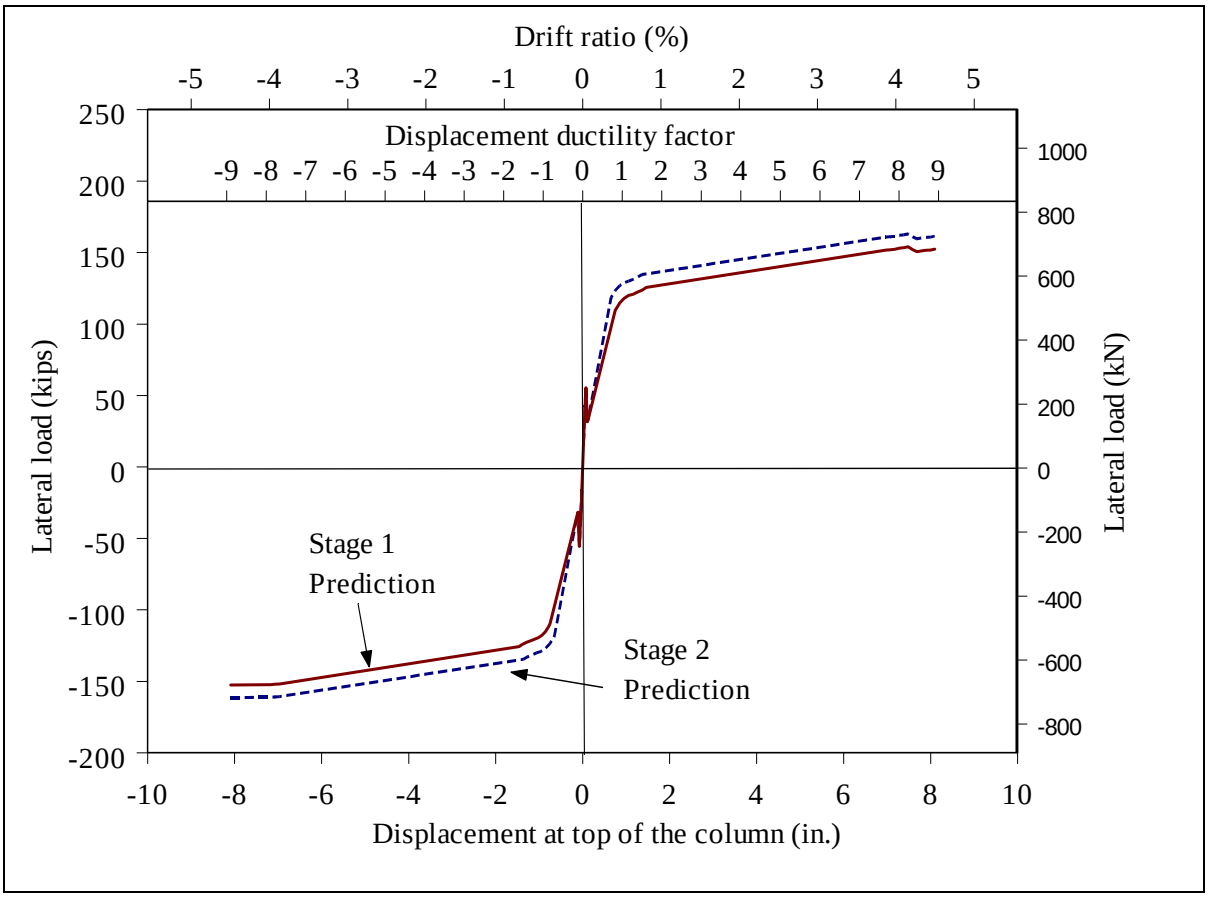

Figure 5.6 Force-displacement prediction for test unit

5.4 Prestress Losses

The anticipated losses in the prestress tendons was calculated according to AASHTO guidelines [1,2] as well as more detailed methods [18] as outlined below for elastic shortening, friction, anchorage seating, and approximated long term losses. It was assumed in the prototype structure that after all losses the tendons would be stressed at $0.60*f_{pu}$ or 162 ksi (1118 Mpa). The jacking stress of each tendon in the specimen took into account the losses as outlined below to achieve a stress level of approximately 60% of the ultimate stress. A summary of the tendon losses is given in Table 5-1.

5.4.1 Elastic Shortening Losses

The elastic shortening loss (Δ_{fpES}) was calculated according to Eqn. 5.5

$$\Delta_{fpES} = \frac{1}{n_j} \sum_{j=1}^{n} (n_j * f_{csj}) \quad (5.5)$$

Where n_j is the number of subsequently stressed tendons and the stress in the concrete, at the location each tendon due to the subsequent tendons is $f_{csj.}$

5.4.2 Friction Losses

The friction loss (Δ_{fpF}) was calculated according to Eqn. 5.6.

$$\Delta_{fpF} = f_{pj} * (\alpha*\mu + K*L) \quad (5.6)$$

Where f_{pj} is the jacking stress; α is angle change of the tendon; μ, the coefficient of friction, was assumed to be 0.25; and K is the wobble coefficient (0.0002 / ft).

5.4.3 Anchorage Seating Losses

The anchorage seating loss (Δ_{fpA}) was calculated according to Eqn. 5.7

$$\Delta_{fpA} = \frac{E * a}{L} \quad (5.7)$$

Where a, the expected seating length, was assumed to be 0.25 in.

5.4.4 Long Term Losses

The long term losses estimated for the test specimen come from contributions of creep (Δ_{fpCR}), shrinkage (Δ_{fpSH}), and relaxation (Δ_{fpR}).

$$\Delta_{fpLT} = \Delta_{fpCR} + \Delta_{fpSH} + \Delta_{fpR} \quad (5.8)$$

The creep loss (Δ_{fpCR}) was calculated according to Eqn. 5.9

$$\Delta_{fpCR} = \frac{E_s}{E_c} K_{cr} (f_{cs} - f_{csd}) \quad (5.9)$$

Where K_{cr} is the 1.6, f_{cs} is the stress in the concrete at the level of prestressing immediately after transfer, and f_{csd} is the stress at the same location due to all superimposed dead loads applied after the post-tensioning is applied.

The shrinkage loss (Δ_{fpSH}) was calculated according to Eqn. 5.10

$$\Delta_{fpSH} = 0.8(17{,}000 - 150*RH) \quad (5.10)$$

Where RH is the relative humidity in percent (assumed to be 70%)

The relaxation loss (Δ_{fpR}) was calculated according to Eqn. 5.11

$$\Delta_{fpR} = 5 - 0.07\,\Delta_{fpF} - 0.1\,\Delta_{fpES} - 0.05(\Delta_{fpSH} + \Delta_{fpCR}) \qquad (5.11)$$

Table 5-1 Specimen theoretical prestress losses in ksi (MPa)

Tendon	Friction (Δ_{fpF})	Anchorage (Δ_{fpA})	Elastic Shortening (Δ_{fpES})	Long-Term Losses (Δ_{fpLT})	Total (Δ_{fpTot})
A	28	12	0	15	55
B	19	19	0	15	58
C	6	45	2	14	67
D	10	26	1	14	51
E	24	14	0	15	53
F	16	84	0	10	110
G	26	22	0	9	58
H	25	10	3	11	49
J	26	10	3	17	56

5.5 Joint Opening

An initial prediction was made as the whether the joints were likely to open during the test. The anticipated moment at the joint locations from both the dead load and seismic loads transferred from plastic hinging of the column was compared to the theoretical cracking moment at the joint. Figure 5.7 and Figure 5.8 show how this theoretical moment demand at the joint locations compared to the decompression moment as well as a cracking moment when a tensile strength of $6\sqrt{f'_c}$ is assumed. . Figure 5.7 shows that the moment range expected in the test (the blue line) stays within the bounds of the decompression

moments meaning that no tensile strains were expected during the first stage of testing. As shown in Figure 5.8 where the moment demand curve meets the cracking capacity curve, the joints nearest to the pier were expected to undergo some opening during the second stage of testing,

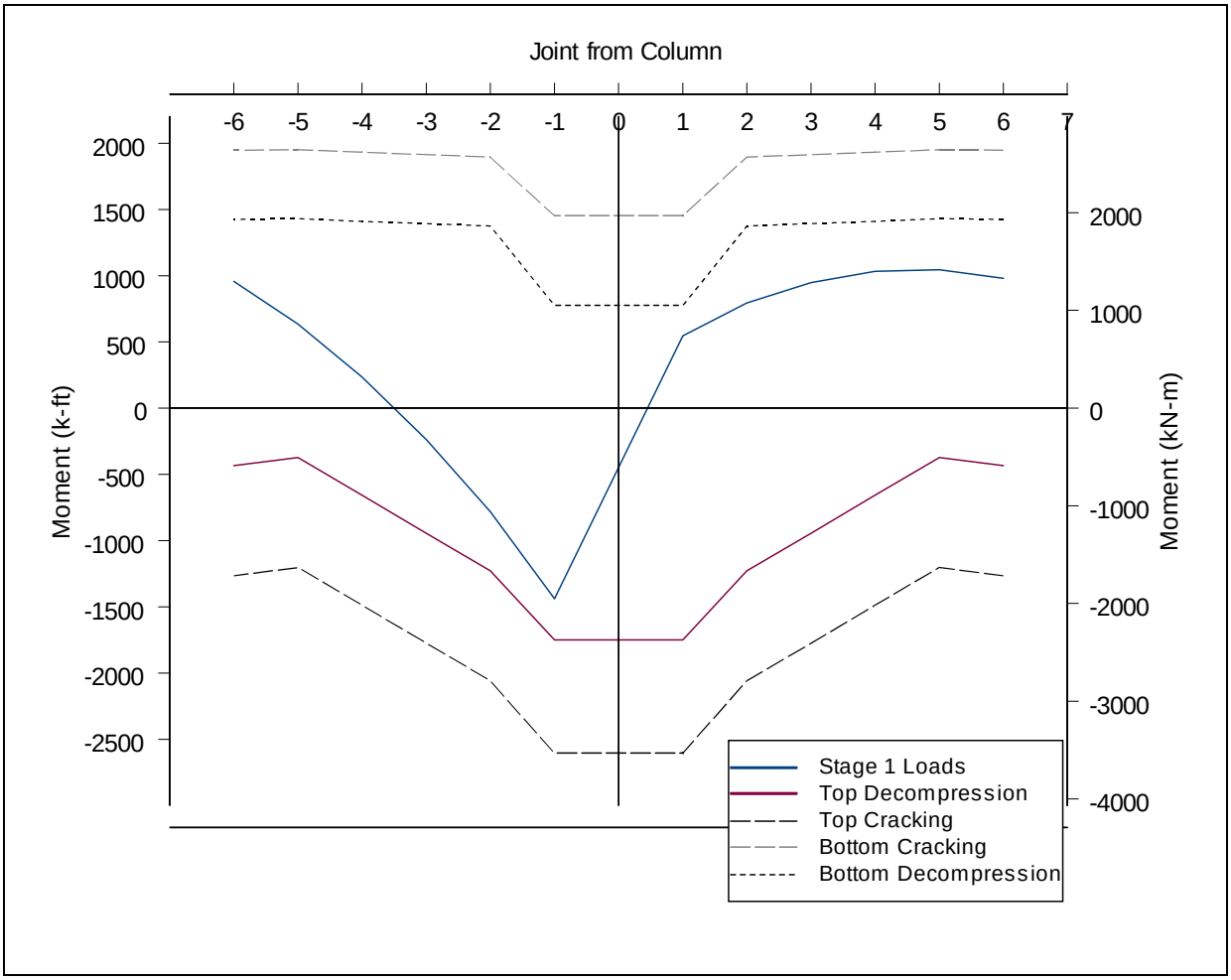

Figure 5.7 Joint opening prediction for stage 1

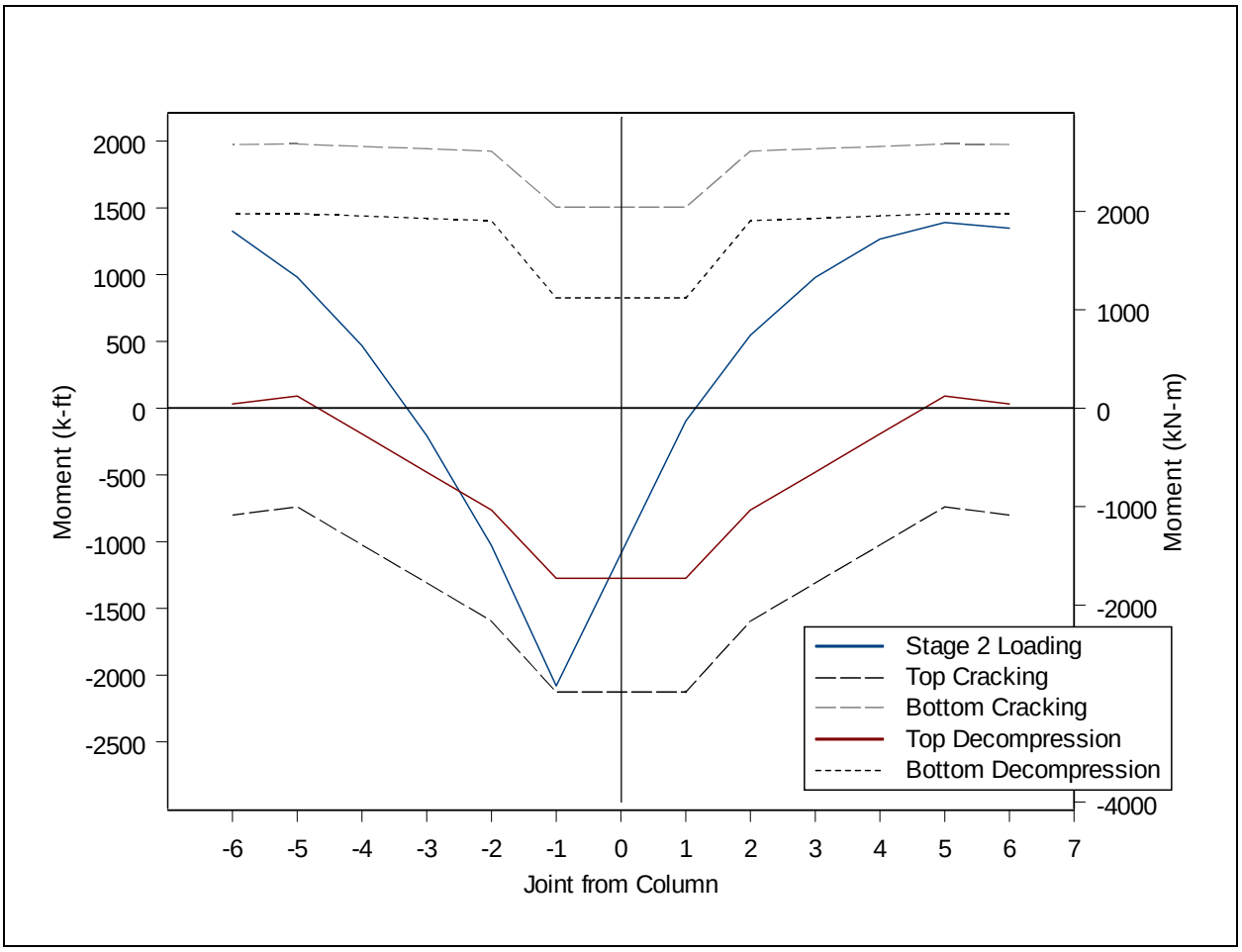

Figure 5.8 Joint opening prediction for stage 2

6 Test Observations

6.1 Overview

Test observations are presented for each stage of the test. The formation and size of cracks as witnessed during the test are explained. Additional photographs of the marked and unmarked crack patterns are found in the photo appendix section. Cracks were marked at the peaks of the first cycle at each ductility level. The cracks were marked with a blue pen in the positive (northward) push, and a red pen in the negative (southward) direction. Photographs and discussions of the joint opening and closing are also explained.

6.2 Test Stage 1

Testing of the bridge structure began on June 10th. After the vertical loads and boundary condition moments were applied to the structure, cyclic loading began. The first loading peak reached was at a displacement equivalent to half the theoretical yield displacement ($0.5\Delta_y$). At this level some hairline flexure cracks appeared in the column (Figure 6.1). After yield displacement (Δ_y) was reached the cracks were imperceptible when the seismic loads were removed from the bridge. At ductility level 2 (μ=2) the flexure cracks on the tension side spread down the column. Shear cracks also formed on the east and west faces of the column (Figure 6.2). The largest crack width measured at μ=2 was a 0.4 mm tension crack near the top of the column. During the early cycles of testing the bridge exhibited a propensity to twist likely due to some construction irregularities likely in the column. The actuators were programmed to inhibit this twist and the applied torque from the actuators was closely monitored. After the completion of stage1 testing the actuator control program was changed to better control the twisting while limiting the torque forces put into the

system. At μ=4 there was significant flexural cracking throughout the column shown with and without marked cracks (Figure 6.3 and Figure 6.4). There was not yet any spalling of the concrete at μ=4. The initiation of short vertical cracks running between the large tensile flexural cracks near the top on the corners signified the initiation of spalling, but none had yet occurred. This was significantly different from the testing of a similar column in a severe bi-directional loading path [7] in which spalling began before μ=4 was reached.

Up to the end of testing stage 1 no significant cracking was evident in the superstructure joints. At the highest ductility level of stage 1 a slight hairline crack was seen in the first joint opening. This was likely the reopening of a creep or shrinkage crack in the closure pour region. When the seismic loads were removed the hairline crack was no longer visible.

Figure 6.1 Marked crack pattern on north and west faces at initial displacement level of $0.5\Delta_y$

Figure 6.2 Marked crack pattern on north and west faces of column at μ=2

Figure 6.3 Marked crack pattern on north and west faces of column at μ=4

Figure 6.4 Unmarked crack pattern on south and east faces of column at μ=4

6.3 Test Stage 2

The second stage of testing began on August 17th. The first cycle was a repeat of the μ=4 cycle at the end of stage 1. During stage 2 openings in the superstructure joints nearest the column were evident under the same ductility level achieved previously (μ=4). The total crack width at the joint was measured to be approximately 0.4 to 0.5 mm. This was the combined crack widths of each side of the 3 inch closure gap. A close up of this crack at the joint is shown in Figure 6.5. The maximum crack width in the column was measured as between 2.5 and 3 mm. At μ=5 extensive spalling of the concrete in the corner regions began (Figure 6.6), and the superstructure joint crack was measured at approximately 0.6 mm. At μ=6 the joint crack was measured at around 0.8 mm and in subsequent cycles and increased ductility levels was not seen to exceed this level by much. No opening of any joints other than those nearest the column was observed. Through the entire loading pattern upon removing the seismic loads the superstructure cracks would close. At ductility levels of μ=6 and μ=8, the column had severe flexural cracking present (Figure 6.7 and Figure 6.8). In the final cycles of the test heavy spalling occurred at all corners of the column. No spalling occurred in the wall section. The test was concluded after two cycles at μ=8 because of concerns of stability of the bridge specimen if it was more heavily damaged. Deterioration of the column would have continued with more cycles and higher ductility levels, leading to failure of the column.

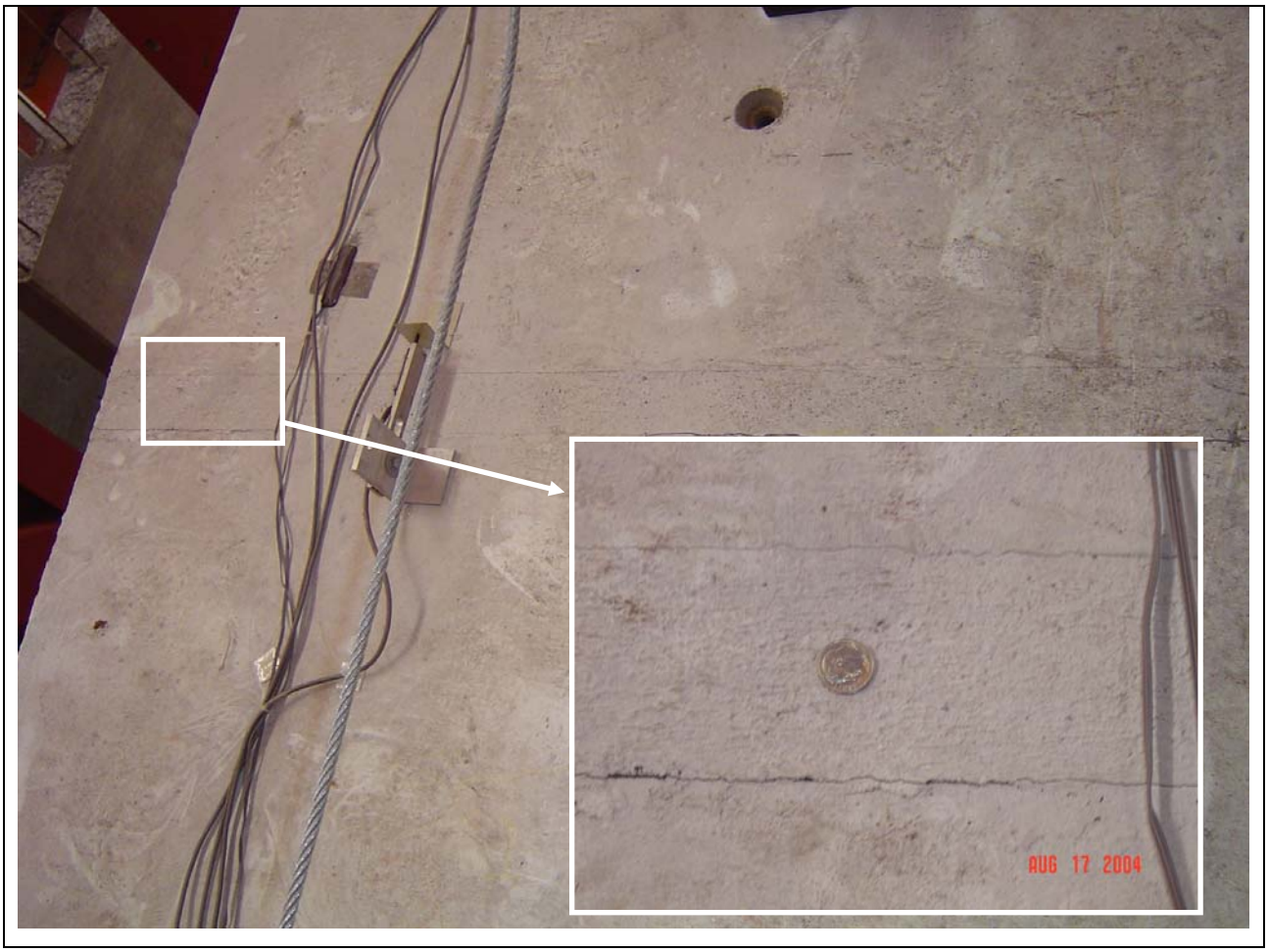

Figure 6.5 Top of joint crack close up during stage 2 at μ=4

Figure 6.6 Spalling of column south face corner regions at μ=5

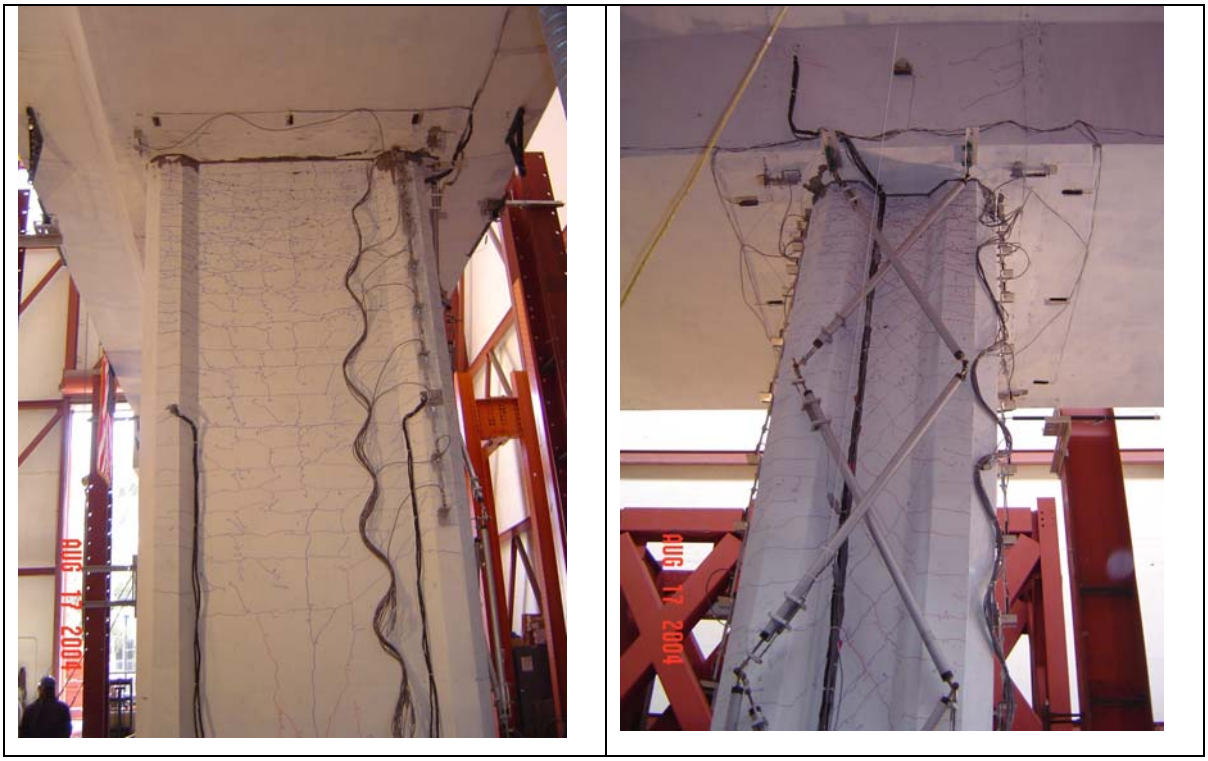

Figure 6.7 Marked crack pattern on north and west faces of column at μ=6

Figure 6.8 Marked crack pattern on north and west faces of column at μ=8

7 Discussion of Test Results

7.1 Overview

Chapter 7 examines the measured results of each stage of the test. The hysteretic behavior of the bridge system is presented and compared between the two stages of the test. System displacements are examined and relevant strain gauge data is presented. Also the measured joint behavior is presented in detail.

7.2 Test Stage 1

7.2.1 Force-Displacement Behavior

The force-displacement data for stage 1 of the test unit, along with the initial prediction is shown in Figure 7.1. The overall performance was typical of a well-confined, reinforced concrete column showing high-energy dissipation capacity, high displacement ductility. The response at each ductility level was similar during the first and second cycles. The earlier monotonic prediction for the stage 1 is also shown on the graph. The prediction underestimated the strength of the column by about 7%, likely due to variations in material properties and construction irregularities. Some of the irregular loops and glitches near the zero load mark were due to controlling the test specimen and bringing it back to a stable position at the end of each day's testing. The shear displacements were insignificant compared to the flexural displacements according to the measurements taken.

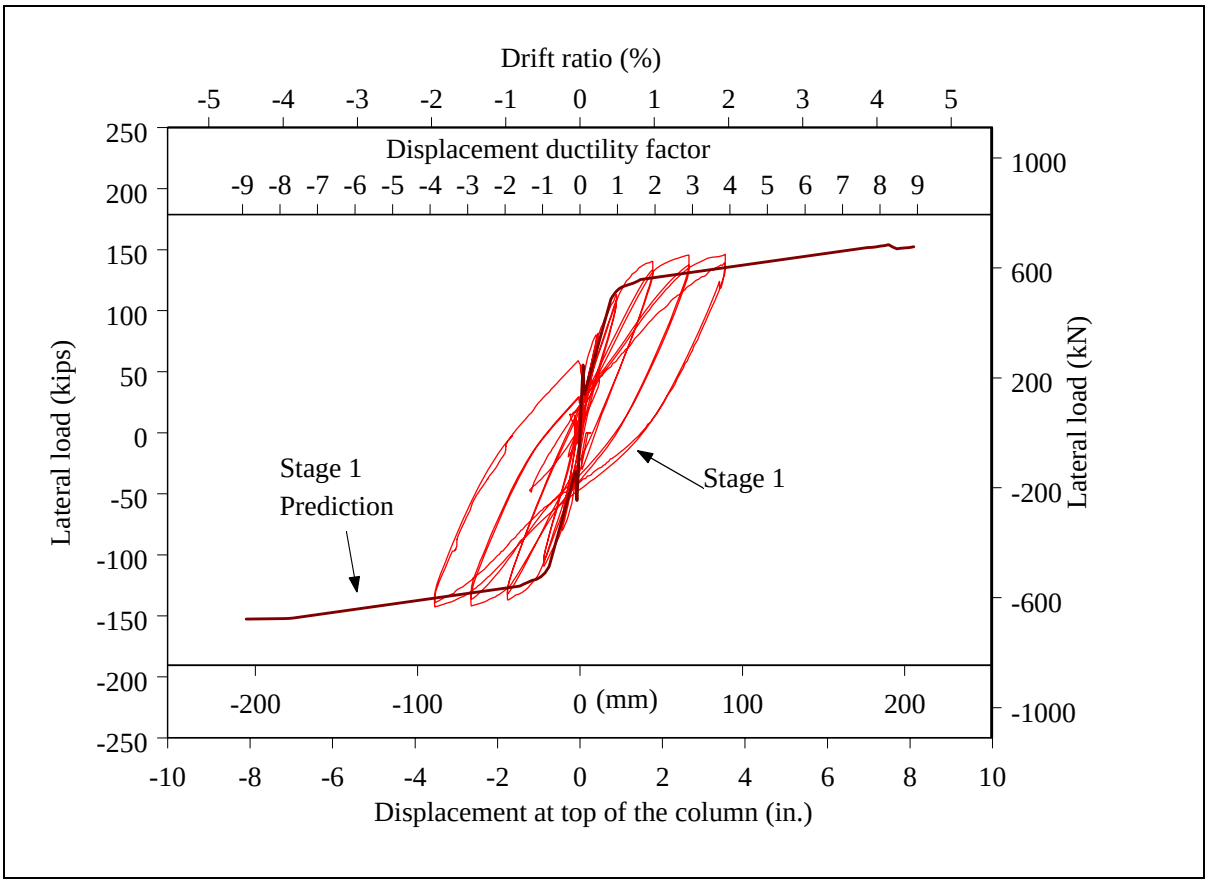

Figure 7.1 Stage 1 force-displacement diagram

7.2.2 Curvature

The curvature profile of the column for stage 1 of the test is shown in Figure 7.2. With the height measured from the base of the column, the formation of the plastic hinge zone at the top of the column is evident. The theoretical yield curvature (Φ_y) is shown on the positive and negative sides of the graph. In the higher ductility levels the curvature significantly exceed Φ_y at a height of approximately 118 inches giving a plastic hinge length of around 30 in (760mm).

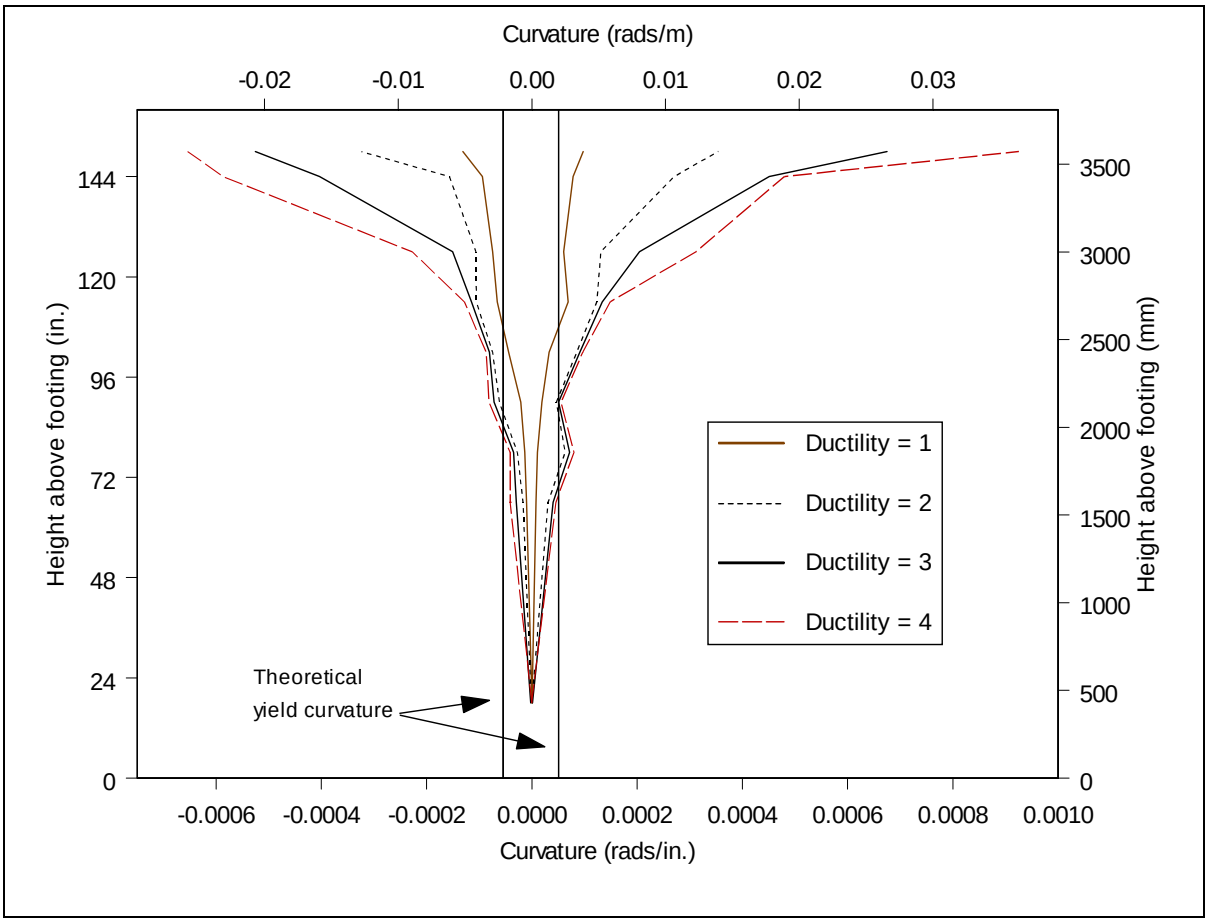

Figure 7.2 Stage 1 curvature profile

7.2.3 Longitudinal Bar Behavior

Several of the longitudinal bars in the column were instrumented to capture the strain profile of the bars. Figure 7.3 shows the locations of the gauged longitudinal bars. The tensile strains along the lengths of these bars at varying ductility levels are shown in Figure 7.4. The gaps in the graph arise from damaged gauges. At increasing displacement levels more gauges were damaged resulting in more gaps. Using a theoretical yield strain of 0.005 (5000 microstrain) the spread of the plastic hinge down the column is evident. At μ=4 the apparent plastic hinge length is around 30 in. (760mm). This corroborates with the

data from the curvature instrumentation. The strain penetration of the longitudinal bars into the pier segment appears to be around 12 in. (305mm) at μ=4.

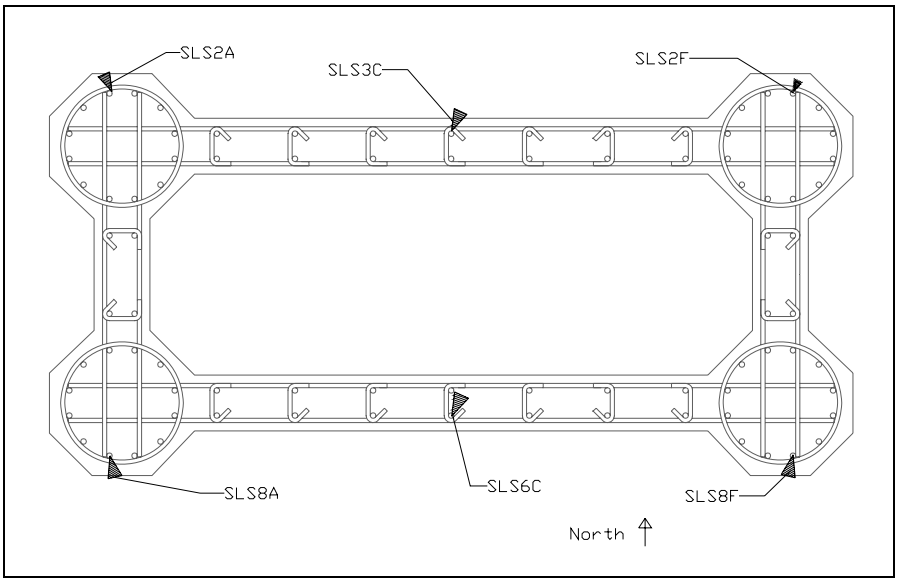

Figure 7.3 Location of gauged longitudinal bars

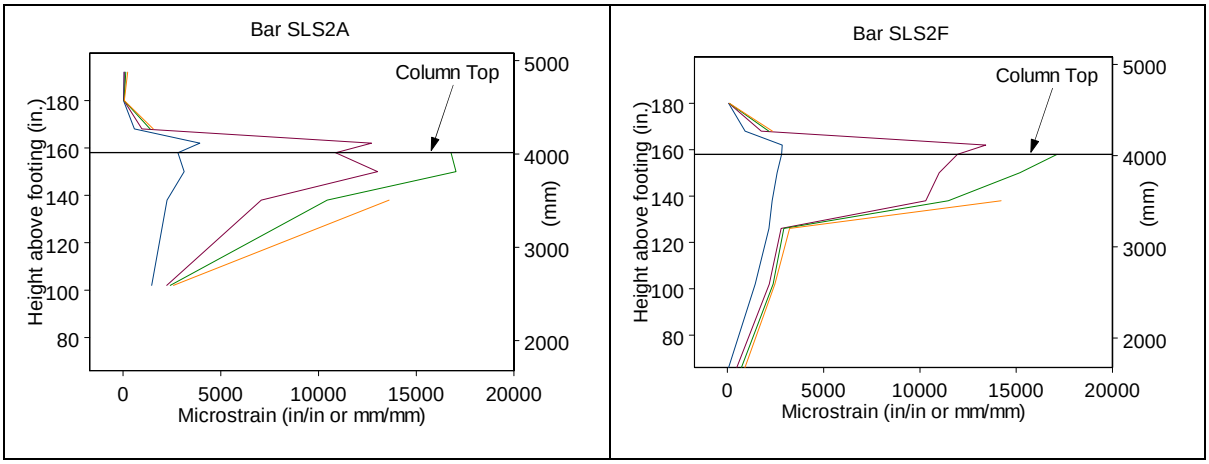

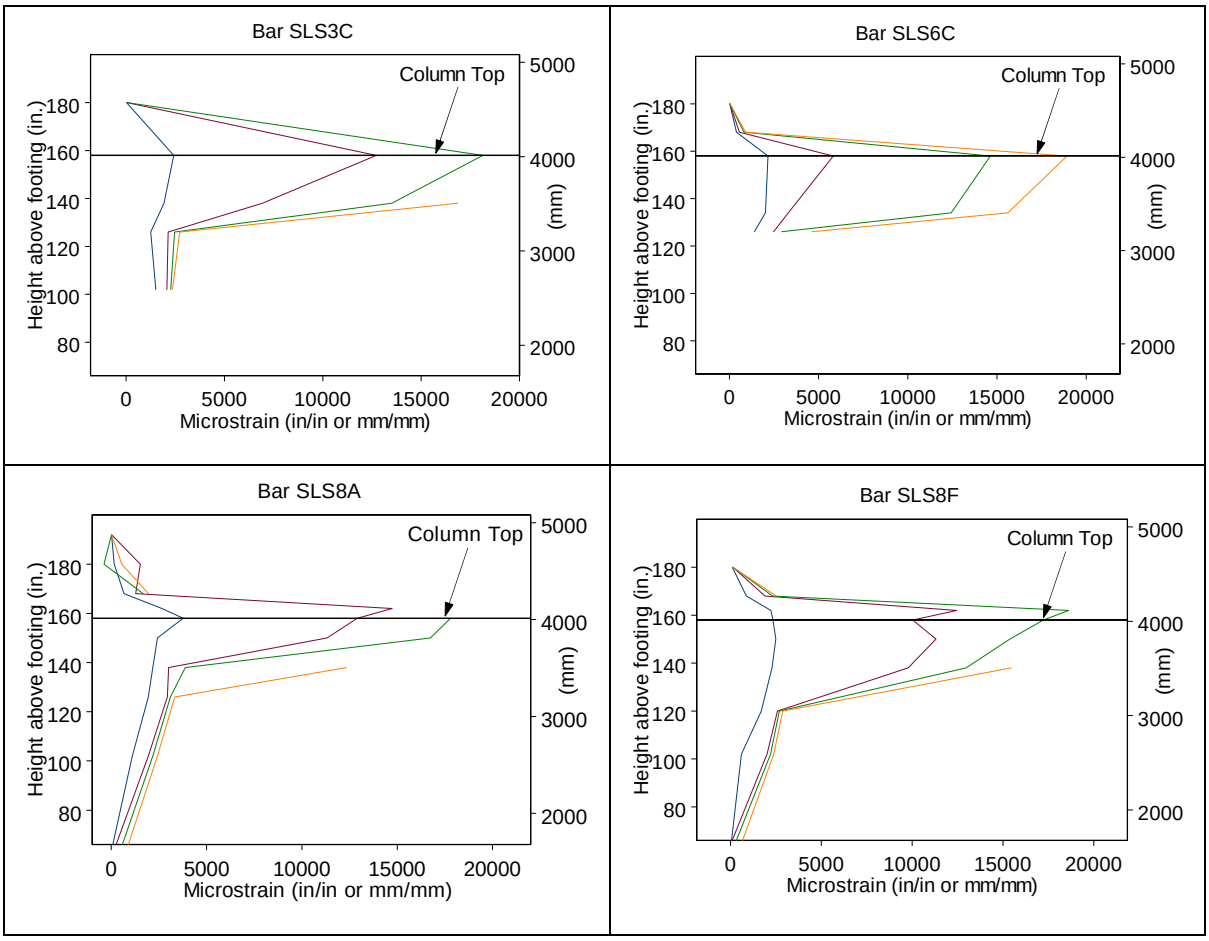

Figure 7.4 Longitudinal bar strain profiles for stage 1 at increasing ductility levels

7.2.4 Transverse Bar Behavior

The transverse bars in the short wall of the column were gauged to measure shear along the length of the column. The locations of the gauged bars are shown in Figure 7.5. At the top and bottom of the column the strain path is irregular due to cracking and the transfer of the forces into the pin respectively. However along most of the column length the strains in the transverse reinforcement were fairly constant. This can be seen in Figure 7.6. The strain in the bars did not exceed the theoretical yield strain (ε_y). Some inherent irregularities due to construction and possibly material differences led to a propensity

towards some twisting of the column during testing. Because the base of the column was a pin the loading actuators solely inhibited the twisting in order to keep the bridge structure loading in one direction. Because of this a small toque force was seen in the column and some differences were seen in the column strain reading for the push and pull directions. This data is presented in the appendix.

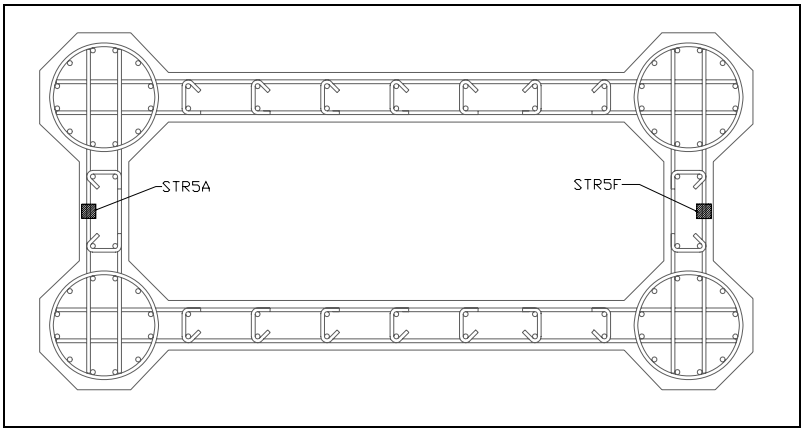

Figure 7.5 Location of gauged transverse bar

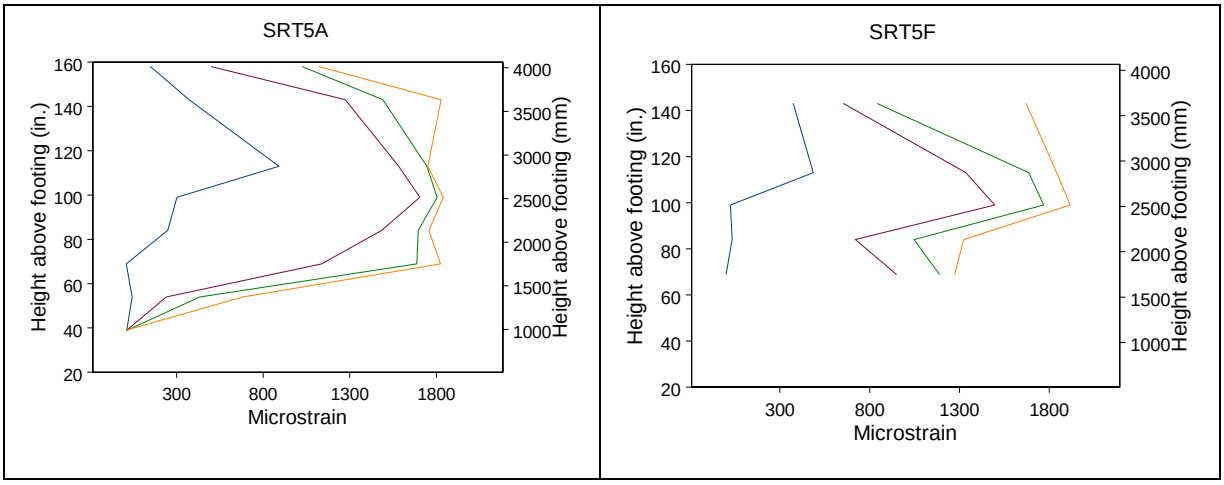

Figure 7.6 Strain profiles of the transverse reinforcement at increasing ductility levels

7.2.5 Joint Behavior

As noted in section 6.2, no large cracks or opening appeared during stage 1 of the testing. However, in examining the data some very small cracks did begin to form at the joints nearest to the column. The hysteretic behavior of one of these joints is shown in Figure 7.7. The initial state of the joint shown in the figure is after the boundary conditions have been applied, thus the data does not begin at the graph's origin. The change in stiffness as the joint cracked is apparent in the bilinear stiffness of the data. Also a hairline residual crack on the order of 0.001 in. (0.025mm) formed at the joint.

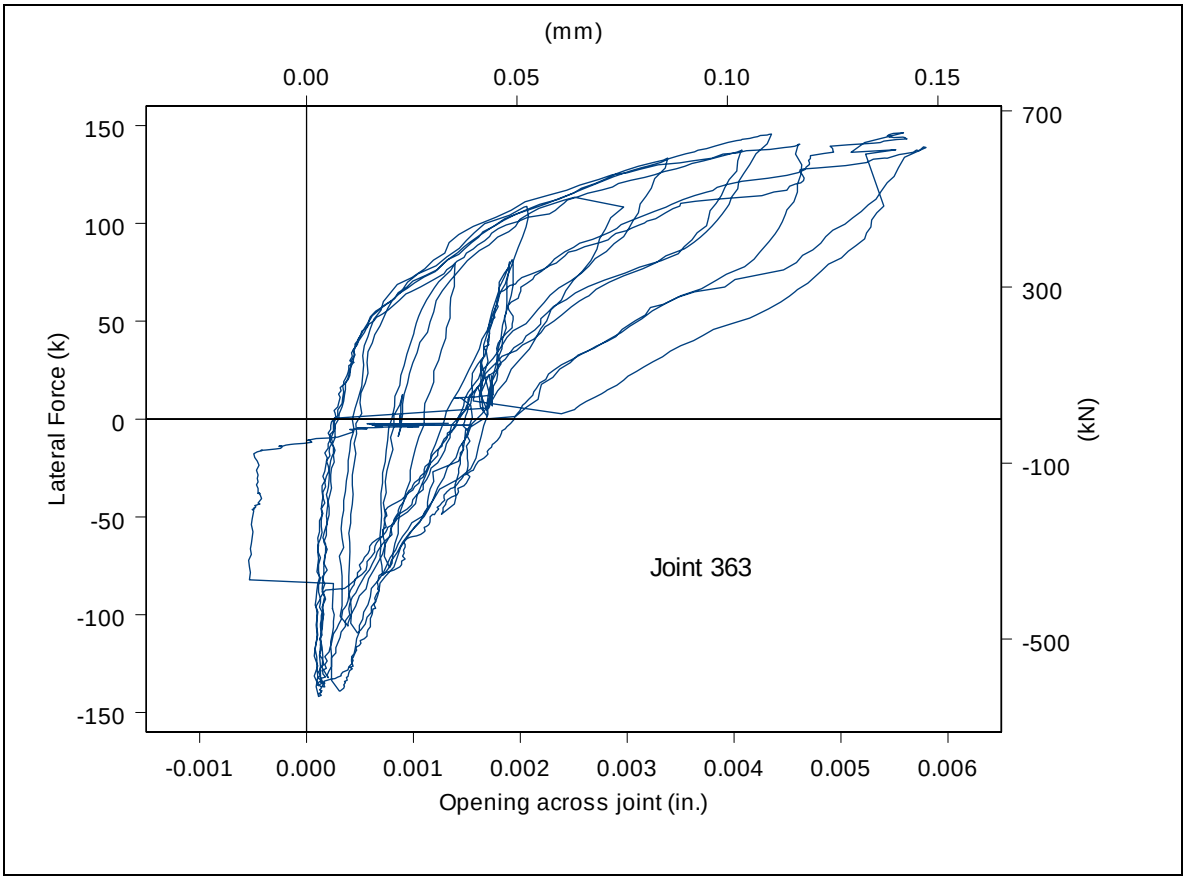

Figure 7.7 Joint opening during stage 1

7.3 Test Stage 2

7.3.1 Force-Displacement Behavior

The stage 2 performance is shown in Figure 7.8, superimposed on the force-displacement data from stage 1. Similarly to the data from the first stage, the force-displacement diagram of the system shows a stable hysteresis loop. The flexural capacity of the column increased due to the higher axial load used in stage 2. Similarly to stage 1, the initial monotonic prediction was slightly exceeded. After μ=4 the lateral load increases very little signifying a nearly perfectly plastic hinge at the column top. This accounts for the little additional opening of the superstructure joints as further displacement levels were reached.

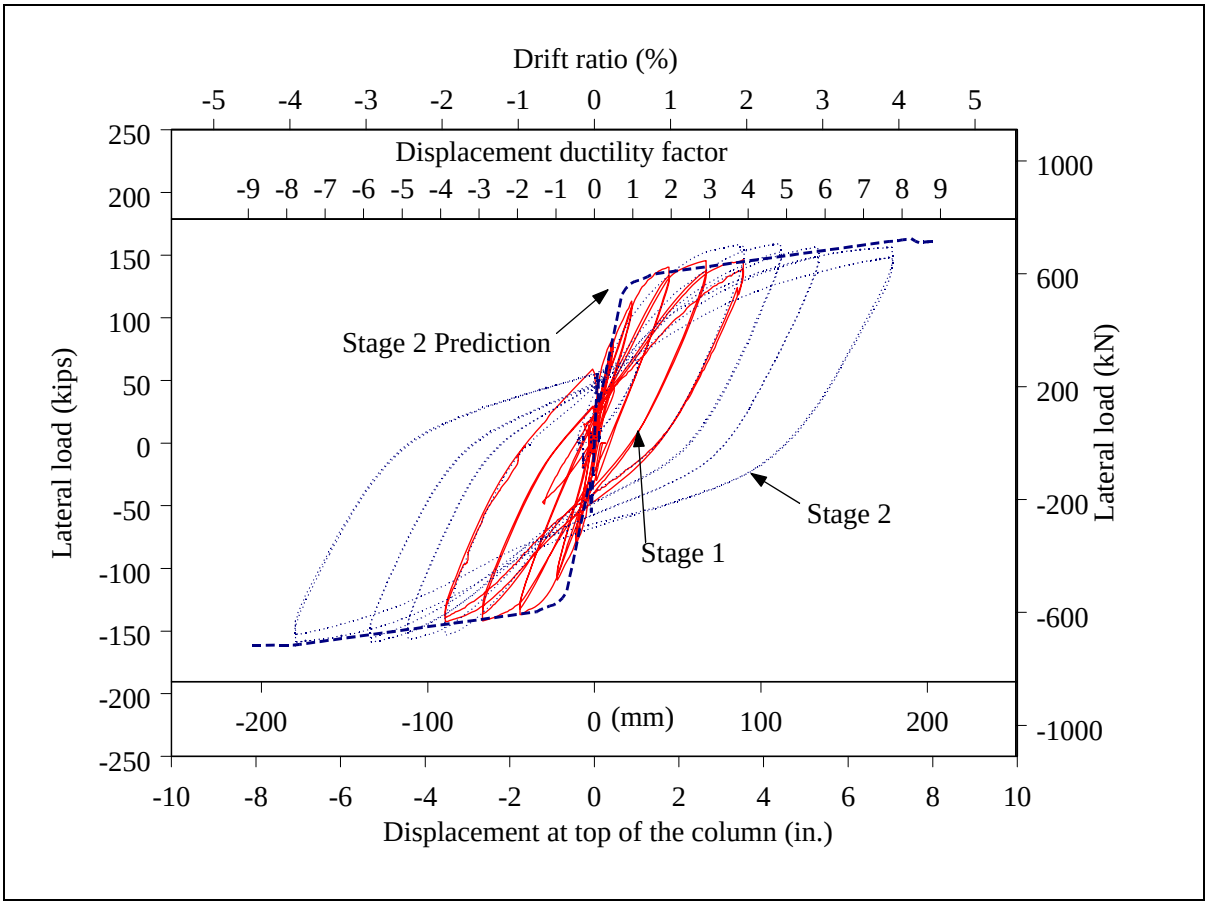

Figure 7.8 Stage 2 force-displacement diagram

7.3.2 Curvature

The stage 2 curvature profile is shown in Figure 7.9. The range of curvature greatly exceeding the yield curvature gradually crept down from the top of the column as higher ductilities were reached. In the final cycles at μ=8, the total plastic hinge length appears to be around 48 in (1219 mm).

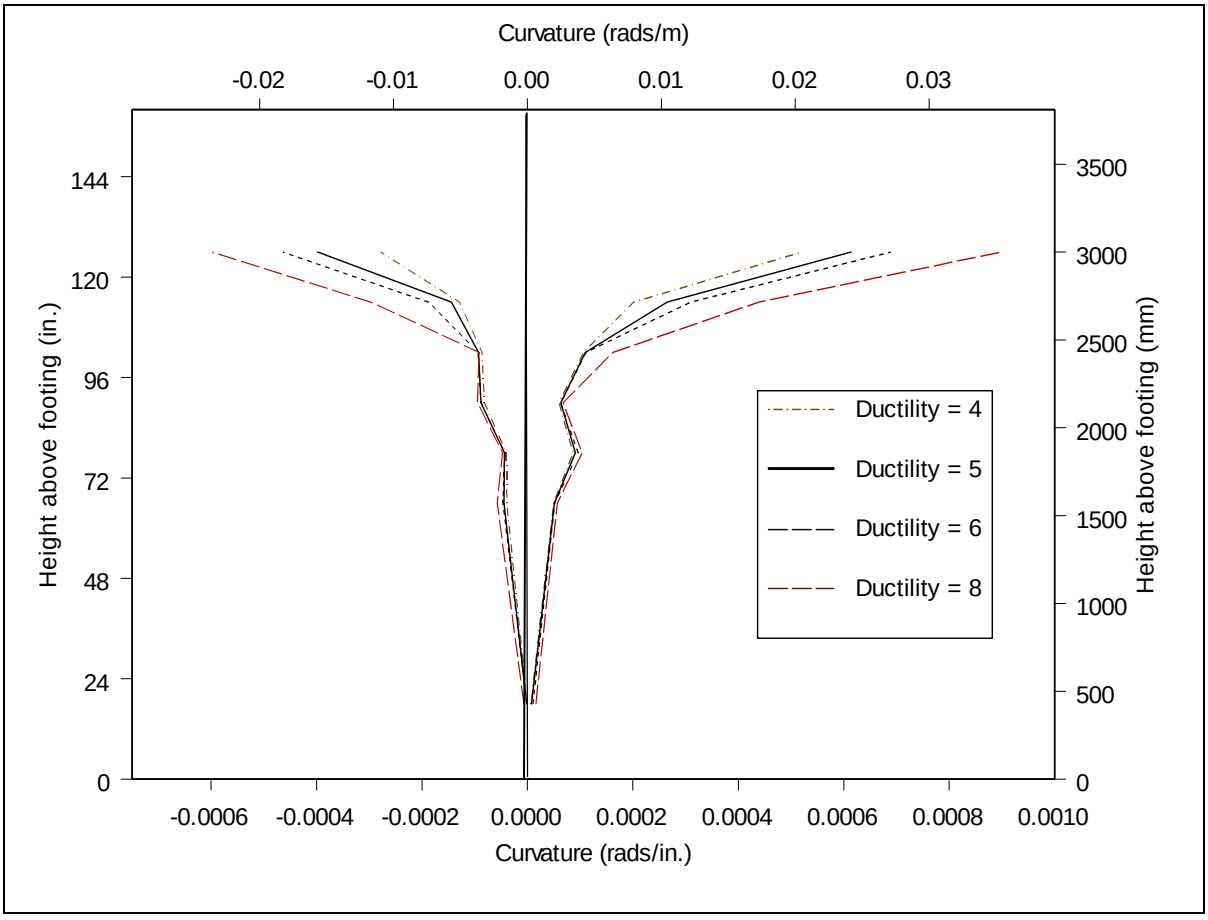

Figure 7.9 Stage 2 curvature profile

7.3.3 Longitudinal Bar Behavior

The tensile strains along the lengths of the longitudinal bars during stage 2 of the test are shown in Figure 7.10. For the location of the bars refer to Figure 7.3. Assuming a theoretical yield strain of 0.005 (5000 microstrain) the spread of the plastic hinge down the column is evident. At μ=4 the apparent plastic hinge length is 30 in. (760mm) as at the end of testing stage 1, while at μ=8 it is approximately 48 in (1220mm). Although it is difficult to see because many gages were damaged, the strain penetration into the pier segment also increased significantly from the 12 in. (305mm) at the end of stage 1.

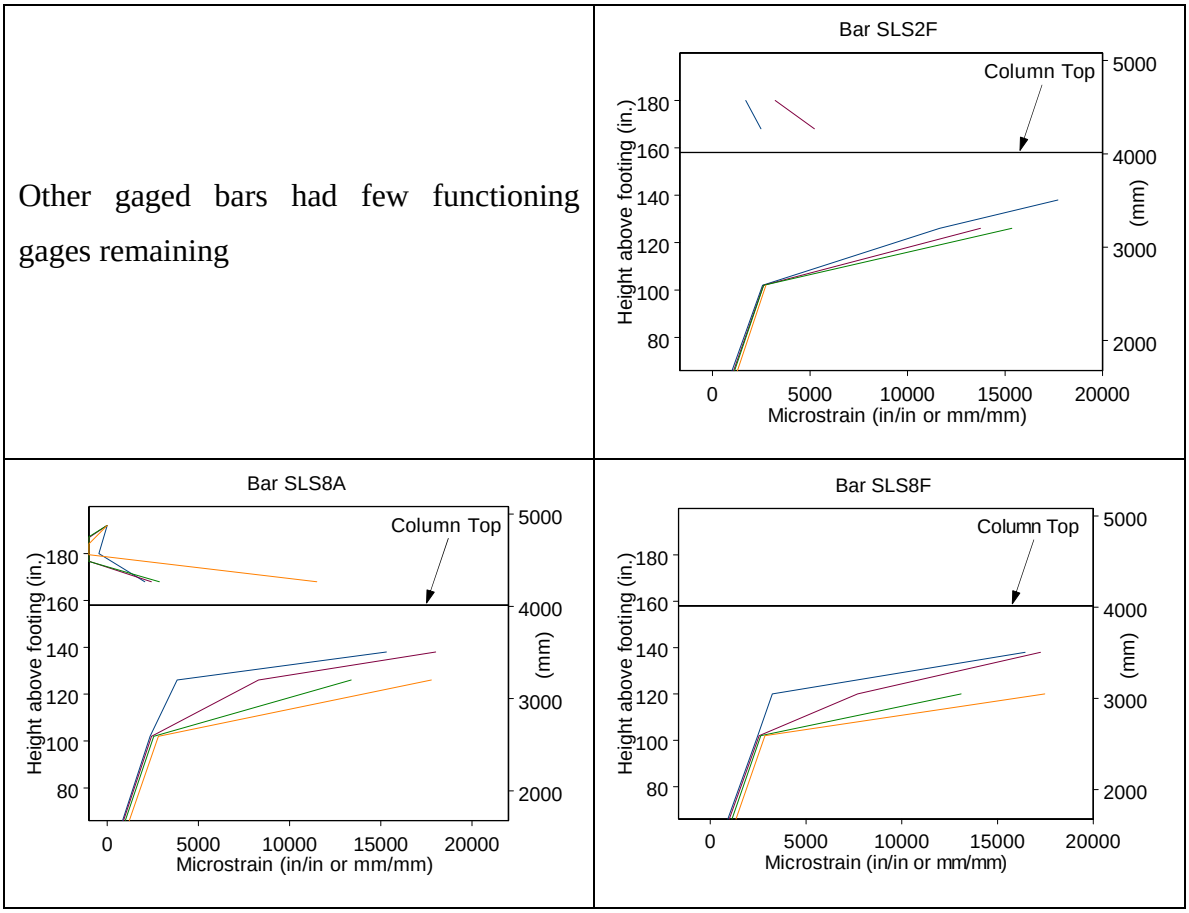

Figure 7.10 Longitudinal bar strain profiles for stage 2 at increasing ductility levels

7.3.4 Column-Superstructure Interaction

As seen in the force-displacement data for stage 2 of the test, due to the additional vertical load applied to the column the capacity and stiffness of the column increased. This increase in stiffness as well as the additional moment caused by the higher vertical load caused some opening of the joints nearest the column. Any increase in column stiffness will cause higher moments to be transferred to the superstructure under similar displacements. However once the joint opens the flexibility of the entire system increases. Definitive data from the single test verifying this result was difficult because of the effect of the increased vertical loads. Further analysis and investigation will be included in the subsequent report detailing the analysis portion of the project.

One area of the column-superstructure interaction where relevant data was gained was in the pier segment. During stage 1 of the test there was no significant opening of the joints nearest to the column and subsequently the gauged bars in the pier segment saw very low strains. The vertical headed-bars placed at each corner of the pier segment with the intent of picking up the shear forces (refer to Figure 2.5) saw strains on the order of 4% of the yield strain (ε_y) with a maximum of 200 microstrain throughout stage 1. During stage 2 of the test when the joints opened somewhat, the strains in these bars increased to around 25% of ε_y. The locations of two of these bars as well as their strains during stage 2 are shown in Figure 7.11.

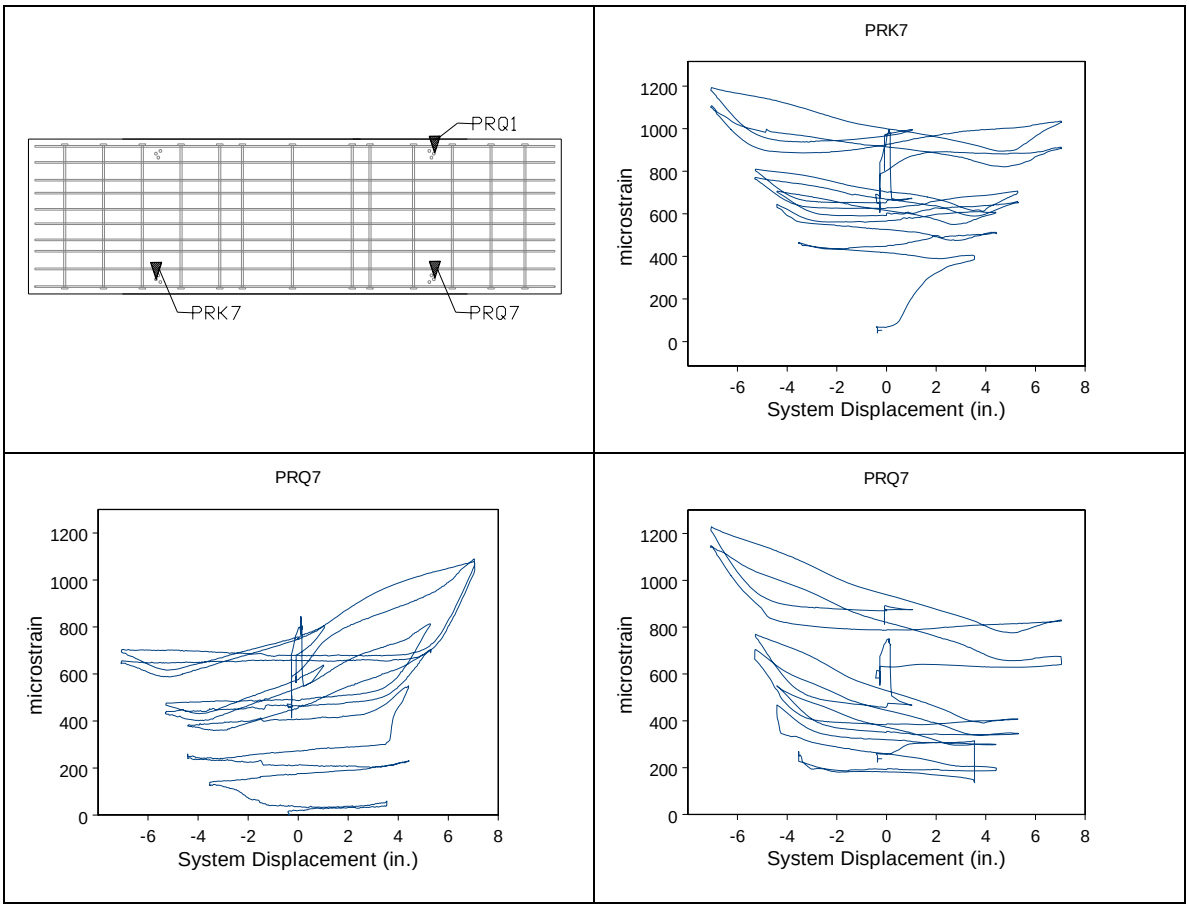

Figure 7.11 Strain of corner pier segment headed bars during stage 2

7.3.5 Joint Behavior

Clear opening of the joints nearest the column was seen during stage 2 of the test. The opening data of the joints on either side of the column is shown in Figure 7.12. The hysteretic behavior of the joint is shown, with energy dissipation likely do to debonding of the tendon and spreading of the crack down the sides of the superstructure. The joint loops are offset likely because of calibration of the instruments or possibly shifting during the weeks of testing. Figure 7.13 illustrates the differences between stages 1 and 2 at μ=4. It can be seen that the stiffness of the joint opening is greatly reduced due to the larger

openings in stage 2. Due to the boundary conditions differences between the stages the graphs appear to cross separate origins.

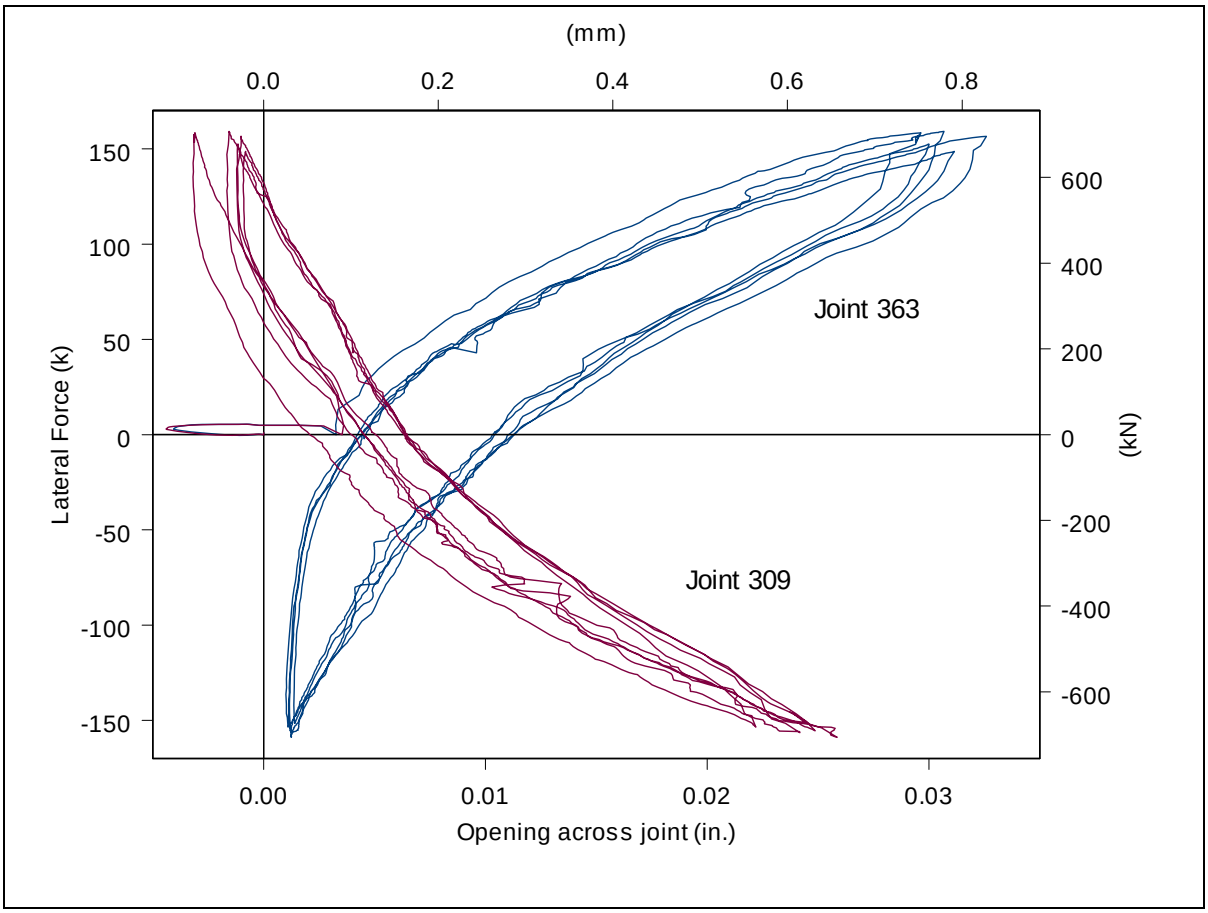

Figure 7.12 Joint opening during stage 2

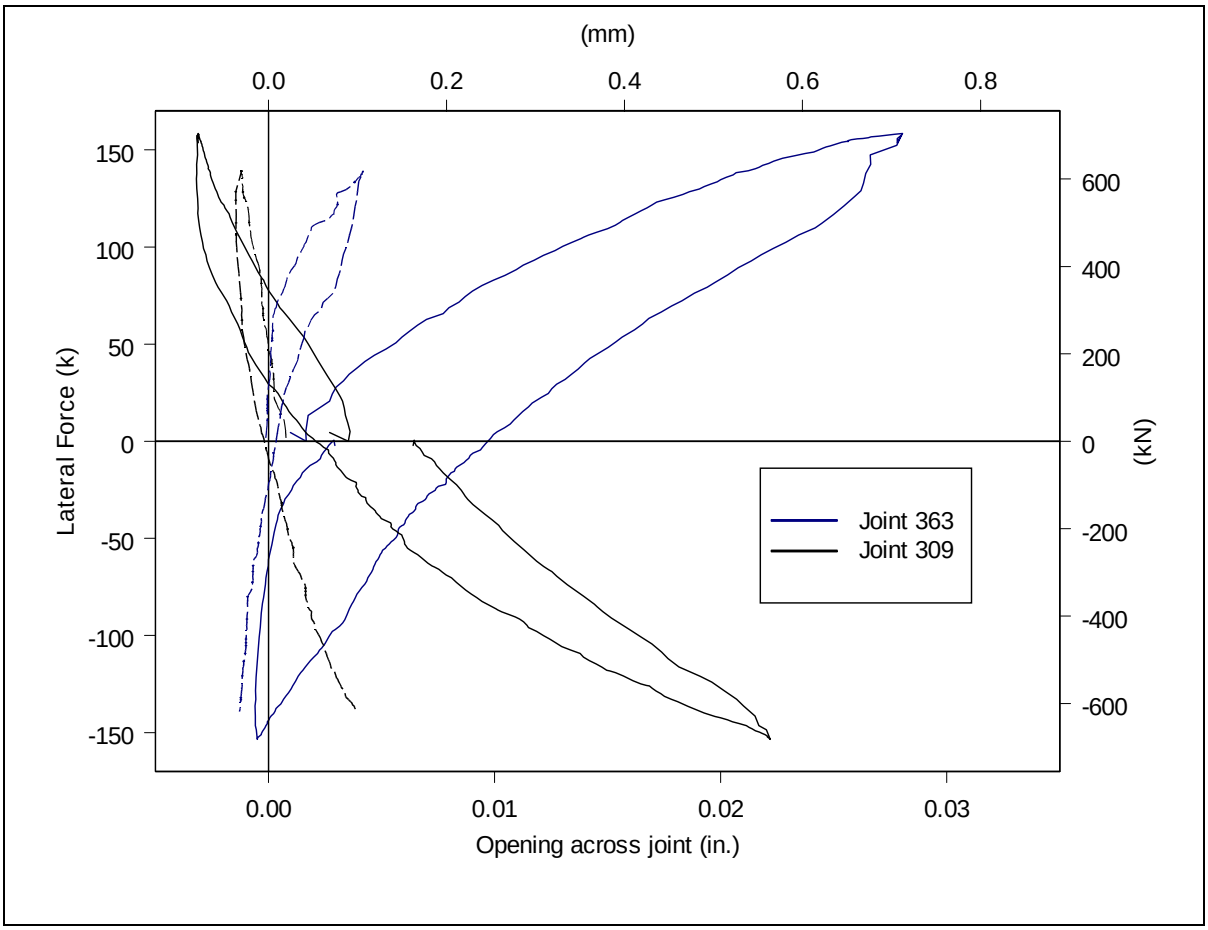

Figure 7.13 Comparison of joint opening at μ=4 between stages 1 and 2

8 Conclusions

8.1 Overview

This report discussed the design and testing of a half-scale bridge system built using the balanced cantilever method of precast segmental construction. Issues regarding design and analysis of precast segmental bridges are discussed based on the results from the segmental bridge system test as well previous phases of the testing program [6]. Issues for future research are highlighted where applicable.

8.2 Joint Performance

Despite not being noticed visibly during stage 1 of the test, the joints began to crack at the locations of the cast-in-place closure joint. The cracking was only at the top surface of the superstructure joints. The hairline cracks that formed along the joint were not easy to see, and closed up completely upon unloading as evidenced by their not being visually recognized during or immediately after the end of stage 1 testing. This cracking was likely due to a lack of tensile strength across the joint after decompression of the Prestress force occurred. At the interface between the pier segment and the CIP closure (or the first segment and the CIP closure) it should be assumed that there is no tensile strength from the concrete at that interface. No other joints were seen to open during any stage of testing.

In the second stage of testing the joints nearest to the column experienced noticeable opening. The cracks were seen to form at the first peaks of loading, and to open and close throughout the cyclic loading of the bridge. No residual damage in the joint region occurred and upon unloading the joints closed again. The crack width did not expand

greatly as the system displacements rose from a ductility of 4 to ductility 8, this was due to the small increase in moment transferred from the column during these cycles as the column had already formed a plastic hinge. The crack widths ranged from approximately 0.5 to 0.8 mm. The crack was not located completely on one or the other side of the 3 in. closure gap, but progressed along one or both sides in a non-uniform manner. The opening and closing of the joints was shown through the data collected to be stable, and to dissipate some energy as the crack propagated down the sides of the superstructure. The crack was never seen to lengthen more than halfway down the superstructure sides.

The combined effect of the reduced number of tendons and the increased load caused the joints to open. An area of future research could isolate these variables to gather specific experimental data related to the change in stiffness to compliment the analytical work currently in progress as the continuation of this program.

Areas of interest for future research include the change in behavior of the joints as the bonded tendons gradually debond. This change in the stiffness of the tendons would have an effect on the opening of the joints. Also, different design levels that allow more opening of the joints and spread displacement capacity from the column to the superstructure through the joints could likely allow for greater displacement capacities while reducing the residual damage sustained by the bridge system. A more severe combined longitudinal and transverse loading of the superstructure segments could clarify possible issues dealing with the shear transfer during extensive opening of the joints.

8.3 Column Performance

The overall performance of the column was typical of a well-confined, reinforced concrete column showing high-energy dissipation capacity, high displacement ductility, and stable hysteretic response. The response at each ductility level was similar during the first and second cycles. The amount of damage to the column was limited due to the unidirectional loading used in the test. Extensive spalling of the cover concrete occurred after μ=4. The system was not brought to failure due to stability issue and possible future uses of the test unit. However failure was certain to occur in the confined corner elements of the column by rupture of the longitudinal or spiral reinforcement or crushing of the corner element concrete.

At a displacement ductility level of 4 the plastic hinge length was similar to that predicted. However, at the extremely high displacement levels (μ=8), after significant spalling of the unconfined concrete had occurred, the plastic hinge length continued to extend down the column reaching a length approximately 1.5 times longer than the initial prediction. This was corroborated between both the curvature and longitudinal bar strain data during each stage of the test.

Further research involving precast segmental columns would compliment the findings of this bridge system test.

8.4 Other Remarks

This test provided two ideas regarding seismic design of precast segmental bridges. First that it is possible to apply the existing bridge design philosophy of limiting all damage to the column with this type of bridge provided the prestressing steel and column strengths are properly designed. Second, when the joints are allowed more flexibility and less prestressing is used, the behavior of the system is not compromised by minor opening of the joints. These findings are limited by the fact that the test used only loading in the longitudinal and vertical directions and that adding transverse loading may cause additional damage or changes to the system behavior once the joints open. This is a likely area of future research.

The pier segment design intended to safely transfer shear forces through to the column once the joints open was accomplished by the vertical headed bars placed at each corner of the pier segment. These were seen to take significantly more load during the stage of the test in which the joints open. Other than this modification the pier segment used was similar to those of CIP bridges. It should be noted that no access opening through the pier segment was used in the design as this highly complicated the already congested region of the pier segment. The access holes on the bottoms of the superstructure midspan segments functioned as the entry point into the center of the box girder sections.

9 Appendices

9.1 References

1. R.J.G. MacGregor, M.E. Kreger, and J.E. Breen, *Strength and Ductility of a Three-span Externally Post-tensioned Segmental Box Girder Bridge Model,* Prepared for the Center for Transportation Research, Research Report 1209-2F, University of Texas at Austin, April, 1991
2. A.N.A. Hindi, M.E. Kreger, and J.E. Breen, *Enhancing the Strength and Ductility of Post-tensioned Segmental Box Girder Bridges,* Prepared for the Center for Transportation Research, Research Report 1209-2G, University of Texas at Austin, April, 1991
3. AASHTO, *Standard Specifications for Highway Bridges*, 14th Edition, 1989
4. AASHTO, *Guide Specifications for Design and Construction of Segmental Concrete Bridges*, 2nd Edition, 1999
5. Caltrans. *Seismic Design Criteria.* Version 1.1, July 1999.
6. S.H. Megally, M. Garg, F. Seible, and R.K. Dowell, *Seismic Performance of Precast Segmental Bridge Superstructures,* Research Report SSRP-2001/24, University of California at San Diego, CA, May 2002.
7. K.P. Burnell, S.H. Megally, and J.I. Restrepo, *Cast-In-Place Hollow Rectangular Column Test, Preliminary Results Summary.* Submitted to Caltrans. May 7th, 2003.
8. ASBI. *Recommended Practice for Design and Construction of Segmental Concrete Bridges.* April 2000.

9. E.M. Hines, A. Dazio, and F. Seible. *Structural testing of the San Francisco-Oakland Bay Bridge east span skyway piers*. Structural Systems Research Project SSRP 2002/01, University of California, San Diego, La Jolla, CA 2002
10. E.M. Hines, F. Seible, R.K. Dowell, and A. Dazio. *Structural testing of the San Francisco-Oakland Bay Bridge east span skyway Structures: Longitudinal Pier Test*. Test Report TR 200-21, University of California, San Diego, La Jolla, CA 2000
11. M.J.N. Priestley, F. Seible, and G.M. Calvi, *Seismic Design and Retrofit of Bridges*. Wiley, New York, 1996.
12. Bond Area Scaling
13. E.M. Hines, F. Seible, and M.J.N. Priestley, *Cyclic tests of structural walls with highly-confined boundary elements,* Structural Systems Research Project SSRP 1999/15, University of California, San Diego, La Jolla, CA 1999
14. ANATECH Corporation, *ANDRIANNA-User's Guide*, Version 1.0, 1999
15. J.B. Mander, M.J.N. Priestley, and R. Park, *Seismic Design of Bridge Piers*, Research Report 84-2, Department of Civil Engineering, University of Canterbury, Christchurch, New Zealand, 1984
16. M.P. Collins, and D. Mitchell, *Prestressed Concrete Structures*, Prentice-Hall, London, 1991
17. M. Menegotto, and P.E. Pinto, "Method of Analysis for Critically Loaded Reinforced Concrete Plane Frames Including Changes in Geometry and Non-Elastic Behavior of Elements under Combined Normal Force and Bending," I. A. B. S. E., *Symposium on the resistance and ultimate deformability of structures acted on by well-defined repeated loads*, Lisbon, Portugal, 1973

18. E.G. Nawy, *Prestressed Concrete: A Fundamental Approach*, 2nd Edition, Prentice Hall, Upper Saddle River, New Jersey, 1996

9.2 Construction Photos

Figure 9.1 Reinforcement and placing of the footing and pin

Figure 9.2 Corner spirals with gauges in place

Figure 9.3 Placement of corner spirals and bottom of column reinforcement

Figure 9.4 View of wall reinforcement in column

Figure 9.5 Column during construction prior to pouring top portion

Figure 9.6 Placing forms for pouring top of column

Figure 9.7 Pier segment reinforcement

Figure 9.8 Tendon anchor and bottom of superstructure reinforcement cage

Figure 9.9 Steel forms used for casting superstructure segments, interchangeable inner form

Figure 9.10 Tendons and reinforcement in segment

Figure 9.11 First completed segment (later scrapped because the bottom blisters are backwards)

Figure 9.12 Unloading and storage of segments awaiting placement

Figure 9.13 Placement of 1st pair of segments

Figure 9.14 Continuing placement of 1st pair of segments

Figure 9.15 Pouring 3” closure gap

Figure 9.16 1st pair of segments in place and epoxied with temporary prestressing bars

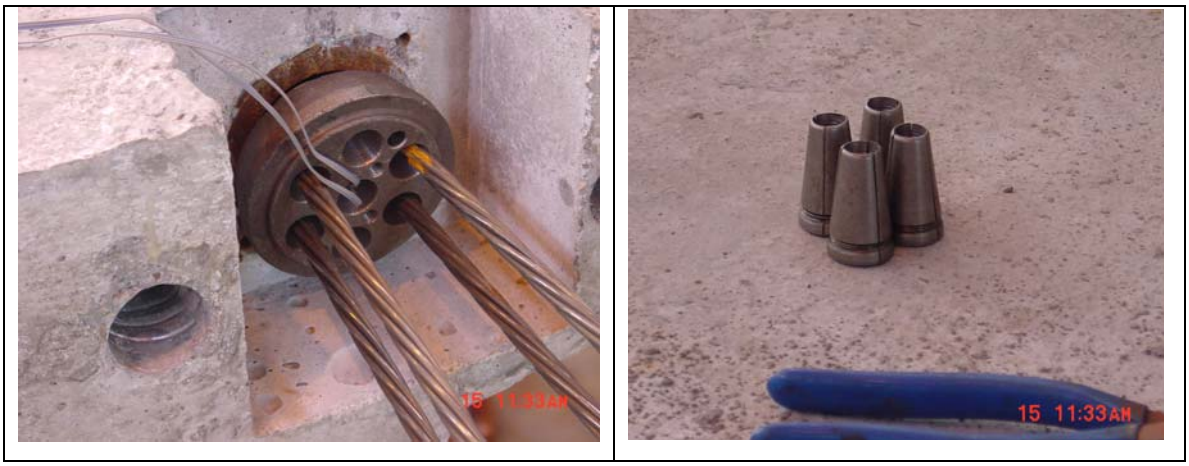

Figure 9.17 Tendon wedge plate and wedges

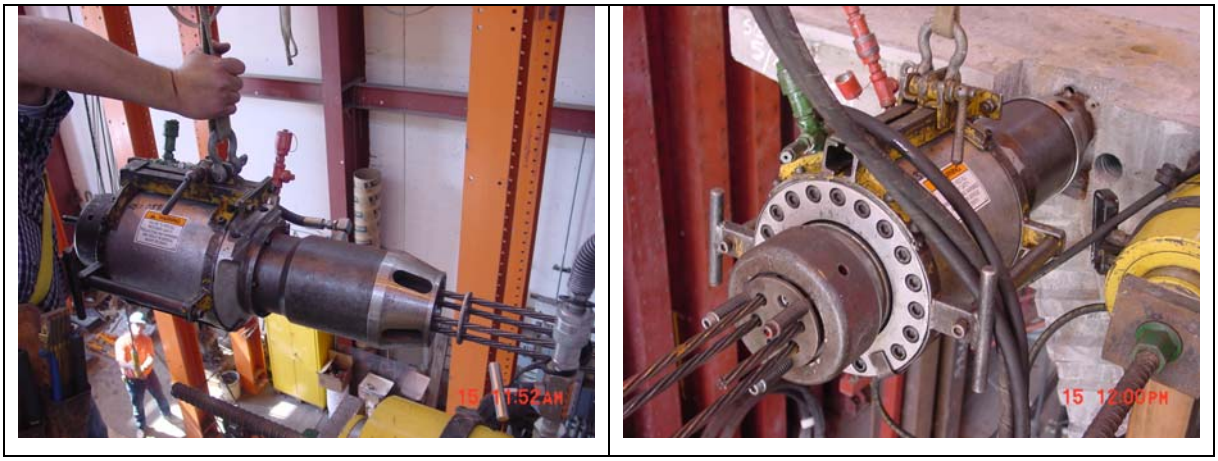

Figure 9.18 Stressing the tendon

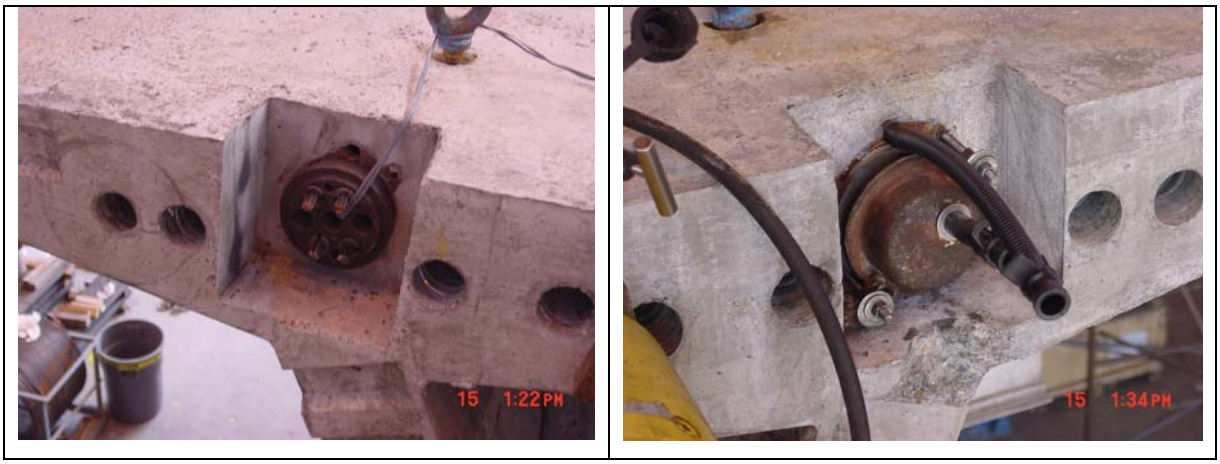

Figure 9.19 Cutting off tendon tails and placement of grout caps

Figure 9.20 2nd pair of segments installed

Figure 9.21 After all segments have been installed and top tendons stressed

Figure 9.22 Placement of end blocks and fixtures

Figure 9.23 Test during placement of actuators

Figure 9.24 Damaged test unit after final testing cycles

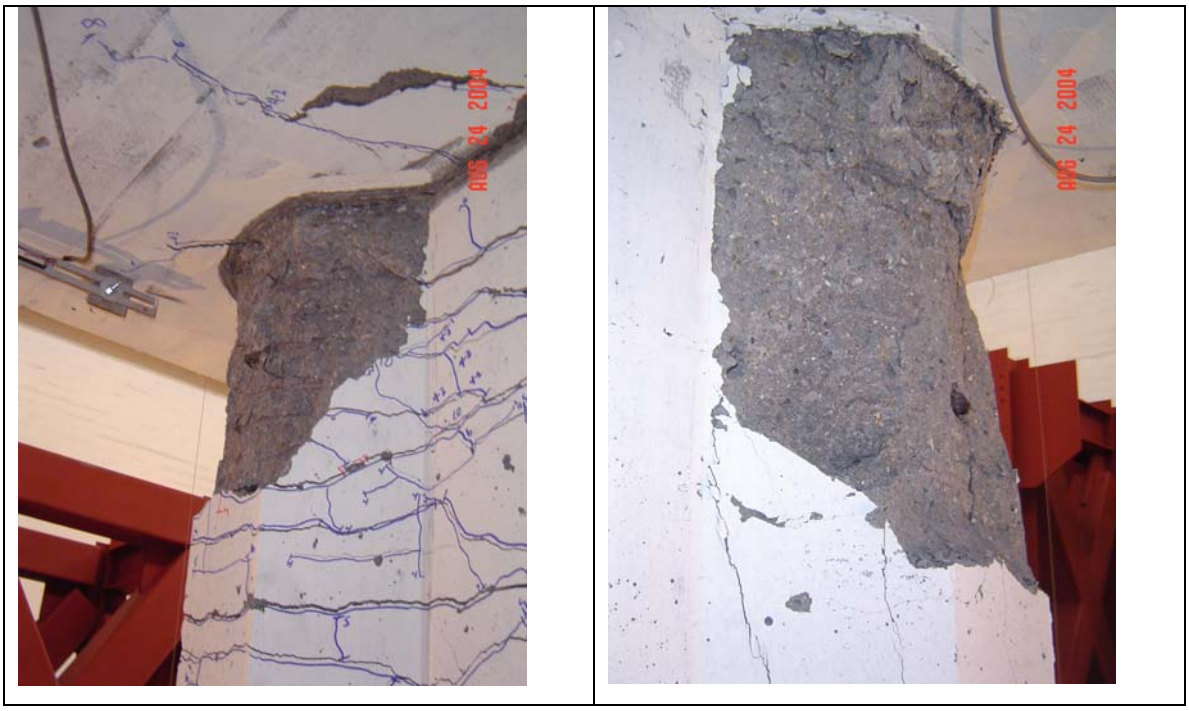

Figure 9.25 Spalling at top corners at conclusion of testing

Figure 9.26 Column displacement and pin rotation close-up

9.3 Additional Data

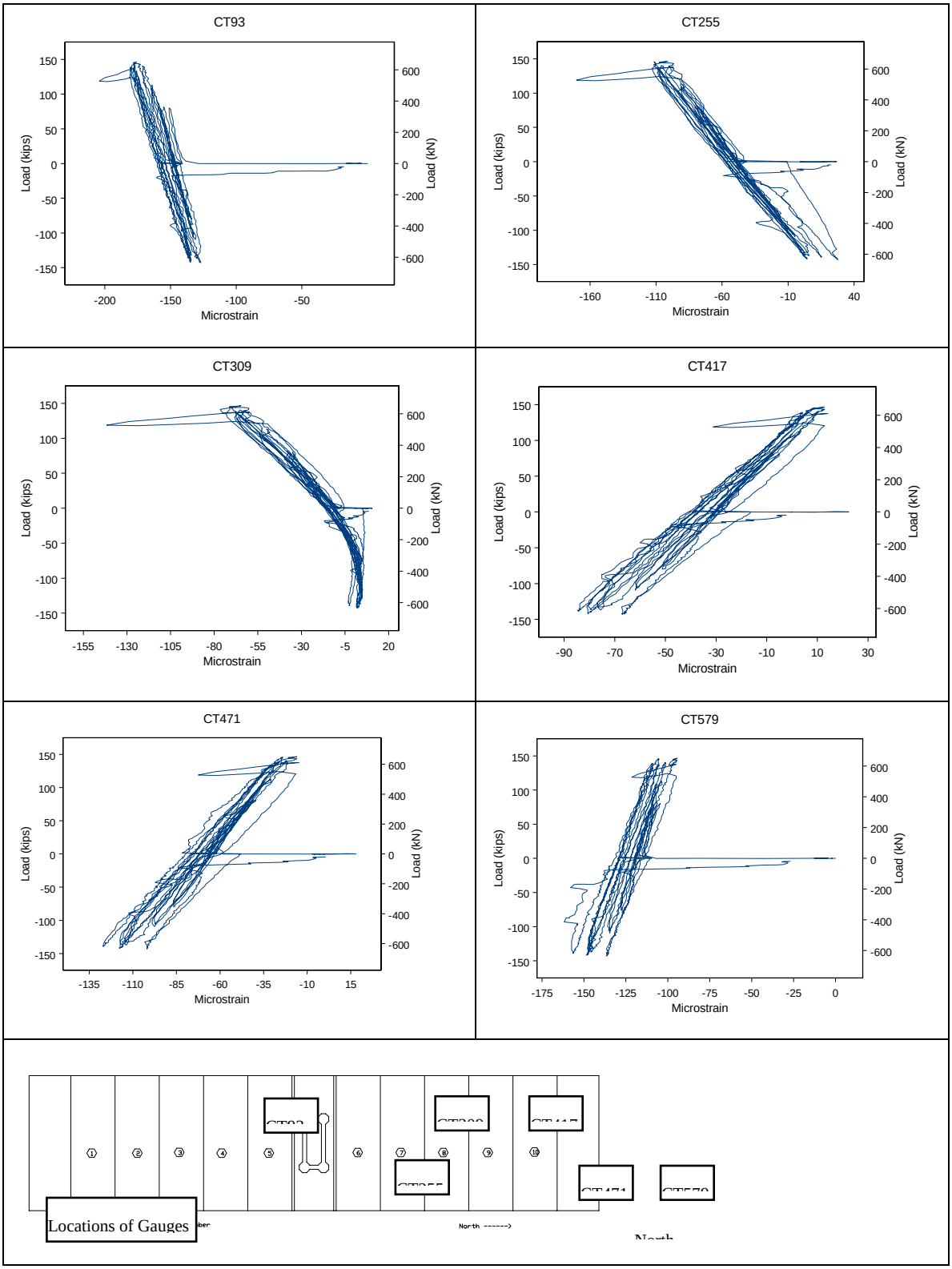

Figure 9.27 Concrete top surface strains for stage 1

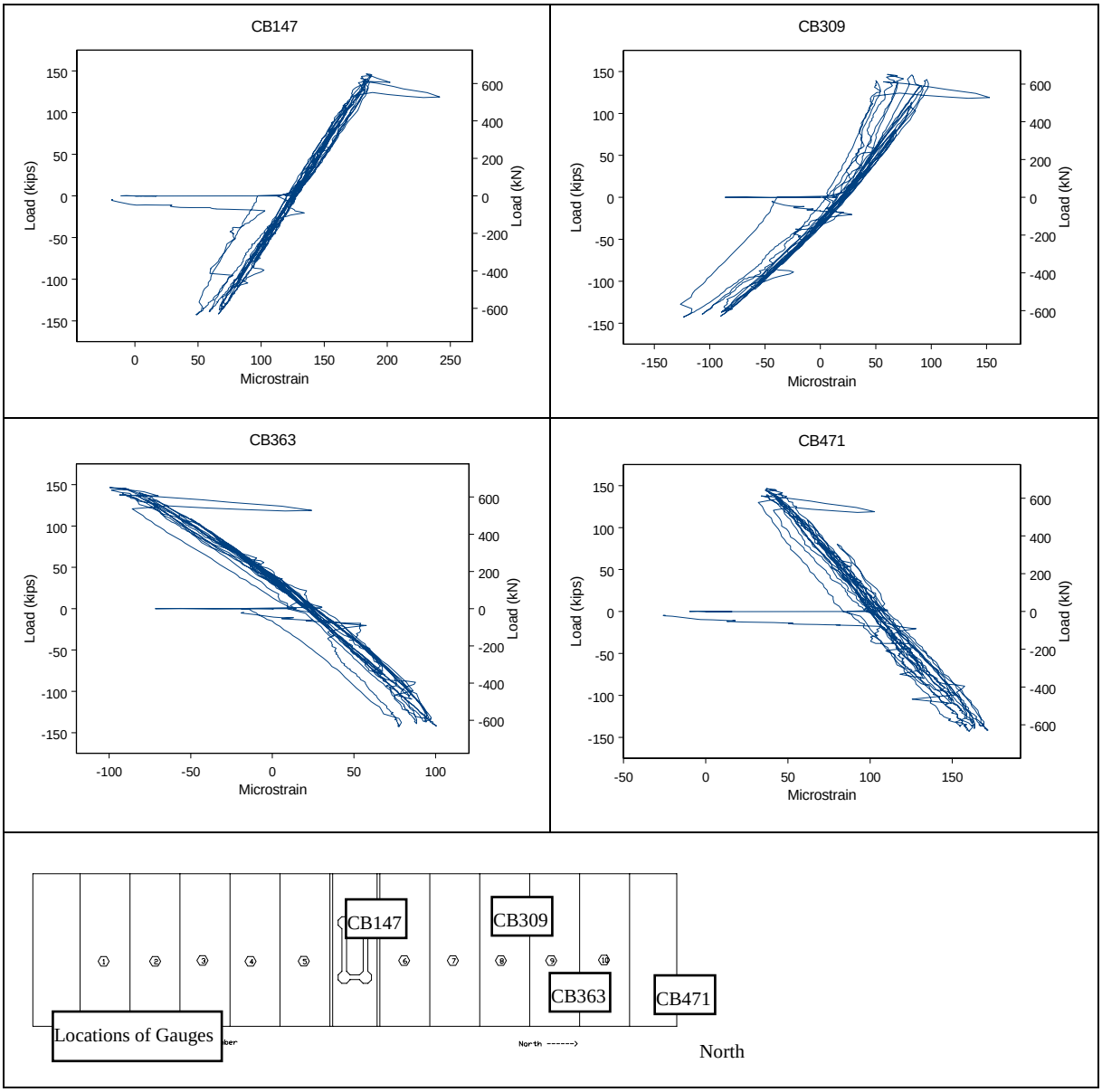

Figure 9.28 Concrete bottom surface strains for stage 1

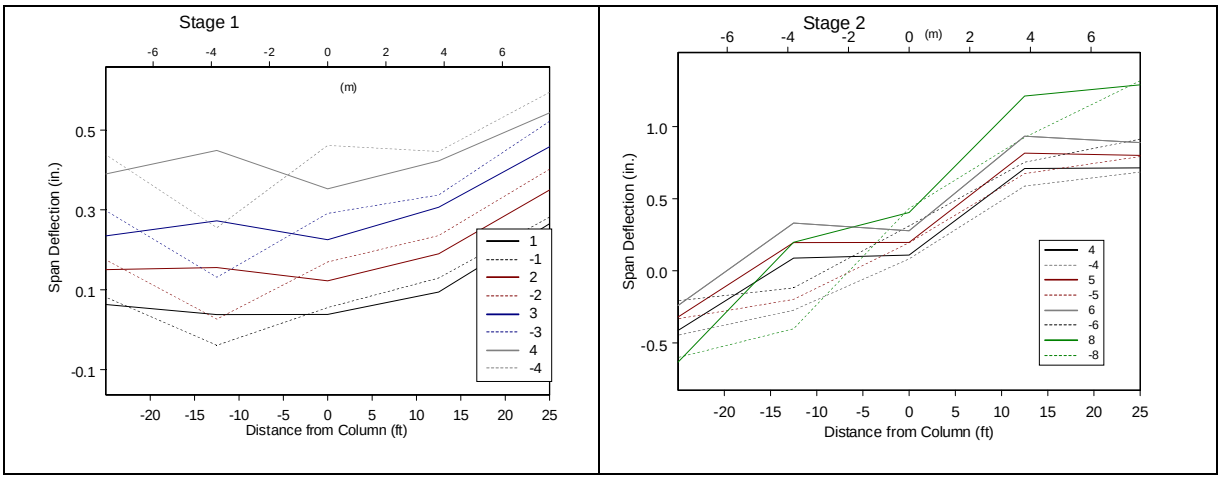

Figure 9.29 Span deflections

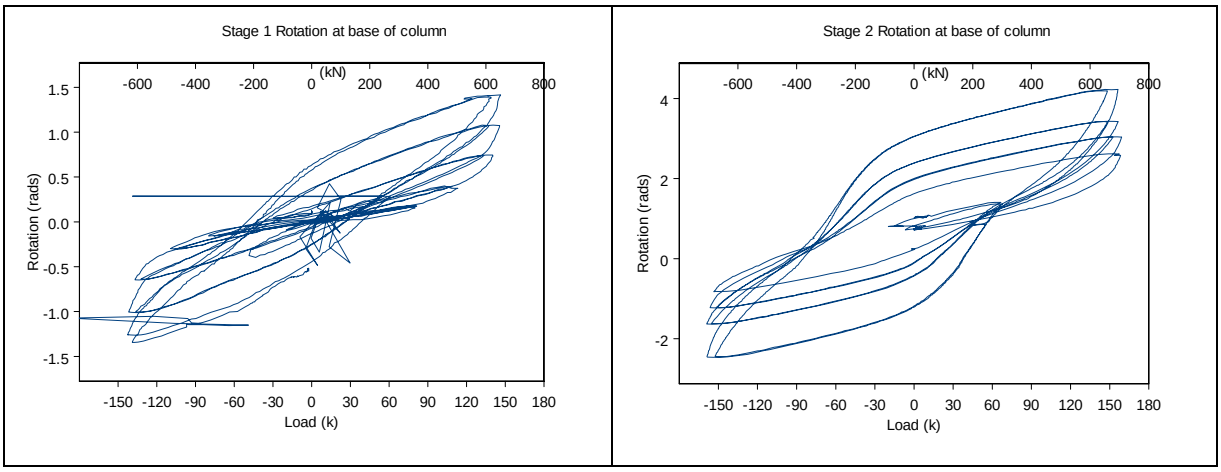

Figure 9.30 Column bottom rotations

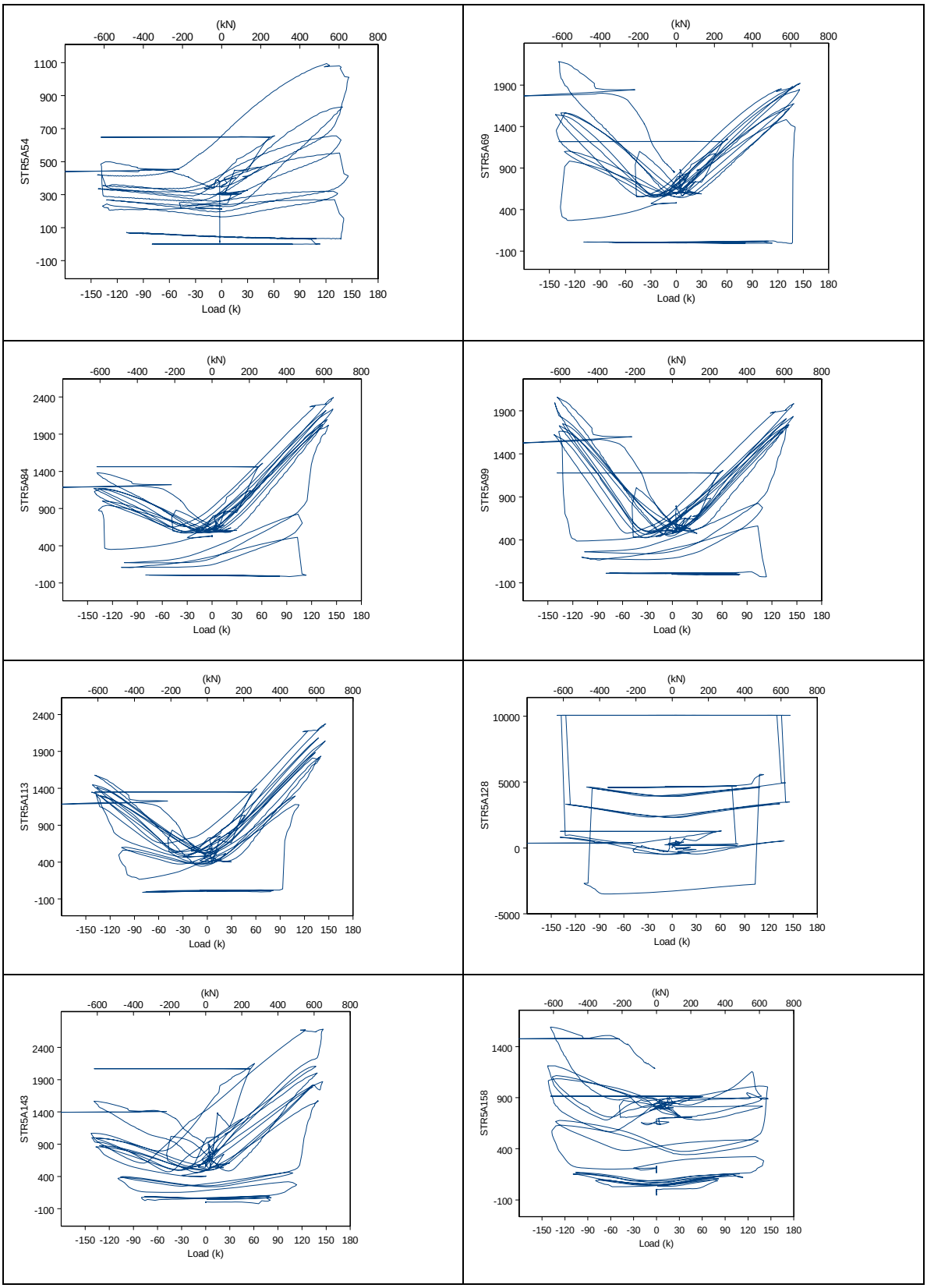

Figure 9.31 Transverse bar strains at location 5A for stage 1

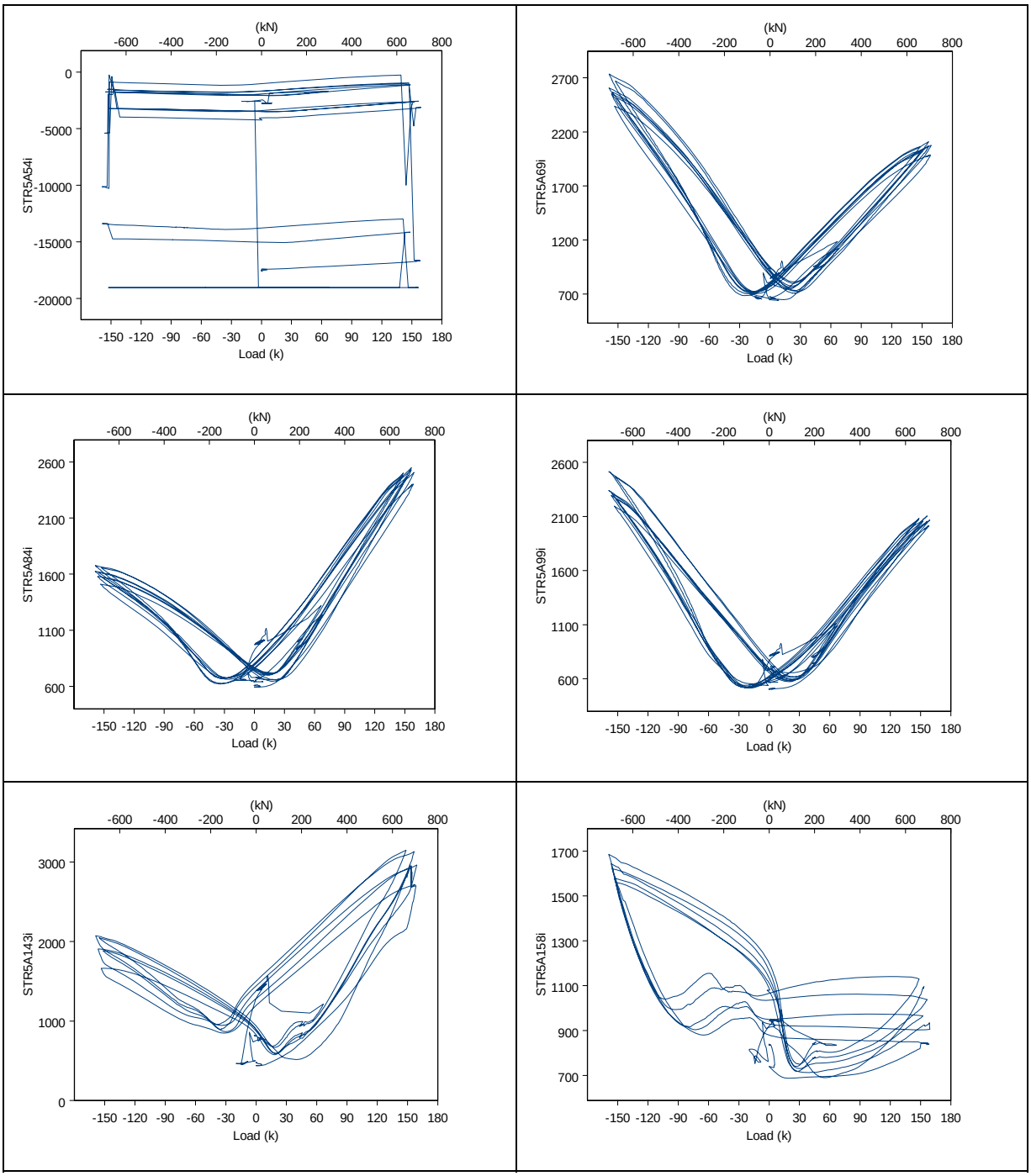

Figure 9.32 Transverse bar strains at location 5A for stage 2

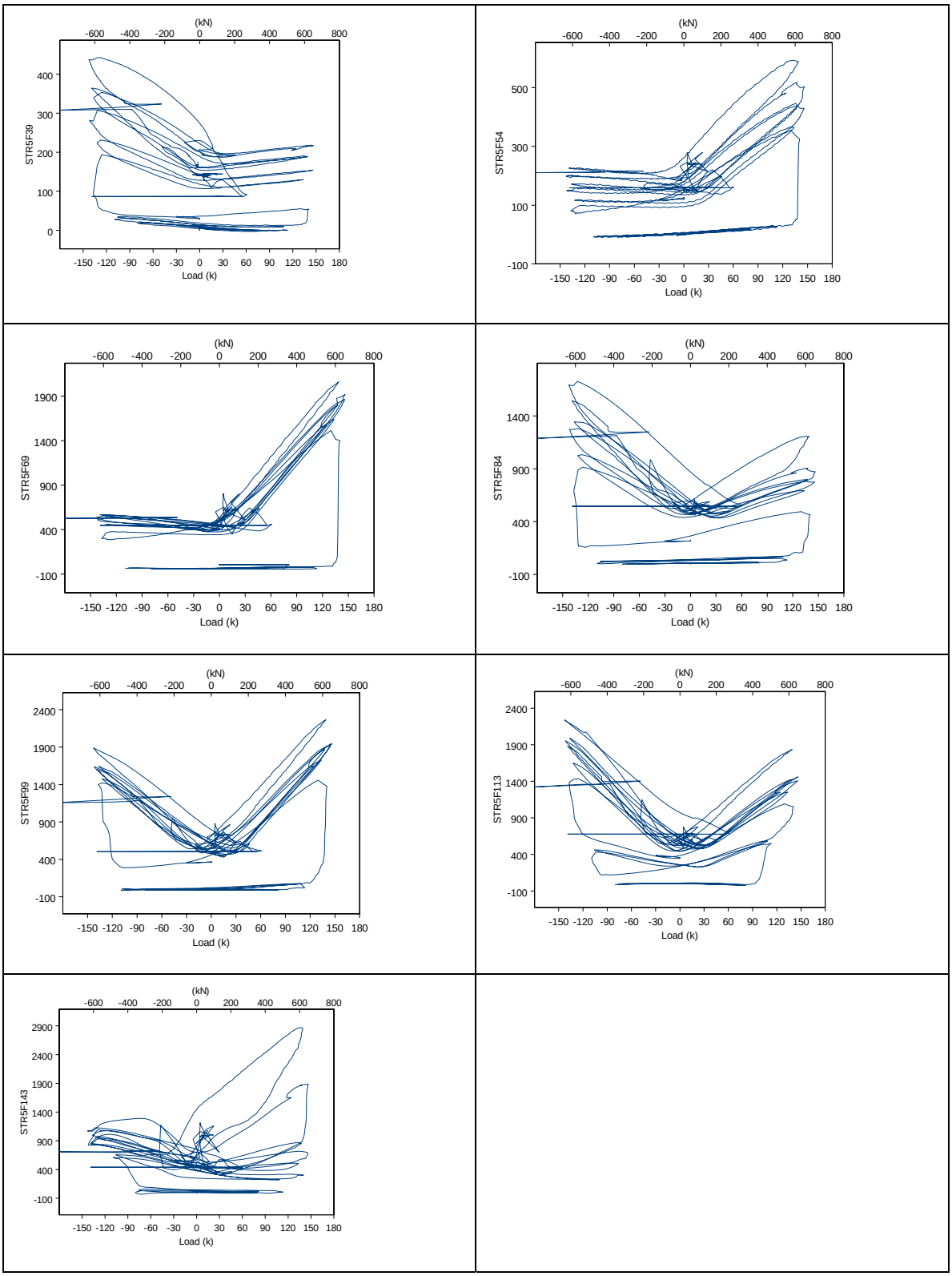

Figure 9.33 Transverse bar strains at location 5F for stage 1

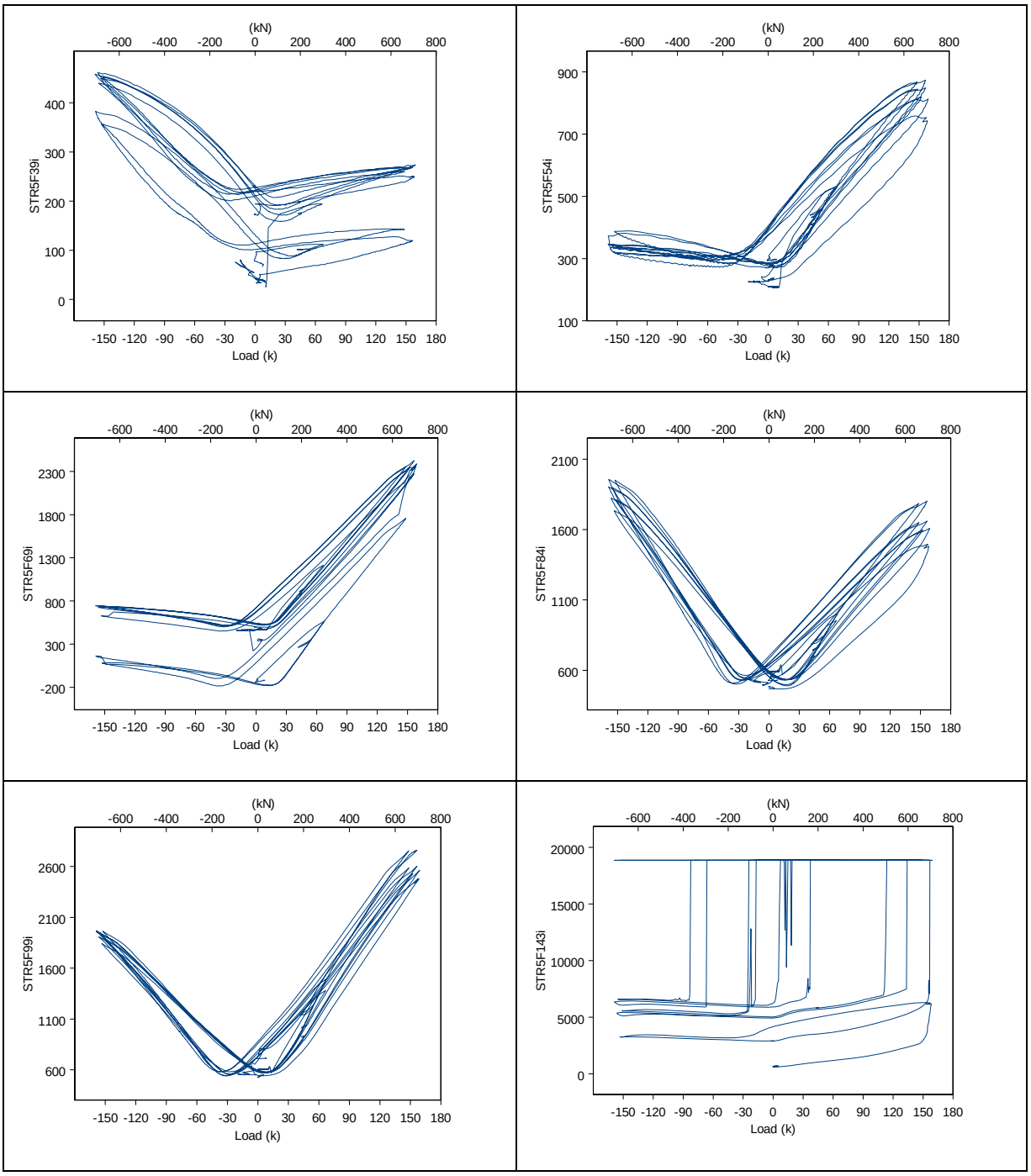

Figure 9.34 Transverse bar strains at location 5F for stage 2

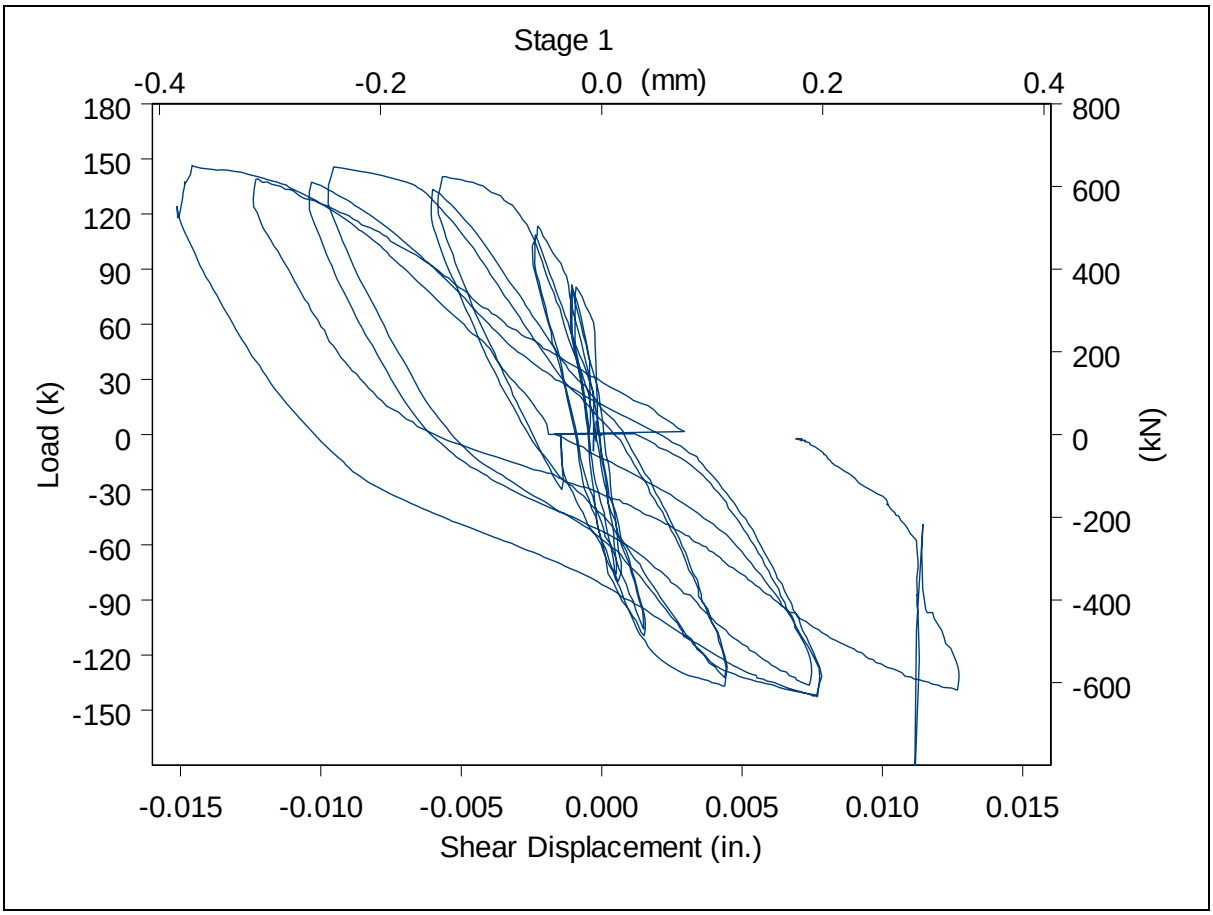

Figure 9.35 Shear deflection during stage 1

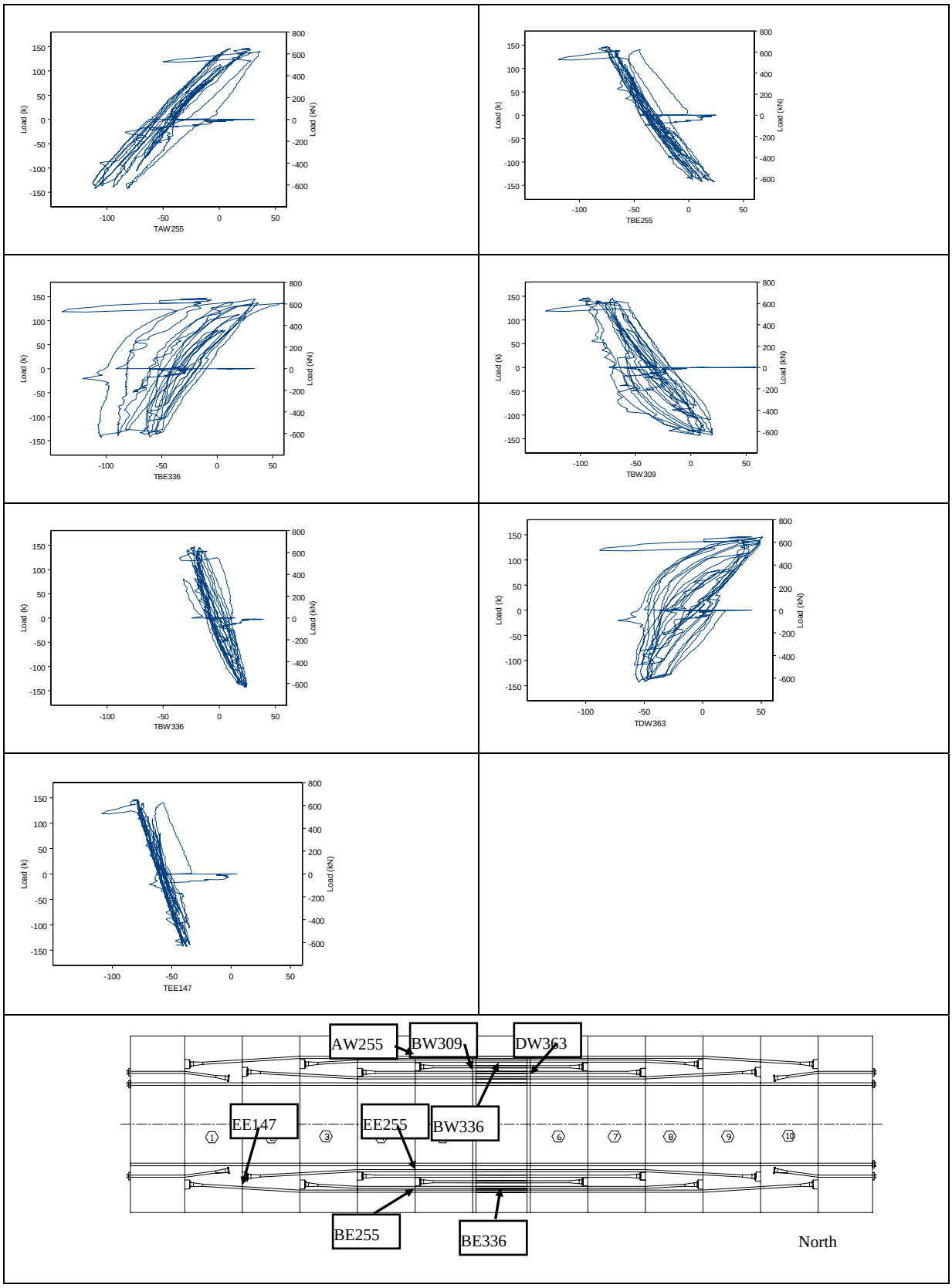

Figure 9.36 Tendon gauge microstrains for stage 1

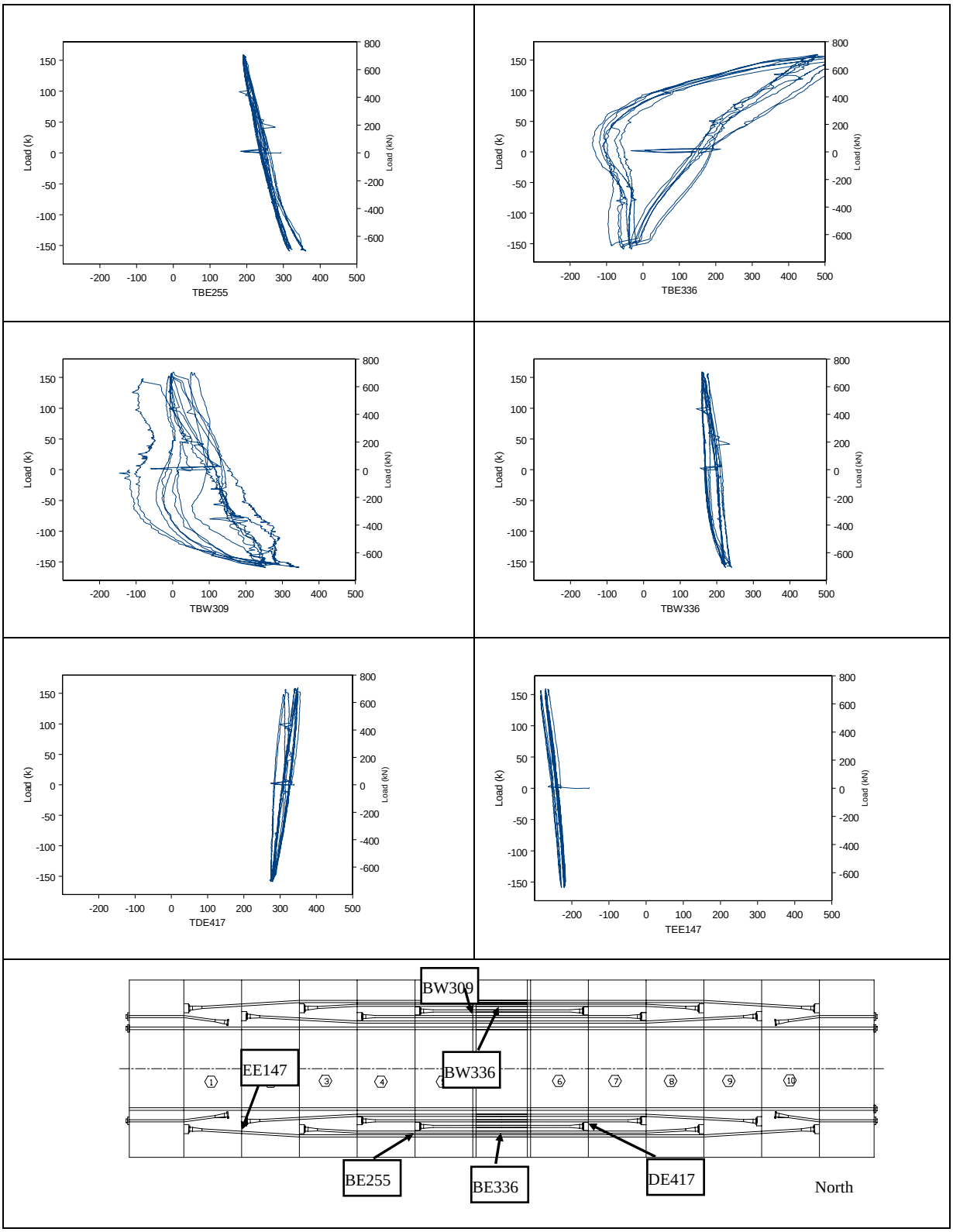

Figure 9.37 Tendon gauge microstrains for stage 2